THESIS

Presented to Faculdade de Engenharia da Universidade do Porto

to obtain the degree of Master of Science of Universidade do Porto

Specialty: Mechanical Engineering – Structural Analysis

Failure Analysis of GRP Pipes Under Compressive Ring Loads

Last revision: March 31st, 2005

by

Hugo Faria

No. 030550004

To be defended in _____, the _____, 2005, before the jury nominated by FEUP

Abstract

The need of evaluating the mechanical behaviour of glass-fibre reinforced plastic (GRP) pipes when installed in the sub-soil, for example, leads to test and simulation methodologies under compressive ring loads.

The present study focused on the experimental and numerical analysis of GRP pipes under ring compressive loading condition. Short and long-term experimental procedures, as well as numerical models, simulating those loading conditions were carried out.

The main objectives were comparing results achieved in different test conditions and evaluating the applicability of numerical analysis for structure's characterization.

Keywords

GRP pipes; ring load; mechanical tests; creep; damage

Resumo

A utilização de metodologias de ensaio e simulação de tubagens em plástico reforçado com fibra de vidro (PRFV) sob carregamento de compressão lateral pretende avaliar o seu comportamento em instalações no sub-solo, por exemplo.

Este estudo incidiu sobre a análise experimental e numérica de tubagens PRFV nessas situações de carregamento de compresão lateral. Foram realizados procedimentos experimentais de curta e longa duração, bem como modelos numéricos, simulando aquelas condições de carregamento.

Os objectivos principais foram a comparação entre os resultados e comportamentos estruturais verificados nas diferentes condições de ensaio e a avaliação da aplicabilidade da análise numérica para caracterização da estrutura.

Palavras-chave

Tubos PRFV; carregamento anelar; ensaios mecânicos; fluência; dano

Acknowledgements

The experimental tasks presented in this study were carried out in the Laboratory of Mechanical Tests (INEGI/CEMACOM) and in the Laboratory of Technological Tests (FEUP/DEMEGI) without whose equipments and technicians they would not been viable. Concerning to that I must express my recognition for the work initiated by those who preceded me, André Vieira and João Reis.

The first steps in the development of the numerical models were given aside with André Roque, whose precious contribution I thank.

Furthermore, I have to enhance the good work environment which Unidade de Materiais Compósitos of INEGI, CEMACOM, received me with. I cannot leave to thank the unit's direction, in the person of Professor António Torres Marques, the availability, efficient advices and the freedom I was transmitted for the best prosecution of the study.

To professors Rui Miranda Guedes and Marcelo Moura my recognition goes, of course, for the total availability and capacity demonstrated in the advising and orientation of this work, but, over all, it goes for the notable easiness with which they had provided me months of pleasant joint work.

Agradecimentos

As tarefas experimentais apresentadas neste estudo foram realizadas no Laboratório de Ensaios Mecânicos (INEGI/CEMACOM) e no Laboratório de Ensaios Tecnológicos (FEUP/DEMEGI) sem cujos equipamentos e recursos humanos não teriam sido viáveis. A esse respeito quero exprimir o meu reconhecimento pelo trabalho iniciado pelos que me antecederam, André Vieira e João Reis.

Os primeiros passos no desenvolvimento dos modelos numéricos foram dados em conjunto com André Roque a quem agradeço a preciosa colaboração.

Ao mais, tenho de realçar o bom ambiente de trabalho com que a Unidade de Materiais Compósitos do INEGI, CEMACOM, me acolheu. Não posso deixar de agradecer à direcção dessa mesma unidade, na pessoa do Prof. António Torres Marques, a disponibilidade, os conselhos eficazes e a liberdade que me foram transmitidos para a melhor prossecução do trabalho.

Aos professores Rui Miranda Guedes e Marcelo Moura o meu reconhecimento vai, naturalmente, para a total disponibilidade e capacidade demonstradas no aconselhamento e orientação deste trabalho, mas, sobretudo, também para a notável facilidade com que me proporcionaram meses de agradável trabalho conjunto.

Table of Contents

1. Introduction

Fibre reinforced polymers (FRP) are a practical alternative to metals in applications where corrosion, weight, environment and other factors limit the use of metals. In piping systems, glass-fibre reinforced plastic (GRP) pipes have been increasingly introduced and are now an important class of engineering structures.

Within their typical applications, either in mechanical structures or civil infrastructures GRP pipes are, frequently, exposed to complex service environment conditions of a range of combinations of stress, time, temperature, moisture, radiation, chemical, and gaseous environments and are expected to perform for fifty years or more [1].

The lack of understanding the fundamental parameters controlling long-term materials performance necessarily leads to over-design and in-service prototype evaluations and, furthermore, inhibits greater utilization.

Additionally, the current standards treating normalization/certification of GRP pipes typically require test durations of 10000 hours and high number of specimens. Even though it is felt that these strong requirements are reasonable, concerning to the confident utilization needs of many applications, the fact is that they are restrictive for the improvement and innovation of new products. Testing times of that long also lead end users to avoid confirmation tests.

FRP materials should be required to pass a series of specifications based on inherent and residual mechanical, physical, and thermal properties after accelerated service environment exposure conditions [1]. The main purpose of developing new test methods with determined preconditioning temperatures, time and environment conditions, is imposing accelerated ageing to the specimens, reducing test time.

By being designed either for gravitational or pressurized transportation of fluids, GRP pipes are typically tested under ring deflection and/or internal pressure conditions. In this study, focused in the ring deflection condition, they were conducted standard and alternative test methods under that loading condition. This loading configuration seems to be appropriated to approximately simulate in laboratory the solicitations verified in a sub-soil installation.

One condition and limitation of the existing methods is the implicit assumption that the mechanisms responsible for the long-term material failure are the same at different load levels. The failure mechanisms originated by the new methods being developed should be as close as possible to those ones verified in real service conditions. So, it is intended to develop damage phenomena similar to those that lead to long-term loss of integrity and failure.

The pipe behaviour in a ring deflected condition is then evaluated by three different test methods, differing in the controlled parameter and/or duration:

- Initial failure strain tests
- Creep Tests
- Relaxation Tests

Determining the characteristics related to creep and relaxation phenomena of these materials and understanding the phenomena is critical to further use of FRP composites in civil infrastructure [1].

There are two main technologies to produce large volumes of FRP pipe: filament winding (1) and centrifugal cast. Some manufacturers also use hybrid methods comprising the two philosophies in the same production. Four different types of GRP pipes, from four different manufacturers have been selected for the test campaigns.

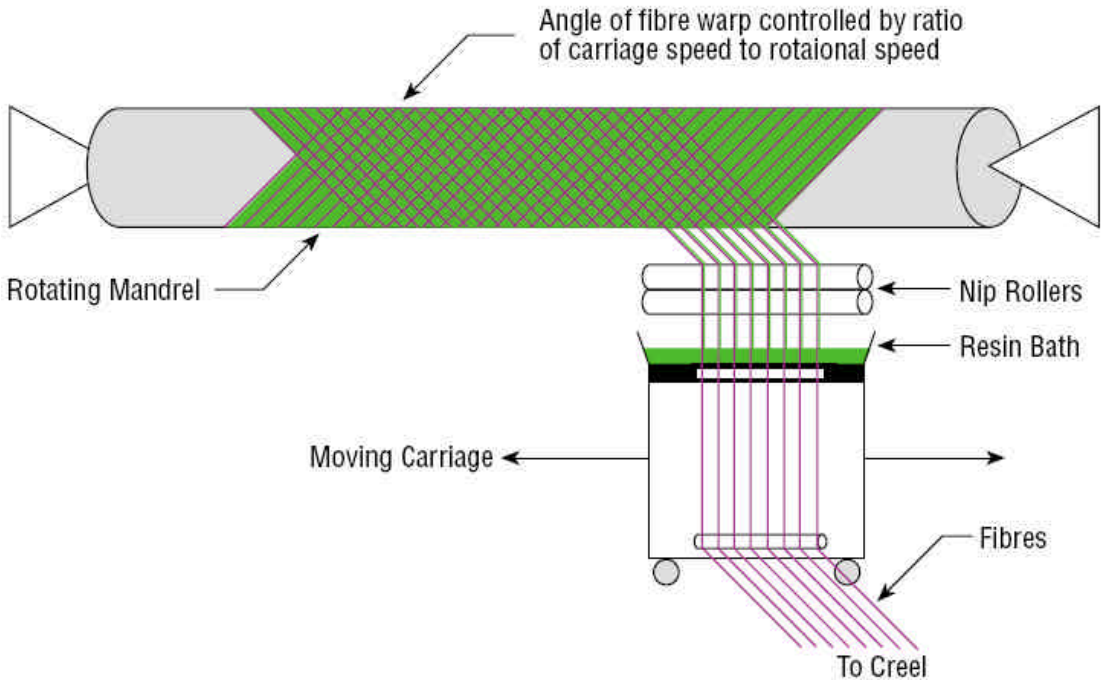

Fig. 1 – Schematic view of filament winding process on FRP pipes [2]

Resulting properties depend on the construction materials, fibre geometry, lay-up thickness, fibre pretensioning and quality of the manufacturing process. That dependence on several parameters makes important to evaluate also the initial properties of the pipes. That is why short-term, static tests were conducted, too.

Besides the experimental procedures, numerical models were developed in order to complement the analysis. Evaluating the reproducibility of the damage mechanisms and the admissible values for several parameters such as fibers elastic stress limit, strain energy release in mode I delamination (G_{Id}) and strain energy release in fibre rupture in mode I (G_{If}) were the main objectives of numerical modeling. It was used a 2D finite element methodology integrating cohesive interface elements with a known softening law developed by M. Moura and J. Gonçalves [3-5]

In this report the experimental and the numerical results achieved will be presented, as well as the main conclusions retrieved from their comparison and analysis. The first two chapters refer to the initial study developed over the state of the art and the current standards defining methodologies for evaluating GRP pipes.

2. State of the Art

Laminated FRP structures assume specific behaviour due, not only to the mechanical properties of their components (strength, elastic modulus, elastic stress limit, etc) but also to the imposed geometry to each ply in the laminate.

Most of reinforcement fibers have better elastic properties than the polymeric matrix. Hence, the global properties of the composite structure appear to depend mostly of the reinforcement properties (fig.2).

However, quantifying those global properties is not as simple as it seems to be. In terms of the initial mechanical performance of the assembled materials, the four main factors governing the fibers contribution are:

1. Basic physical properties of the fibers;
2. Quality of the matrix-fibre interface;
3. Quantity of fibers (V_F);
4. Geometry and fibers orientation.

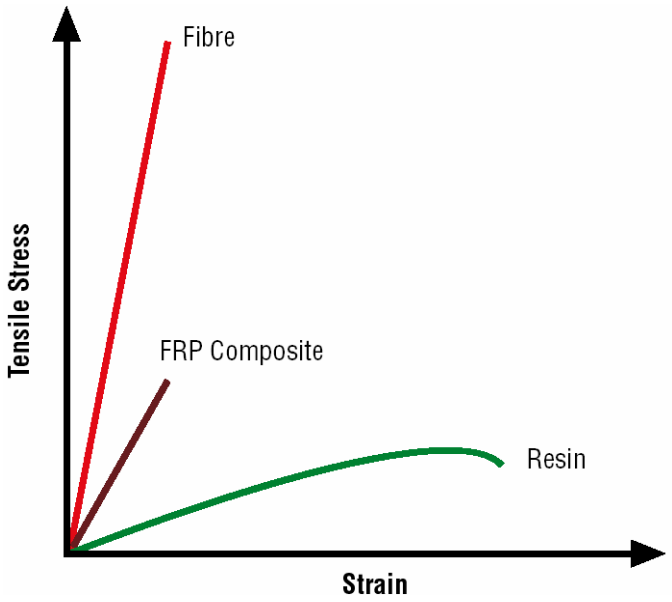

Fig. 2 – Contribution of fibre and resin to the global performance of a FRP [2]

It is, however, relevant to notice that these materials have time-dependent performance, due to creeping, stress relaxation, ageing effects, moisture absorption, temperature, etc.

The compliance and strength of polymeric composite materials may then change over time in high temperature or long service applications. To avoid failures due to unexpected loss of strength after long periods of time, it is imperative that accelerated tests be developed to determine long-term strength properties [6].

When layering up two plies with different fibre orientation angles, +f and - f for instance, the submission to a unidirectional tensile stress field will introduce interlaminar shear stresses, due to the difference between the corresponding strain fields (fig.3). Delamination may then occur.

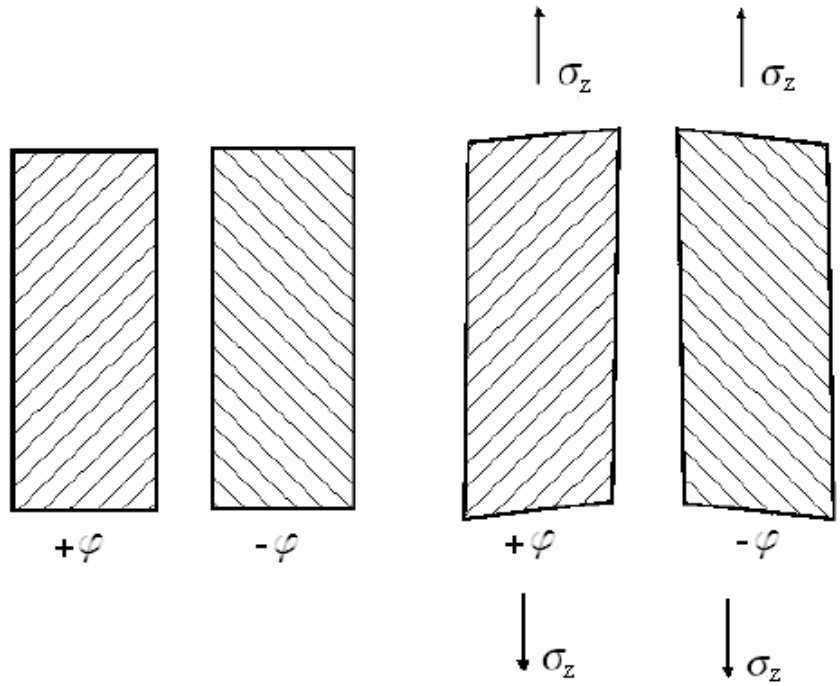

Fig. 3 – Individual behaviour of plies with different fibre orientation angle [7]

Compressive load along the fibres direction may lead to ‘microbuckling’ of fibres that induce local damages (fig.4).

One relevant property of all resins is their ability to support degradation while absorbing water and increasing the specific weight. The way that water affects the fibre/resin interface in each ply is a significant damage inducer mechanism to account with.

A polymer chain having an epoxy backbone is substantially better than many other resin systems at resisting the effects of water. Such systems have shown to confer excellent chemical and water resistance, low water transmission rate and very good mechanical properties to the polymer [2].

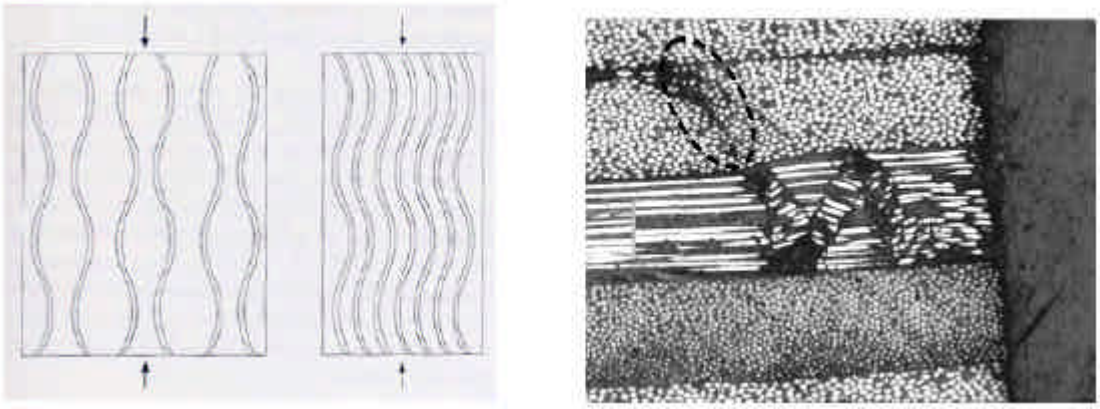

Fig. 4 – 'Microbuckling' of fibres introduced by compressive load [7]

Polyester and epoxy resins show degradation when absorbing water due to the ester groups in the molecular chains (fig.5). A thin polyester laminate maintains only 65% of its interlaminar shear resistance after submersion in water for one year, while an epoxy laminate keeps 90% of its ability [2].

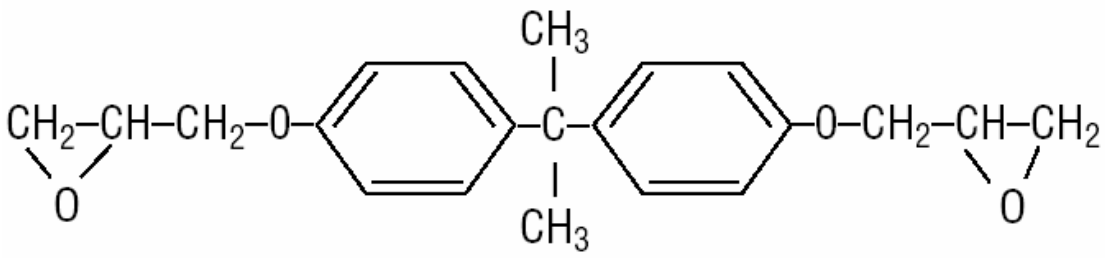

Fig. 5 – Typical molecular structure of an epoxy resin [2]

Figure 6 shows the different behaviour of polyester and epoxy resins when conditioned under water at 100ºC during a few hours. Such environment leads to an acceleration of damage processes.

The leakage failure of a filament-wound fibre-composite vessel, subjected to a combined internal pressure and axial loading, is commonly viewed as a result of progressive damage produced by the coalescence of micro cracks, thus creating a through-thickness crack path prior to complete loss of the tube's structural load-bearing capability. The nature of the problem is very complicated, since it involves the initiation and accumulation of various damage mechanisms in a heterogeneous and anisotropic medium under complex loading conditions [8].

Penetration of water in the wall may change significantly the long-term behaviour of the pipe due to the ageing effects.

In water distribution and sewerage systems the loss of mechanical properties is due to material creeping, plasticity, resin hydrolysis, and chemical attack of the interface fibre/resin by fluid.

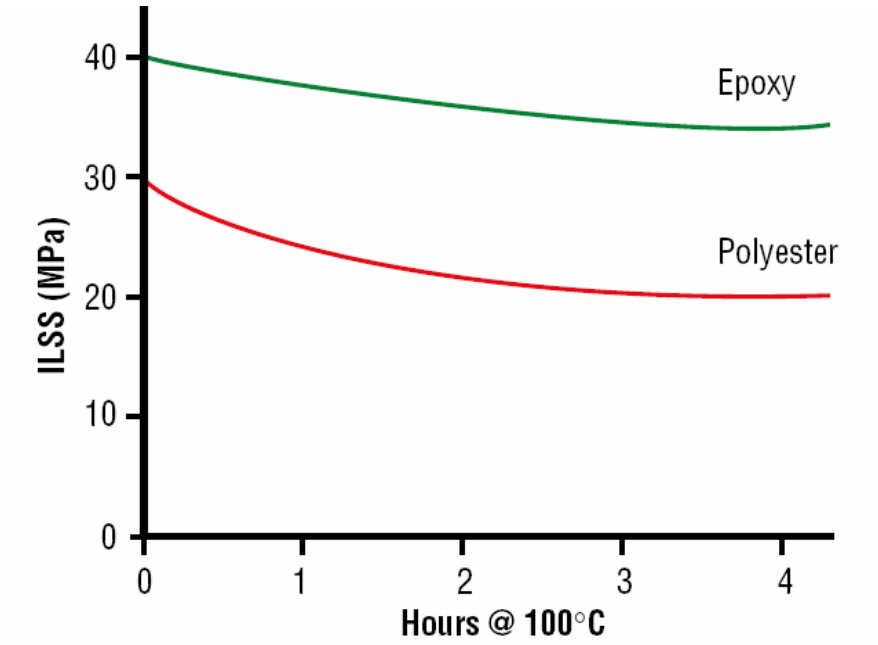

Fig. 6 – Effect of periods of water soak at 100ºC on resin interlaminar shear strength [2]

Concerning to the analytical study, a model that let us simulate the laminate composite structure response, *r*, to an external solicitation, *p*, will have a time dependent generic formulation like

$$r(t) = \Phi[x, p(t)] \qquad 0 < t \leq t \qquad (1)$$

where *x* represents the parameter's vector. The principal methods to achieve an appropriate formulation for *?* operator differ, primarily, in the scale of observation used in the analysis (fig.7) [9].

The damage mechanisms, its effects, the predominance of ones on others, although having been object of several studies, are not well dominated, once there is not, for now, a reliable analytical model, capable of predict long-term properties of these structures.

One local effect of porosity is increasing the stress concentration, which becomes particularly relevant when it occurs in the fibre/resin or ply/ply interface. As so, the

corresponding parameter to account for in a model should be *K* (stress concentration factor). With this philosophy, many other parameters would be considered.

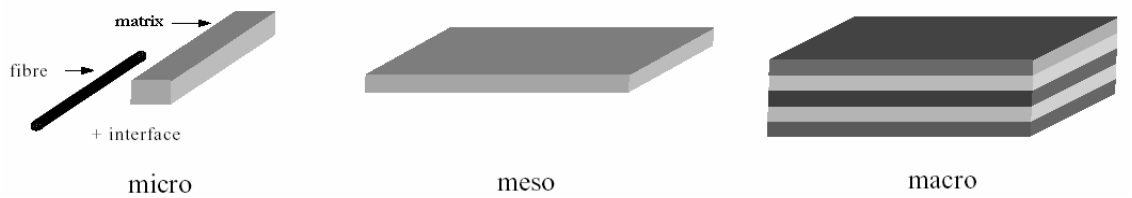

Fig. 7 – Three different scales of observation [9]

In a mesoscopic scale analysis, the essential variables to define the ply state at each time *t*, can be separated in two main groups: the visible and measurable variables (total strain *e*, temperature *T*) and internal variables (microstructure, damage effects).

Total strain *e* depends on its elastic, e^e, and inelastic, e^{in}, components which can be calculated from the Clausius-Duhem's inequation relating to the density of free energy at each moment [10], where e^{ve} and e^{vp} are the viscoelastic and the viscoplastic components.

$$e = e^e + e^{in} = e^e + e^{ve} + e^p + e^{vp} \tag{2}$$

One reasonable approach shall be the one that includes only the relevant parameters (physical, material, environmental) and conducts to a better simulation of real service conditions. So, the environmental conditions and the way they influence and degrade the structural properties are main fields for future research and modelling.

Computational demanding of the model is another characteristic to account for.

Fabrice Richard and D. Perreux [9] developed an analytical model based on thermodynamics of irreversible processes in which inelastic strains should be determined by dissipative energy calculus.

The main problem associated to this conception, is in determination of the mathematical formulation of energetic potentials and, on the other side, on its measurement, once a relevant portion of the energy dissipation results in heat transfer.

Another theoretical model, based on Lekhnitskii's anisotropic elasticity theory, developed by C. S. Chouchaoui e O. O. Ochoa [11], with no inclusion of damage

phenomena, establish constitutive equations for different cases of load (traction, torsion, flexure, pressure), obeying to the restraints of each problem and to the fundamentals of the continuum strains and stresses between plies.

Most of the times, failure by leakage in a laminate is seen as result of coalescence of micro-cracks [8] which propitiate damage progression.

Complementarily, one can say that delaminating, transverse or longitudinal (parallel to fibers direction) cracking are the main damage mechanisms that may lead to long-term loss of structural integrity and are influenced by ageing effects depending on environmental conditions.

The analytical approach by macro structural models introduces some simplifications but one must always attempt to the non-linearities introduced by damage phenomena and other factor that shall not be dismissed. Different mechanical behaviour of a single ply when isolated or integrated (fig.8) denotes the necessity of accounting the differences between different model scales.

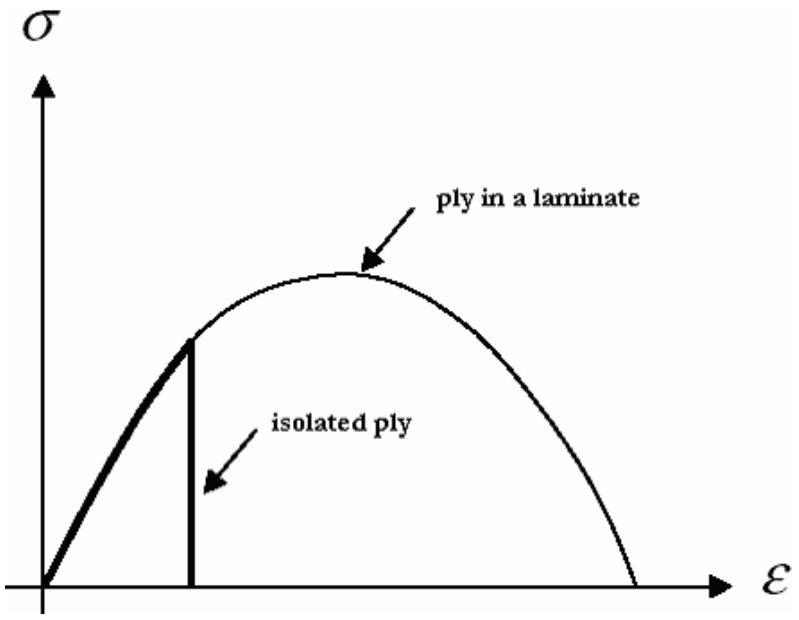

Fig. 8 – Different behaviour of a single ply (isolated or integrated) [9]

Once more, the main concern when modeling composite structures is the correct choice of the parameters to include in the governing equations so that one can satisfactory simulate elasticity, viscoelasticity, plasticity and/or viscoplasticity, damage mechanisms as well as every important phenomena occurring during long-term service conditions.

Experimental procedures and mechanical tests are essential to validate any theoretical model developed. They are also determinant to define the parameters that are relevant to use in the predictive model.

Within the different loading possibilities one must choose those which propitiate plasticity phenomena, micro-cracking, delaminating, as far as possible sequentially sorted so that one can associate each one to the corresponding inducing mechanism.

For instance, increasing progressively the amplitude of a dynamic loading, with intercalary measurements of elastic modulus is a promising test method to evaluate degradation in composite structures.

Certainly is also interesting considering effective properties as input parameters in a model that include damage mechanisms. That is the main focus of a study conducted by L. Parnas and N. Katrici [12] and may consist in relevant simplifications of complex analytical approaches.

One of the goals of the experimental procedures conducted by F. Richard and D. Perreux [9], I. Ghorbel and P. Spiteri [13] among others is the measurement of elastic properties degradation factors. These factors are introduced in the model as parameters such as D_1, D_2, D_3, …, and can be evaluated during progressive loading assays. Next expression shows an example of measurement of elastic modulus degradation:

$$D_i = -\frac{\Delta E_i}{E_i} \tag{3}$$

The failure times of similar test specimens, mainly in creep tests, typically are quite disperse what is due to material variability originated in the manufacturing process [14].

H. Toutanji and S. Dempsey [15] developed formulations including damage mechanisms that are potential tools to analyse the behaviour of such structures as those filament-wounded subjected to different combined load conditions.

N. Tarakçioglu and A. Akdemir [16] analysed experimentally the superficial crack propagation in test specimens with different orientation angles of fibres, showing that the theoretical model based on equations of Newman-Raju of fracture mechanics is inefficient when changing the fibres orientation.

This example reinforces some ideas:

- The analytical models shall be adapted to the case-study or, ideally, sufficiently robust and reliable to comprehend a generalized applicability;
- When using theoretical approaches that don't consider environmental effects, or initial defects, the validation tests shall have a controlled environment so that one can guarantee that scatters in results are only due to variability of material properties;
- Omitting damage factors will conduct to improper modeling once their effects seem not to be negligible;
- Supporting the model in short-term tests may introduce some errors by ignoring the damage mechanisms that may only initiate after several thousands hours in operating conditions.

Hence, in order to improve the knowledge on GRP pipes' behaviour, mechanical tests with different loading configurations shall be developed, as well as methods for evaluation of each parameter's relevance. Based on this experience, test procedures may be profitably updated. Analytical and/or numerical models may also be created in a more reliable way, simulating short and long-term behaviour of GRP pipes.

3. Standards Analysis

The existing European test methods for prediction of long-term behaviour of GRP pipes have been prepared by CEN/TC155/WG14, following the work done by ISO/TC138/SC6, during more than 20 years [17].

In this section will be presented, beyond the basic study of the current European Standards in GRP pipes, some of the procedures pointed to be possible targets of important changes or updates, very soon.

The standards analyzed are related to the mechanical testing procedures under ring deflection condition and the last one, EN 705:1994 [18], describes the predictive extrapolation methods to use complimentarily.

EN 1225 – Determination of the creep factor under wet conditions and calculation of the long-term specific ring stiffness

Based on ISO/CD 10468, this standard specifies a method for determining by extrapolation[1] both the long-term specific ring stiffness and the creep factor for glass-reinforced thermosetting plastics (GRP) pipes under wet conditions.

Thus, the principle is to compress vertically a cut length of pipe to a specified deflection, maintaining the load constant and measuring vertical deflections at intervals of time.

The test apparatus is to be submerged.

It is then expected to have increasingly deflection levels during the test duration by way of a physical process called creeping of materials. The time dependence of this phenomenon (usually a long-term based property) justifies the extrapolation methods.

[1] extrapolation methods should agree with EN705, which is referred for that purposes

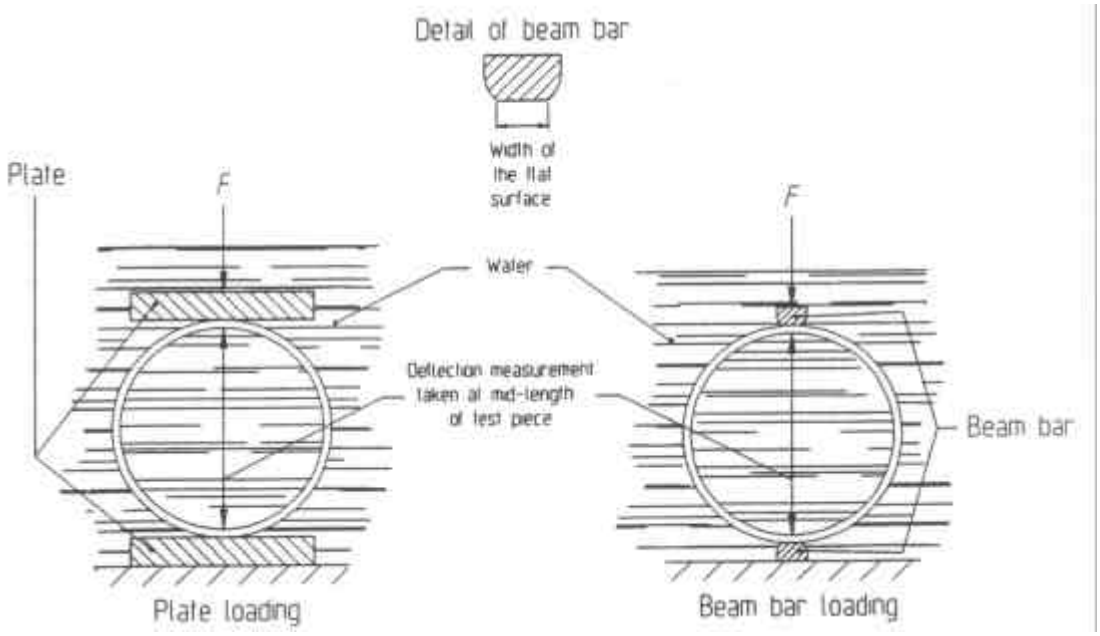

Fig. 9 - Schematic diagram of the test arrangement [19]

- Definitions

Speci.fic Ring Stiffness: A physical characteristic of the pipe which is a measure of the resistance to ring deflection under external load.

This mechanical property of a pipe is defined by the following expression:

$$S = \frac{E\,I}{d_m^3} \qquad (4)$$

where

E is the apparent modulus of elasticity;

I is the moment of inertia in the longitudinal direction per meter length

d_m is the mean diameter of the pipe

Deflection Coefficient: A dimensionless factor which takes into account the theory of second order. It is given by the following equation:

$$f = \left[1860 + \left(2500 \times \frac{y_{x,1,wet}}{d_m}\right)\right] \times 10^{-5} \qquad (5)$$

where

$y_{x,1,wet}$ is the extrapolated long-term vertical deflection (x years, reference position 1, wet conditions.

d_m is the mean diameter of the pipe.

- Procedure

Eventual previous conditioning of test pieces shall be based in the referring standard(s) and the following procedure must be conducted at the specified temperature, too.

The initial specific ring stiffness[2] must be accounted for a reference position (two reference longitudinal lines drawn in the specimen) in order to estimate the load, *F*, required to compress the test piece to between 98.0% and 98.5% of its mean diameter.

Placing the test piece in the apparatus with the pair of diametrically opposed reference lines in contact with the upper and lower bars (or plates), it must be ensured that the contact between the test piece and each beam bar is as uniform as possible and that the bars are not tilted laterally.

Charging rate must then be as slow as necessary to obtain the vertical deflection correspondent to de estimated load in 3 min. and this initial deflection recorded.

Fill the container with water to a level such that the test piece is completely submerged.

Maintaining load constant measures of vertical deflection must be taken at intervals at increments of log(time), such that at least three readings are taken for each decade of log(time). Table 1 presents intervals of time in minutes, hours or days

[2] determined in accordance with prEN 1228

which correspond to successive equal increments of 0.1 in log(t_h) where t_h is the time in hours.

Table 1 – Equal increments of log(t_h) and corresponding times [19]

lg t_h	Time min	h	days
0,1	75,5	1,26	0,052
0,2	95,1	1,58	0,066
0,3	120	2,00	0,083
0,4	151	2,51	0,105
0,5	190	3,16	0,132
0,6	239	3,98	0,166
0,7	301	5,01	0,209
0,8	379	6,31	0,263
0,9	477	7,94	0,331
1,0	600	10,0	0,417
1,1	755	12,6	0,525
1,2	951	15,8	0,660
1,3	1197	20,0	0,831
1,4	1507	25,1	1,05
1,5	1897	31,6	1,32
1,6	2389	39,8	1,66
1,7	3007	50,1	2,09
1,8	3786	63,1	2,63
1,9	4766	79,4	3,31
2,0	6000	100	4,17
2,1	7554	126	5,25
2,2	9509	158	6,60
2,3	11972	200	8,31
2,4	15071	251	10,5
2,5	18974	316	13,2

lg t_h	Time min	h	days
2,6	23886	398	16,6
2,7	30071	501	20,9
2,8	37857	631	26,3
2,9	47660	794	33,1
3,0	60000	1000	41,7
3,1	75536	1259	52,5
3,2	95094	1585	66,0
3,3	119716	1995	83,1
3,4	150713	2512	105
3,5	189737	3162	132
3,6	238864	3981	166
3,7	300712	5012	209
3,8	378574	6310	263
3,9	476597	7943	331
4,0	600000	10000	417
4,1	755355	12589	525
4,2	950936	15849	660
4,3	1197157	19953	831
4,4	1507132	25119	1047
4,5	1897367	31623	1318
4,6	2388643	39811	1659
4,7	3007123	50119	2088
4,8	3785744	63096	2629
4,9	4765969	79433	3310
5,0	6000000	100000	4167

Calculation of the long-term specific ring stiffness under wet conditions for position 1 is achieved using the following equation:

$$S_{x,1,wet} = \frac{f \times F}{L \times y_{x,1,wet}} \tag{6}$$

where

f is the deflection coefficient (equation 5)

F is the constant load applied

$y_{x,1,wet}$ is the extrapolated long-term vertical deflection (x years, position 1, wet conditions)

L is the average length of the test piece.

And the wet creep factor, $a_{x,wet}$, calculation must be determined as follows on:

$$a_{x,wet} = \frac{S_{x,1,wet}}{S_{0,1}} \tag{7}$$

- Comments on EN 1225

The water environment imposed in this standard tends to accelerate the damage progression as it also approximates this test to the usual service conditions of these structures (water supply and sewerage). One must attempt the water chemical properties and their stability during the test.

This standard refers to EN 1228:1997 [22] when it comes to the initial ring stiffness of the pipes.

By reporting the definition of preconditioning conditions to the referring standard(s), EN 1225 allows the existence of different procedures among different manufacturers and/or certification testers which eventually act in the same type of market and applications of GRP pipes.

- Related Standards

EN 761 Plastics piping systems. Glass-reinforced thermosetting plastics (GRP) pipes. Determination of the creep factor under dry conditions

EN 1228 Plastics piping systems. Glass-reinforced thermosetting plastics (GRP) pipes. Determination of initial specific ring stiffness

EN 1394 Plastics piping systems. Glass-reinforced thermosetting plastics (GRP) pipes. Determination of the apparent initial circumferential tensile strength

ISO 7685 Plastics piping systems - glass reinforced thermosetting plastics (GRP) pipes – Determination of initial specific ring stiffness.

ISO 14828 Glass-reinforced thermosetting plastics (GRP) pipes - Determination of the long-term specific ring relaxation stiffness under wet conditions and calculation of the wet relaxation factor

ISO 10952 Plastics piping systems - Glass-reinforced thermosetting plastics (GRP) pipes and fittings - Determination of the resistance to chemical attack from the inside of a section in a deflected condition

EN 1226 – Test method to prove the resistance to initial ring deflection

This standard, which is based on ISO/DIS 10466, describes a method for testing the ability of glass-reinforced thermosetting plastics (GRP) pipes to withstand specified levels of initial ring deflection without displaying surface damage and/or structural failure.

Applying diametrically opposed forces (see figure 10), the test tube must be compressed from zero up to the maximum allowable level of deflection. The increment of deflection must include two stages at two different specified levels of two minutes each.

At these two levels, defined by the referring standard(s), the specimen is inspected for surface damage and/or structural failure (first deflection level) and for structural failure (second deflection level).

Many of the test parameters must be set by the referring standards, such like:

- the two deflection limits of the pipe;
- the length of the test pieces;
- the number of test pieces;
- the test temperature;

- the surface(s) to be inspected for surface damage;
- the characteristics of surface damage and structural failure.

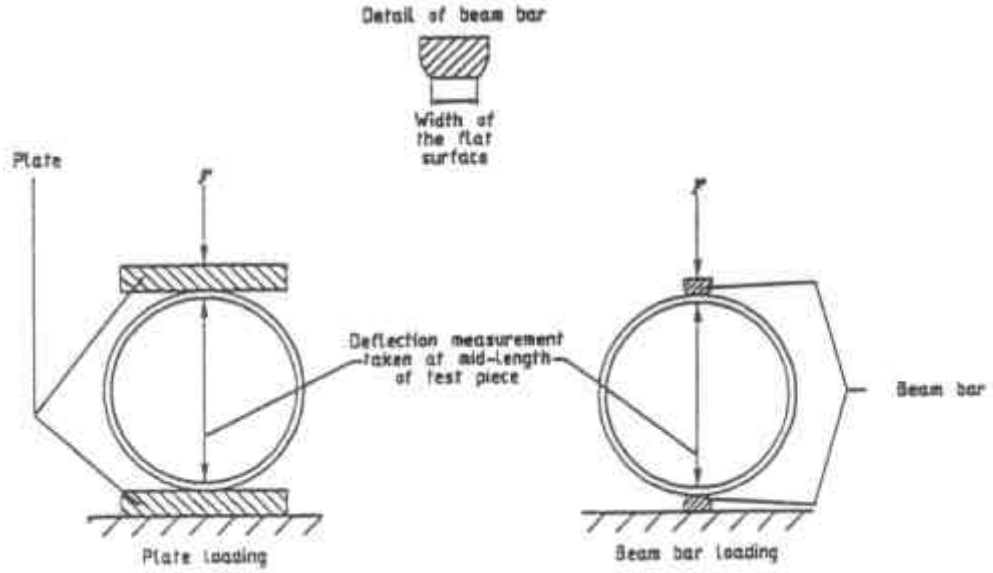

Fig. 10 – Schematic diagram of the test arrangement [20]

- Definitions

Structural Failure: A failure apparent in any of the following forms:

- interlaminar separation;
- tensile failure of the glass fibre reinforcement;
- buckling of the pipe wall;
- if applicable, separation of the thermoplastic liner (coat) from the structural wall.

- Procedure

A temperature shall be specified to conduct the test.

Placing the test piece in the apparatus with the pair of diametrically opposed reference lines in contact with the upper and lower bars (or plates[3]), it must be

[3] limited up to 28% relative deflection measurements in any of the two deflection levels

ensured that the contact between the test piece and each beam bar is as uniform as possible and that the bars are not tilted laterally.

Compressive loading rate must be constant so that the first minimum initial relative vertical deflection is reached to an accuracy of ±2.0 % of the specified value in 2±0.5 min.

First load level (fig. 11) is then recorded and the achieved deflection maintained during another 2±0.5 min in order to proceed the surface inspection.

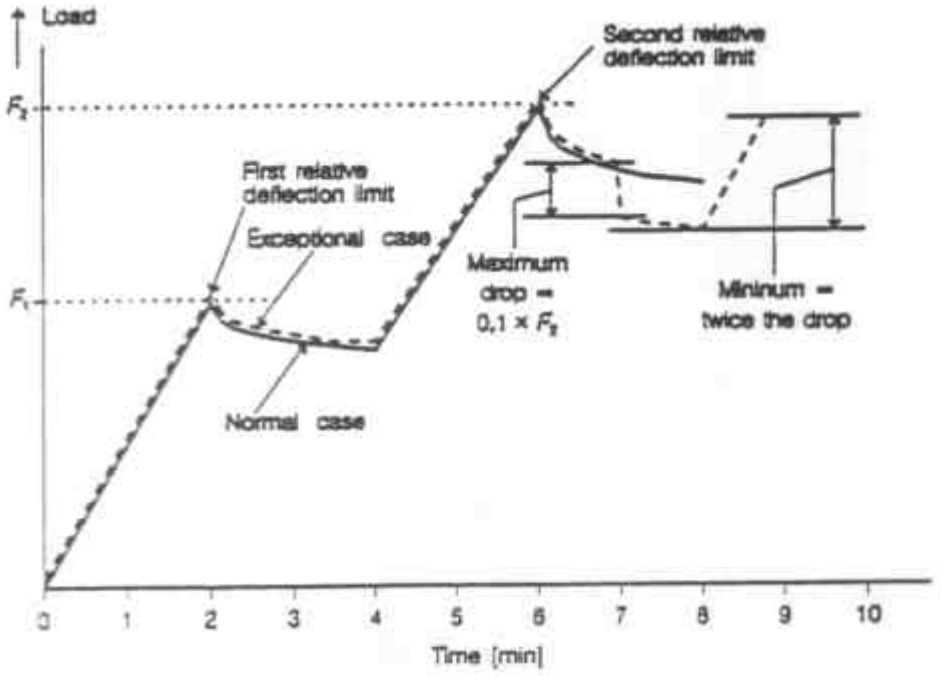

Fig. 11 – Schematic diagram of load versus time [20]

Using either a constant rate of compression or loading, the deflection is increased up to the second minimum initial relative vertical deflection is reached to an accuracy of ±2.0 % of the specified value in 2±0.5 min.

Second load level must be recorded and the achieved deflection maintained during another 2±0.5 min in order to inspect the specimen for structural failure.

At this second stage, load must be continuously recorded so that one can detect one of these phenomena:

- smooth drop of load level;
- instantaneous drop in load of more than 10 %;
- instantaneous drop in load of not more than 10 %.

Considering that failure have occurred or not, depends on the specimen behaviour at second load level stage. In the third case (drop = $0.1F_2$) one must be able to increase load level up to twice of the drop value otherwise failure is registered.

- Comments on EN 1226

The expected drop of load at each deflection level is due to relaxation phenomena during the test time. In these materials, relaxation may induce damage such as fibre and/or interface rupture. The progressive loss of mechanical properties may lead up to loss of structural integrity (delaminating, cracking, etc). That property shall be investigated as far as possible with different testing conditions to evaluate the influence of preconditioning and/or level of deflection.

Although the times set for each period of the test seem to be properly defined, it is relevant to notice (and eventually study) how sensitive these GRP pipes are to the type of charging evolution.

- Related Standards

ISO 10466 Plastics piping systems - glass reinforced thermosetting plastics (GRP) pipes – test method to prove the resistance to initial ring deflection.

EN 1228 / ISO 7685 Plastics piping systems. Glass-reinforced thermosetting plastics (GRP) pipes. Determination of initial specific ring stiffness

EN 1227 – Determination of the long-term ultimate relative ring deflection under wet conditions

Based on ISO/DP 10471.2, this standard specifies a method for determining by extrapolation[4] the long-term ultimate relative ring deflection of glass-reinforced thermosetting plastics (GRP) pipes under wet conditions.

[4] extrapolation methods should be based on EN705, which is referred for that purposes

Using bars or plates[5] to apply diametrically opposed forces, as shown in figure 12, to the test tube, it is expected to obtain increasingly relative deflection states from initial 0% up to rupture (or final deflection if rupture doesn't occur within the maximum time to rupture considered).

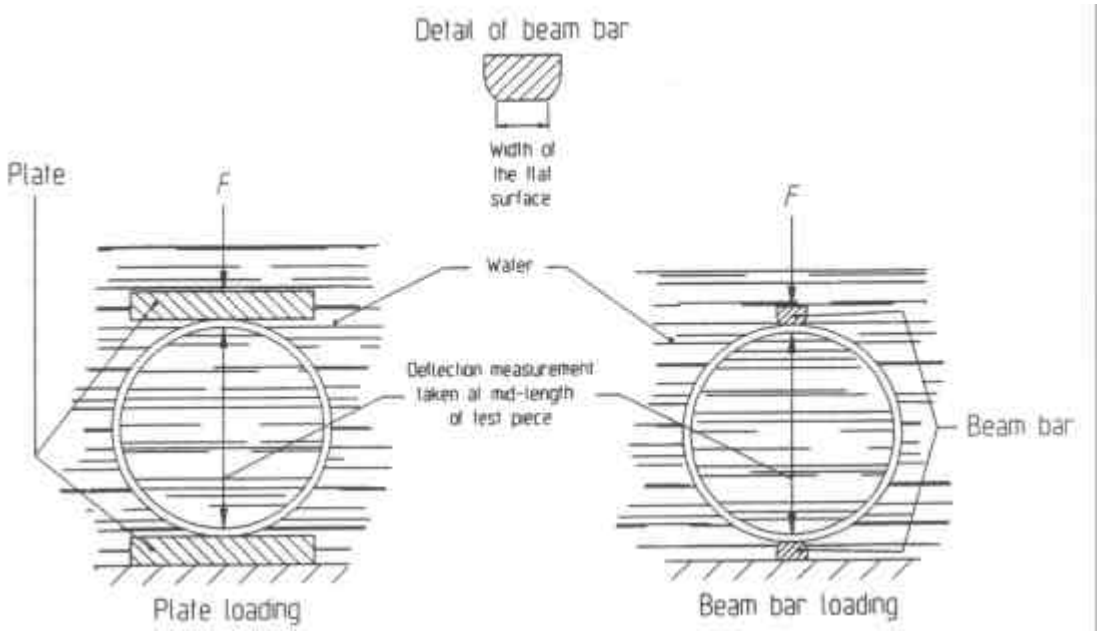

Fig. 12 – Schematic diagram of the test arrangement [21]

- Definitions

Failure: Loss of the structural integrity of the test piece as defined by either of the following conditions:

a) Effective rupture of the pipe wall;
b) Estimated rupture of the pipe wall.

In case b), estimated rupture is derived from the intersection of

1 – the line described by the logarithm of the rate of deflection, log(*r*), versus logarithm of time, log(*t*), as obtained from an individual test (not ruptured yet)

[5] the use of plates is limited up to 28% relative deflection measurements

2 – the line described by the logarithm of the rate of vertical deflection at rupture, $\log(r_u)$, versus logarithm of time, $\log(t_u)$, derived from a series of test pieces.

The equation that describes that intersection is

$$\frac{\log(r)}{\log(t)} = \frac{\log(r_u)}{\log(t_u)} \tag{8}$$

- Procedure

The following procedure must be conducted at the temperature of (23±5)º C.

Placing the test piece in the apparatus[6] with the pair of diametrically opposed reference lines[7] in contact with the upper and lower bars (or plates), it must be ensured that the contact between the test piece and each beam bar is as uniform as possible and that the bars are not tilted laterally.

When filling the container with water to a level such that the test piece is completely submerged, all the apparatus must be prepared for imposing the predetermined load.

Loading rate must be as slow as necessary to obtain the desired static load in 3±0.5 min. and hold that load constant until the test is completed.

From the deflections directly measured, the values of the relative vertical deflections at mid-length of the test piece must be recorded. At least three readings for each decade of logarithm of time, where the time is expressed in hours, must be taken.

The test is completed when either of the following conditions is fulfilled:

a) rupture of the test piece occurs, in which case record the relative vertical deflection and the time to failure;
b) the test has continued for at least 10000 h without rupture and both the following conditions are fulfilled:
    1) pipe wall rupture has been detected in at least 16 other test pieces and;

[6] compressive loading machine, water container, dimensional measuring devices
[7] drawn in the specimen

2) for at least two of those 16 test pieces, the time to failure exceeded 6000 h.

When the conditions in b) have been satisfied, the failure is estimated as described above (see eq.8) and the complementary equations are:

$$\log r = w - z + \log w' \quad (9)$$

where

$$w = a + b \times z + c \times z^2 + d \times z^3 + e \times z^4 \quad (10)$$

$$w' = b + 2 \times c \times z + 3 \times d \times z^2 + 4 \times e \times z^3 \quad (11)$$

$$z = \log t \quad (12)$$

where

a, b, c, d and e are coefficients;

t is the time, in hours.

and

$$\log r_u = f + g \times \log t_u - t_v \times s_u \quad (13)$$

where

f, g are coefficients

t_v is *Student's t*

s_u is the standard deviation of the values of $\log r_u$

The load to deflect the test piece must be calculated so that the resulting time to failure for each individual test stays conformed with the distribution of the times to failure specified in the referring standard.

The long-term ultimate vertical deflection in wet conditions is obtained by extrapolation of the data in accordance with EN 705:1994 [18].

- Comments on EN 1227

The evolution of deformation when a constant static compressive load is imposed is due to the damage phenomena generation and growth during the test time (delaminating, cracking, etc.) with progressive loss of mechanical properties up to loss of structural integrity (creeping).

The water environment is used to accelerate this damage progression as it is also a way of simulating real service conditions.

Although the specification of the exact number of test tubes is submitted to the referring standard(s), the imposed condition of at least 16 valid tests so that further statistical analysis can be validated lead us to a high number of specimens. Here again one have relevant economical aspects to be considered.

It must be assured a neutral and stabilized water (pH of 7±2) environment.

- Related Standards

ISO 10471 Glass-reinforced thermosetting plastics (GRP) pipes - Determination of the long-term ultimate bending strain and the long-term ultimate relative ring deflection under wet conditions

ISO 10952 Plastics piping systems - Glass-reinforced thermosetting plastics (GRP) pipes and fittings - Determination of the resistance to chemical attack from the inside of a section in a deflected condition

EN 1228 – Determination of initial specific ring stiffness

Based on ISO/DIS 7685.2, this standard specifies a method for determining the initial specific ring stiffness of glass-reinforced thermosetting plastics (GRP) pipes.

In either the two methods specified, a cut length of pipe is to be loaded throughout its length to compress it diametrically. In each one of these two methods either plate or beam bar loading (fig.13) can be used in the test apparatus.

The two methods given, A and B, may be used (within the specified deflection) for any diameter. The difference between them is in the parameter controlled during the assay.

After applying the load to achieve the initial deflection specified in the referring standard, either the load is kept constant (method A) or the deflection is (method B).

In the first case (method A) the final deflection is determined. In the second case (method B) the final load being applied is the determined parameter.

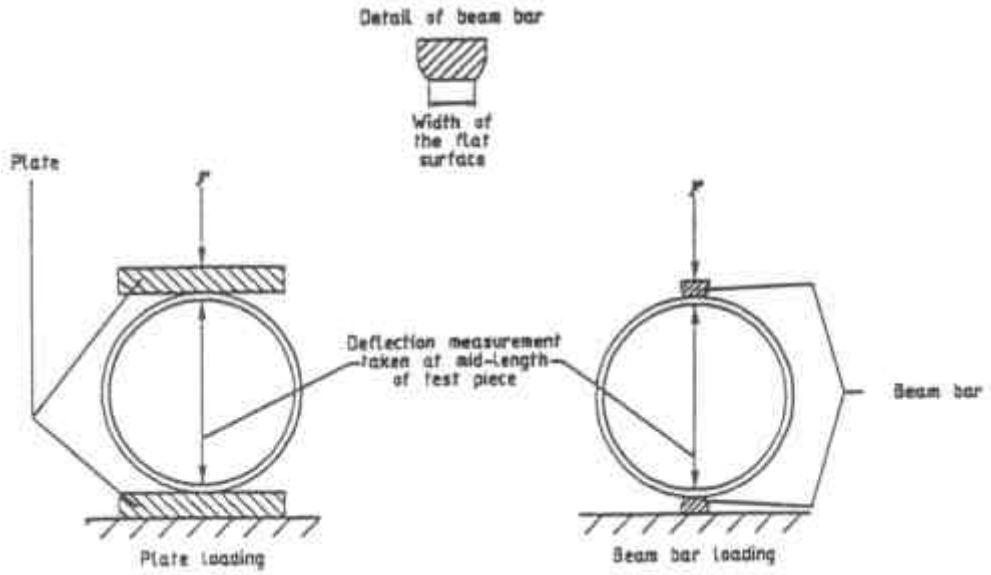

Fig. 13 - Schematic diagram of the apparatus [22]

It is then expected to have increasingly deflection levels during the test duration (method A) or decreasing load (method B) by way of physical processes called creeping and/or relaxation of materials. These are time dependent phenomena and so, the test duration will be determinant in its appearance.

- Definitions

Specific Ring Stiffness: A physical characteristic of the pipe which is a measure of the resistance to ring deflection under external load.

This mechanical property of a pipe is defined by the following expression:

$$S = \frac{E\,I}{d_m^3} \qquad (14)$$

where

E is the apparent modulus of elasticity;

I is the moment of inertia in the longitudinal direction per meter length

d_m is the mean diameter of the pipe

- Procedure

The length of the test pieces should be as specified in the referring standard(s). Pre-conditioning (or not) the test pieces is up to referring standard(s) as well as the choice of the test temperature. Unless otherwise specified, specimens must be stored at the test temperature prior to testing. Straight lines shall be drawn on the inside or the outside along the length of the test piece and repeated at 60º intervals around its circumference, to serve as reference lines.

Placing the test piece in the apparatus with the pair of diametrically opposed reference lines in contact with the upper and lower bars (or plates), it must be ensured that the contact between the test piece and each beam bar is as uniform as possible and that the bars are not tilted laterally.

- ***Method A*** (using constant load):

The compressive load should be applied until a relative deflection between 2.5% and 3.5% is reached in 60 ± 10 seconds under one of the following conditions:

a) at a constant rate;
b) in three increments of load.

The load is then to be kept constant for 2 min and the final deflection measured and registered.

- ***Method B*** (using constant deflection):

The compressive load should be applied until the relative deflection specified in the referring standard is reached in 60 ± 10 seconds under one of the following conditions:

a) at a constant rate;

b) in three increments of load.

The deflection is then to be kept constant for 2 min and the final applied load measured and registered.

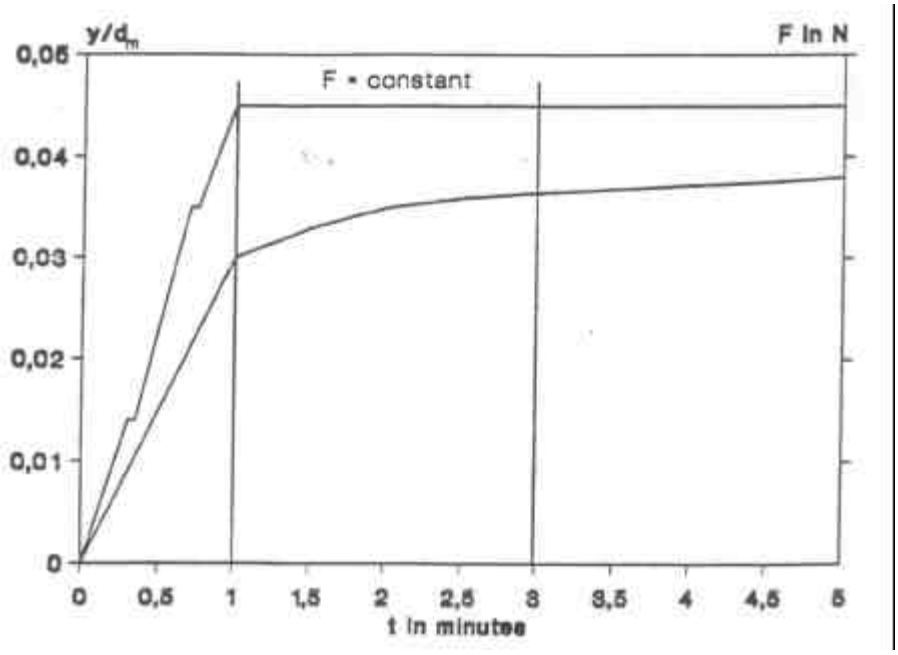

Fig. 14 – Load and corresponding deflection versus time (using loading condition b) [22]

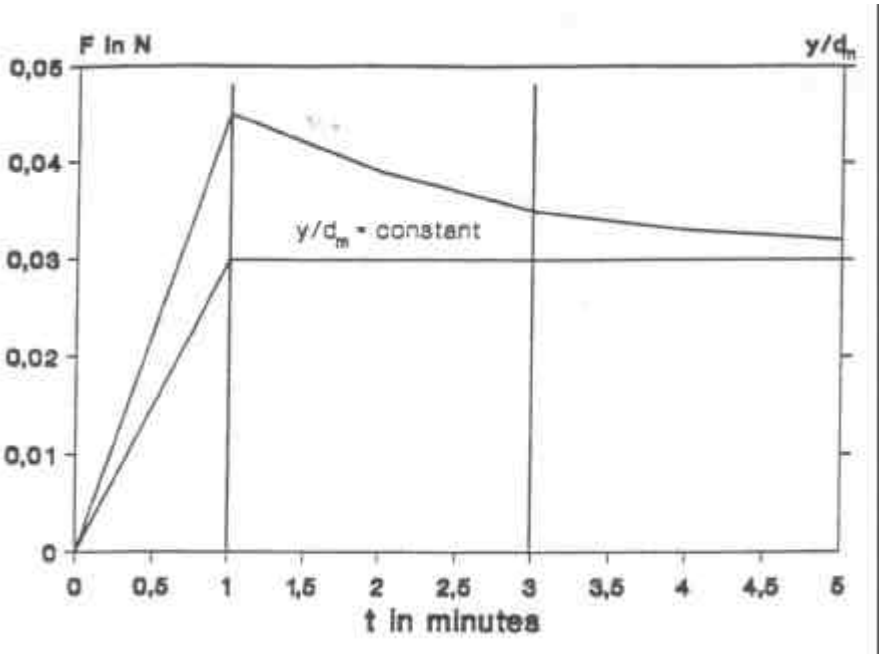

Fig. 15 – Deflection and corresponding load versus time (using loading condition a) [22]

Note: An estimate of the probable compressive load required to achieve a relative deflection can be made from knowledge of the nominal stiffness (SN).

- Comments on EN 1228

This standard describes two different methods that, by defining distinct charging conditions, lead to different processes of mechanical degradation of the specimen to be tested. As so, *method A* uses creeping and *method B* uses stress relaxation to degradate the specimen after reaching the specified level for load and deflection, respectively.

The choice of the correct method to apply, either *A* or *B*, for testing procedures according to EN1228 [22] is, then, to be criteriously done, once different in service applications may demand different residual mechanical properties to be evaluated.

- Related Standards

EN 1394 Plastics piping systems. Glass-reinforced thermosetting plastics (GRP) pipes. Determination of the apparent initial circumferential tensile strength.

ISO 7685 Plastics piping systems - glass reinforced thermosetting plastics (GRP) pipes – determination of initial specific ring stiffness.

EN 705 – Methods for regression analysis and their use

Regression analysis is a very common method for prediction of properties by extrapolation of a series of values obtained by validated tests.

This European Standard, which is based on ISO/TC138/SC6/WG1/N197, describes the procedures intended for analyzing the regression of test data, usually, with respect to time.

The referring standards require estimates to be made of the long-term properties of the pipe for such parameters as circumferential tensile strength, deflection and creep.

Statistical techniques for data analysis of destructive tests were investigated. Many of these simple techniques required the logarithms of the experimental data to

a) be normally distributed;
b) produce a regression line with negative slope;
c) have a sufficiently high regression correlation.

The fulfillment of the last two conditions does not guarantee the satisfaction of the first condition. Further investigation resulted in the adoption of the covariance method to treat those tests which present skewed distributions of data.

The results from non-destructive tests, such as creep or changes in deflection with time, often satisfy the three conditions and so, in that cases, simpler procedures can be used.

So, this European Standard specifies procedures suitable for the analysis of data which, when converted into logarithms of the values, have either a normal or a skewed distribution.

The extrapolation using these techniques typically extends the trend from data gathered over a period of approximately 10000h, to a prediction of the property at 50 years.

- Methods

Data are analyzed for regression using methods based on least squares analysis which can accommodate the incidence of a skew and/or normal distribution and the applicability of a first order or a second order polynomial relationship.

The three methods of analysis used comprise the following:

i. ***Method A***: covariance using a first order relationship;
ii. ***Method B***: least squares with time as the independent variable - first order relationship;
iii. ***Method C***: least squares with time as the independent variable - second order relationship.

Both methods A and B, must be used to fit a straight line of the form

$$y = a + b \times x \tag{15}$$

where:

y is the logarithm (log) of the property being investigated;
a is the intercept on the y axis;
b is the slope;
x is the logarithm (log) of the time, in hours.

i. ***Method A***

For method A, one must primarily calculate the following variables as necessary in accordance with the data suitability, functional relationships, described next.

$$Q_y = \frac{\sum (y_i - Y)^2}{n} \tag{16}$$

$$Q_x = \frac{\sum (x_i - X)^2}{n} \tag{17}$$

$$Q_{xy} = \frac{\sum (x_i - X)(y_i - Y)}{n} \tag{18}$$

where:

Q_y is the sum of the squared residuals parallel to the y axis divided by n

Qx is the sum of the squared residuals parallel to the x axis divided by n

Q_{xy} is the sum of the squared residuals perpendicular to the line, divided by n

Y is the arithmetic mean of the y data, i.e.

$$Y = \frac{\sum y_i}{n} \tag{19}$$

X is the arithmetic mean of the x data, i.e.

$$X = \frac{\sum x_i}{n} \tag{20}$$

x_i, y_i are individual values

n; is the total number of results (pairs of readings for x_i, y_i)

NOTE: If the value of Q_{xy} is greater than zero the slope of the line is positive and if the value of Q_{xy} is less than zero then the slope is negative.

The suitability of data is then evaluated by calculating r^2 and r as follows:

$$r^2 = \frac{Q_{xy}^2}{Q_x \times Q_y} \tag{21}$$

$$r = \sqrt{r^2} = \frac{Q_{xy}}{\sqrt{Q_x \times Q_y}} \tag{22}$$

If the value of r^2 or r is less than the applicable minimum value given in table 2 data should be rejected as not being suitable for further analysis.

To find a and b for the functional relationship line

$$y = a + b \times x \tag{15}$$

it must be set

$$\Gamma = \frac{Q_y}{Q_x} \tag{23}$$

and then a and b calculated using the following equations:

$$b = -\sqrt{\Gamma} \tag{24}$$

$$a = Y - b \times X \tag{25}$$

Table 2 – Minimum values for the squared, r^2, and linear coefficient of correlation, r, for acceptable data from n pairs of data [18]

(n - 2)	Minimum values r^2	Minimum values r	(n - 2)	Minimum values r^2	Minimum values r
11	0,6416	0,8010	23	0,3816	0,6177
12	0,6084	0,7800	24	0,3689	0,6074
13	0,5781	0,7603	25	0,3569	0,5974
14	0,5506	0,7420	30	0,3070	0,5541
15	0,5250	0,7246	35	0,2693	0,5189
16	0,5018	0,7084	40	0,2397	0,4896
17	0,4805	0,6932	45	0,2160	0,4648
18	0,4606	0,6787	50	0,1965	0,4433
19	0,4425	0,6652	60	0,1663	0,4078
20	0,4256	0,6524	70	0,1443	0,3799
21	0,4099	0,6402	80	0,1273	0,3568
22	0,3953	0,6287	90	0,1139	0,3375
			100	0,1031	0,3211

NOTE: In table 1 and elsewhere in this standard, the equations and corresponding values for r^2 and r are given, for convenience of use in conjunction with reference data published elsewhere in terms of only r^2 or r.

When calculated the variances, C, one can check the suitability of the data for extrapolation. Intending to extrapolate the line, it must be considered:

$$T = \frac{b}{\sqrt{va\,riance\ of\ \ slope\ b}} = \frac{b}{\sqrt{C}} \tag{26}$$

Data is to be considered suitable for extrapolation when the absolute value of T, $|T|$, is equal or greater then the applicable value for Student's t, t_v.

ii. ***Method B***

Defining S_y, S_x and S_{xy} as follows

$$S_y = \sum (y_i - Y)^2 \tag{27}$$

$$S_x = \sum (x_i - X)^2 \tag{28}$$

$$S_{xy} = \sum (x_i - X)(y_i - Y) \tag{29}$$

and calculating r^2, r, b and a, using the following equations

$$r^2 = \frac{S_{xy}^2}{S_x \times S_y} \tag{30}$$

$$r = \sqrt{r^2} = \frac{S_{xy}}{\sqrt{S_x \times S_y}} \tag{31}$$

$$b = \frac{S_{xy}}{S_x} \tag{32}$$

$$a = Y - b \times X \tag{33}$$

and the parameter M, which is given by

$$M = \frac{S_x^2}{S_{xy}^2} - \frac{t_v^2 \left(S_x S_y - S_{xy}^2\right)}{(n-2) S_{xy}^2} \tag{34}$$

the evaluation of the suitability of the data is made, considering that:

- if the value of r^2 or r is less than the applicable minimum value given in table 2
- if M is equal to or less than zero

the data should be considered unsuitable for analysis and extrapolation.

iii. ***Method C***

In this case, it is intended to fit a curved (second order) line of the form

$$y = c + d \times x + e \times x^2 \tag{35}$$

Determination of *c*, *d* and *e* is up to the solution system below

$$\sum y_i = c\,n + d \sum x_i + e \sum x_i^2 \tag{37}$$

$$\sum x_i\, y_i = c \sum x_i + d \sum x_i^2 + e \sum x_i^3 \tag{38}$$

$$\sum x_i^2\, y_i = c \sum x_i^2 + d \sum x_i^3 + e \sum x_i^4 \tag{39}$$

and calculating r^2 and r, using the following equations

$$r^2 = \frac{c \sum y_i + d \sum x_i\, y_i + e \sum x_i^2\, y_i - \left[\frac{\left(\sum y_i^2\right)}{n}\right]}{\sum y_i^2 - \left[\frac{\left(\sum y_i^2\right)}{n}\right]} \tag{40}$$

$$r = \sqrt{r^2} \tag{41}$$

and the parameter *M*, which is given by

$$M = \frac{S_x^2}{S_{xy}^2} + \frac{S_{xx}^2}{S_{xxy}^2} - \frac{t_v^2 \left(S_x\, S_y - S_{xy}^2 + S_{xx}\, S_y - S_{xxy}^2\right)}{(n-2) S_y^2} \tag{42}$$

the evaluation of the suitability of the data is made, considering that:

- if the value of r^2 or r is less than the applicable minimum value given in table 2
- if *M* is equal to or less than zero

the data should be considered unsuitable for analysis and extrapolation.

- Comments on EN 705

Changes to this standard have been recently discussed, namely on which concerns to the applicability of linear extrapolations.

It seems properly to note that these three methods are used to fit a straight line or a curved line which is to be considered reliable in terms of its analysis and extrapolation of the material or structural property that is being studied.

Currently, it isn't used to extrapolate parameters such as environment effects, moisture diffusion, damage propagation, etc, i. e., it is not prepared to include or study these parameters by themselves, but in a global observation analysis type.

This isn't necessarily a problem, although it may lead to a not so satisfactory extrapolation of the results, once it can be assumed that the more time it passes, greater is the damage influence, eventually until total loss of integrity.

- Related Standards

ISO/AWI 10928 Plastics piping systems – Glass-reinforced thermosetting plastics (GRP) pipes and fittings – Methods for regression analysis and their use

4. Experimental Program

The two main objectives of the experimental program accomplished within this work were evaluating the applicability of alternative test procedures (being studied in the last few years by different research groups world wide) and supporting further investigation on the relevant parameters governing the short and long-term behaviour of GRP pipes.

The first concern was to evaluate some of the proposed alternative test methods for the determination of long-term properties of glass-reinforced plastic (GRP) pipes, in terms of their applicability rendering a considerable reduction of the time needed for testing with a good level of safety in the long-term estimations when compared to the existing specified ones described before:

EN 1225 Plastics piping systems - Glass-reinforced thermosetting plastics (GRP) pipes - Determination of the creep factor under wet conditions and calculation of the long-term specific ring stiffness
EN 1226 Plastics piping systems - Glass-reinforced thermosetting plastics (GRP) pipes - Test method to prove the resistance to initial ring deflection
EN 1227 Plastics piping systems - Glass-reinforced thermosetting plastics (GRP) pipes - Determination of the long-term ultimate relative ring deflection under wet conditions
EN 1228 Plastics piping systems - Glass-reinforced thermosetting plastics (GRP) pipes - Determination of initial specific ring stiffness

Tests according to the existing standards were also performed in order to create a reference database consisting in the first critical basis for the analysis to develop on the results provided by each of the new approaches.

Different types of GRP pipes from different manufacturers were selected, i.e., some of the test campaigns were performed either on filament wound polyester and epoxy, continuous filament deposition and centrifugal casting pipes.

In the two next sections test procedures are briefly described and the corresponding results are presented, respectively.

Procedures

Several experimental procedures were conducted comprising a ring deflection loading condition. Configurations either with a known deflection rate, constant deflection or with constant load were developed.

"Burn-off" tests were also performed to determine the mass contents of each component/phase and to observe the real layering-up of manufacturer's C specimens. These data were later on used to better understand the pipe's behaviour as well as to define the respective properties in numerical modeling.

A brief description of the testing procedures carried out is presented next.

Initial Ring Stiffness

The initial failure strain tests were performed according to EN1226:1999 which describes a method for testing the ability of glass-reinforced thermosetting plastics (GRP) pipes to withstand specified levels of initial ring deflection without displaying surface damage and/or structural failure [20].

Each of several cut lengths of pipe, supported horizontally, was subjected to a vertical compressive load throughout its length to two specified levels of vertical deflection (fig.16).

The set-up arrangement consists on an upper beam bar connected with the load cell and the moving head, and a lower beam bar. The acquisition system is then nearly disposed (fig.17).

Major axes of beam bars were perpendicular to, and centered on, the direction of application of load. Each beam bar is rigid and its length is equal to the length of the test pieces and the width is (50±5) mm.

Two straight lines, to serve as reference lines, were drawn on the outside along the length of the test piece at 180º to each other. Length of the test piece along each reference line, external diameter and wall thickness, were measured.

The specimens were inspected at the first deflection level for surface damage, and at the second deflection level for structural failure. The test proceeded beyond the second level on all test pieces that haven't failed until then and maximum deflection and load at failure were registered.

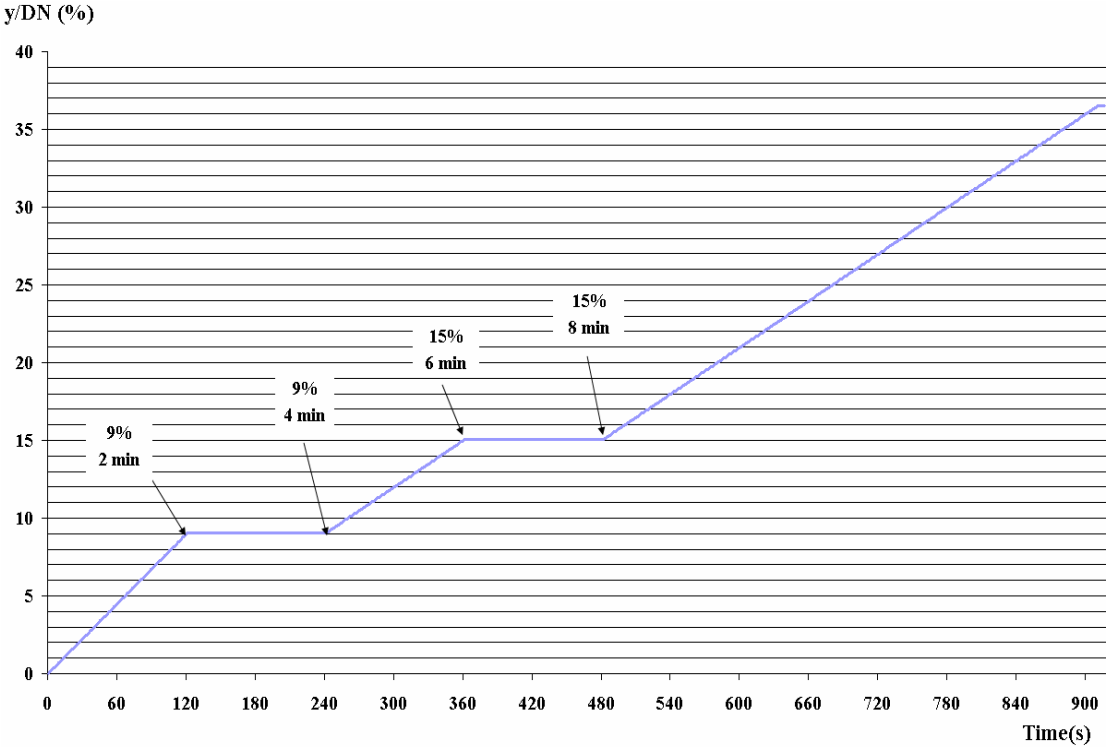

Fig. 16 – Deflection rate and sequence used

Fig. 17 – Compressive loading test apparatus

Creeping In Wet Conditions

The creep tests carried out aimed to determine, by extrapolation, the long-term ultimate relative ring deflection of glass-reinforced plastic (GRP) pipes in wet conditions. These were led according to EN 1227:1997 [21].

Each of several cut lengths of pipe, supported horizontally and submerged, is to be subjected to a vertical load throughout its length. It is intended to use different loads in different test specimens, so that, at the end, one can observe the differences in failure times, such as the deflection increasing during the assays.

The resulting vertical deflections are recorded at given times. The failure times shall be distributed between 0.1h to over 10.000h.

Table 3

	$y_{u,wet,2/DN}$	$y_{u,wet,50/DN}$
SN	%	%
500	40.8	24.4
625	37.8	22.7
1000	32.4	19.4
1250	30.0	18.0
2000	25.7	15.4
2500	23.9	14.3
4000	20.4	12.2
5000	18.9	11.3
8000	16.2	9.7
10000	15.0	9.0

In table 3 one can see the minimum 2-minute initial ring deflections before bore cracking and structural failure, as indicated in EN1796 standard for different values of nominal stiffness (SN).

The parameters $y_{u,wet,2}/d_m$ and $y_{u,wet,50}/d_m$ are the short-term ultimate relative vertical deflection (2 minutes) and the long-term ultimate relative vertical deflection (50 years) under wet conditions, respectively.

Since there are not tabled values for Nominal Stiffnesses higher than 10000N/m^2, therefore $y_{u,wet,50}/d_m$ will be 8.3% and $y_{u,wet,2}/d_m$ will be 13.9%, by extrapolation of the limit curves for S_0=12563[8]. The compressive loads to be applied on the test piece with S_0=12563, in order to obtain a relative vertical deflection equal to the determined

[8] this was the stiffness found in the test specimens to be tested

short-term and long-term ultimate relative vertical deflection, are calculated as follows:

$$F = S_0 \times L \times y_{u,wet,2}/f = 12563\times0.3\times0.139\times0.5\times10^5/[1860 + (2500\times0.139)] \tilde{} \ \underline{\mathbf{11.866\ kN}} \quad (43)$$

$$F = S_0 \times L \times y_{u,wet,50}/f = 12563\times0.3\times0.083\times0.5\times10^5/[1860 + (2500\times0.083)] \tilde{} \ \underline{\mathbf{7.565\ kN}} \quad (44)$$

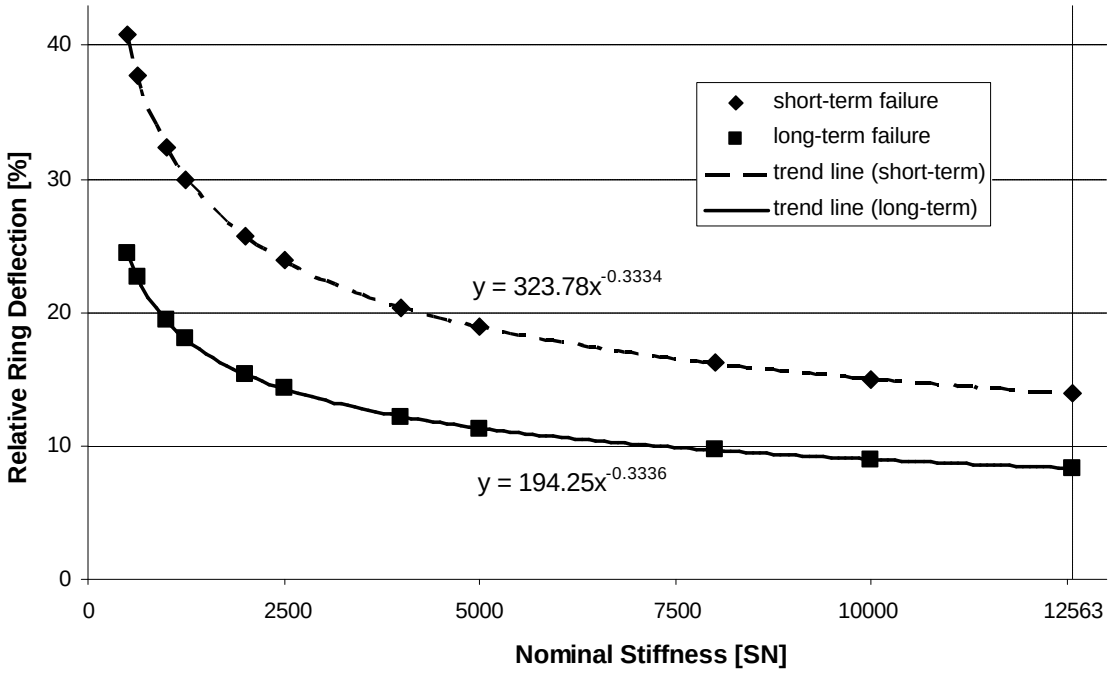

Fig. 18 - Limit curves for bore cracking and structural failure

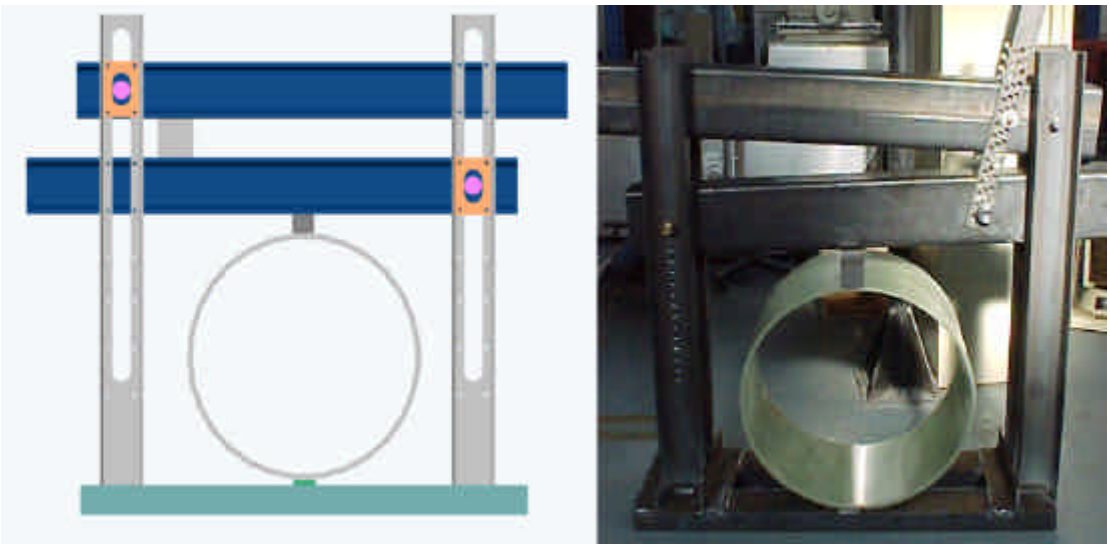

Fig. 19 – Ring deflection machine

Two straight lines, to serve as reference lines, are drawn on the external surface along the length of the test pieces at 180º to each other. Length of the test piece along each reference line, external diameter and wall thickness are measured.

Figure 19 shows a schematic representation of the deflection machine projected for these experimental procedures, and a prototype of that machine.

Stress Relaxation

Relaxation tests, in a ring deflected condition were performed using several specimens of different types of pipes (different manufacturers). These tests were run in accordance with an alternative procedure proposed in a co-normative European research project.

Test pieces used for determination of the stress relaxation in a ring deflection condition, are pre-conditioned under water at 50 ºC for 1000 hours (fig.20).

Fig. 20 – Preconditioning tank

Each of several cut lengths of pipe, supported horizontally, is then to be subjected to a ring deflection condition throughout its length.

The load is measured using load cells during a period of at least 1000 hours[9]. The deflection level to be used in the test is defined based on the expected long-term deflection of each pipe type.

The equipment designed for this purpose is shown in figure 21. It includes a beam under flexure, with two strain gauges, working as a load cell. Those were calibrated so that the relation load *vs* strain is correctly introduced in analysis of the resulting data.

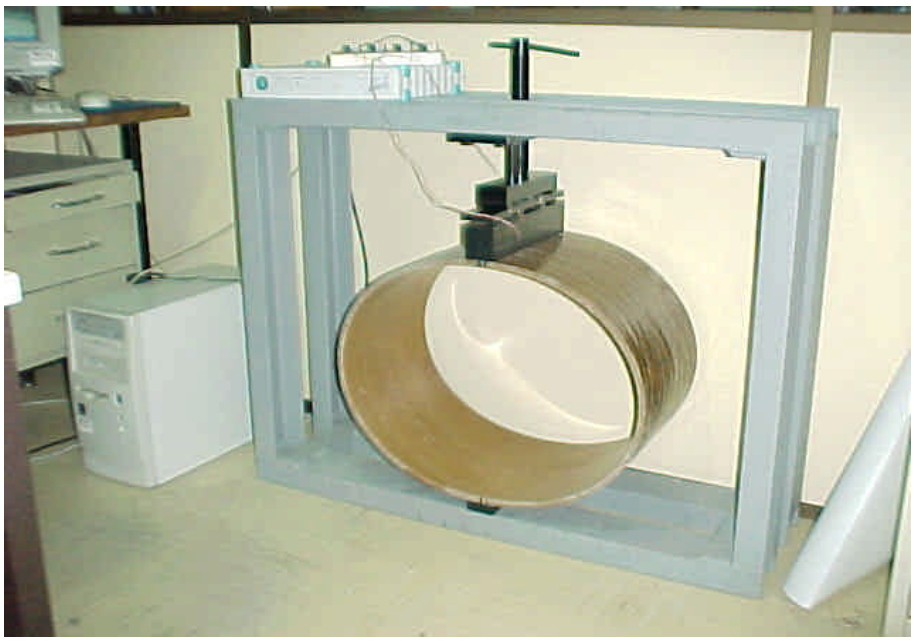

Fig. 21 - Relaxation machine performing a test on a Man. A specimen

Burn-off tests

To assess the mass contents of fibres and resin of the GRP pipes from manufacturer C (because these were the specimens used in larger number for experimental tests and the reference for numerical simulation) burn-off tests according to the portuguese standard NP2216:1988 were conducted.

Five samples accomplishing the specifications of that standard were cut from a spare specimen the mass contents analysis. Several other samples were cut for the purpose of analyzing the geometry of the pipe wall layers. Figure 22 shows one of those samples.

[9] this test period can be extended if a clear shape of the curve *load vs. time* could not be obtained

Fig. 22 – Sample (Manufacturer C, DN500 SN1000) for burn-off tests

The heating system used for degrading and destroy the polymeric phases is presented in figure 23.

Fig. 23 – Burn-off heating system

Results

Initial Ring Stiffness

The machine used for these initial ring stiffness tests was a universal mechanical testing machine INSTRON. The machine is able to achieve and sustain displacement in accordance with the periods specified for the procedures (Figure 16).

Each test piece was a complete ring cut from a pipe type DN500 SN10000 supplied by manufacturer C and made by filament winding and short fibres deposition with 300 mm long (specs 1 to 5).

Table 4 presents geometric measurements initially taken for all five test pieces.

Table 4 – Dimensions of the test specimens

Spec.	DN	SN	L1 [mm]	L2 [mm]	Lmean [mm]	t 1.1 [mm]	t 1.2 [mm]	t 2.1 [mm]	t 2.2 [mm]	t-mean [mm]	Dext [mm]	Dmean [mm]
1	500	10000	300.1	298.6	299.35	11.8	12.1	11.9	12.1	11.96	521.2	509.27
2	500	10000	297.8	298.9	298.35	12.1	12.4	12.9	12.2	12.39	520.7	508.3
3	500	10000	299.0	299.9	299.45	12.1	12.2	12.4	12.0	12.18	521.2	509.0
4	500	10000	298.8	298.8	298.80	11.9	12.3	12.1	12.2	12.11	521.0	508.9
5	500	10000	299.1	299.6	299.35	12.0	12.3	12.3	12.2	12.20	520.7	508.5

Each test piece was compressed at a constant rate so that the first minimum initial relative vertical deflection specified in the referring standard was reached to an accuracy of ±2.0% in 2±0.5 min and the corresponding load F_1 was recorded.

According to EN 1796, for a pipe type SN 10000 the required minimum initial ring deflection before bore cracking occurs in 2 minutes ($y_{2,bore,min}/d_m$) is 9%. So, this deflection was maintained for 2±0.25 min and the corresponding load F_2 recorded, while inspecting the test piece without magnification for surface damage.

Deflection was increased using a constant rate of deflection so that the second minimum initial relative vertical deflection was reached to an accuracy of ±2% of the specified deflection value in 2±0.5 min and recorded the corresponding load F_3.

In accordance with EN 1796, for a pipe type SN 10000 the required minimum initial ring deflection without structural failure in 2 minutes ($y_{2,struct,min}/d_m$) is 15%. This deflection was then maintained for 2±0.25 min and the corresponding load F_4 recorded while inspecting the test piece for eventual structural failure.

Next figures show some instants of the tests conducted for the five test specimens.

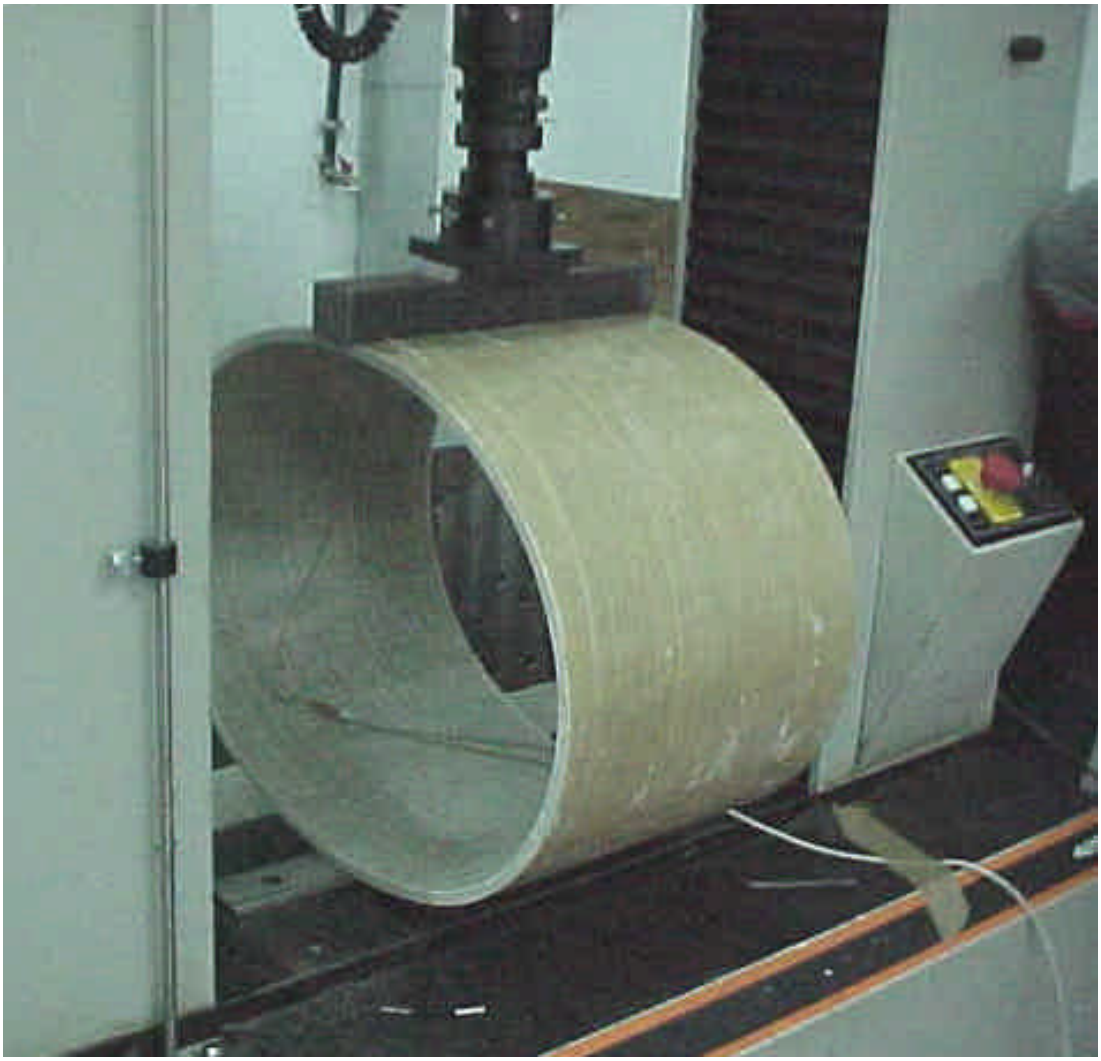

Fig. 24 – Deflecting a test piece (image taken before first specified stage)

The results are displayed in terms of load *versus* time (Fig.28) and strain *versus* time (Fig.29). In both graphics the relative ring deflection curve (y/DN) is also displayed.

Figure 30 shows the *P*-***d*** curves that present two discontinuities, each one, relating to the stages imposed to each specimen during the tests. Observing these results, it may be verified a stress relaxation phenomenon at each stage.

The offset of reaction ring force and strain curves of test piece 1 (after second deflection stage) is due to an initially limitation for a maximum relative deflection of 30% of the testing machine. This limit was then enhanced up to 50%.

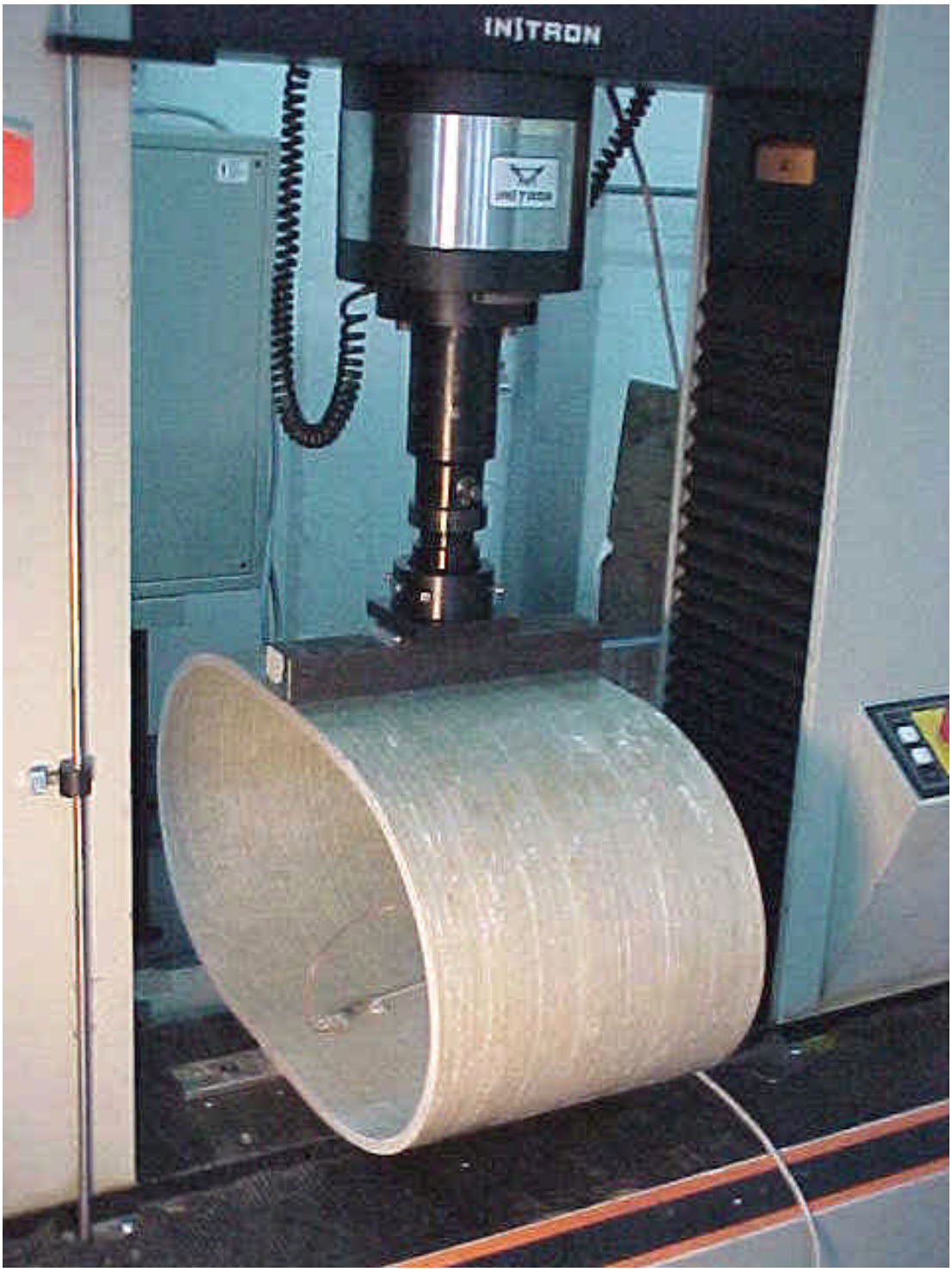

Fig. 25 – Deflecting the test piece (image taken after second deflection stage)

Furthermore, strain results showed in figure 29 are incomplete since strain gauges had failed before structural failure of the pipe wall occurs. So, it was not possible to evaluate the circumferential strain at failure for each test specimen.

Figure 30 relates the reaction ring force with the respective relative ring deflection at each instant of the tests.

Only test piece 5 showed no bore cracking after the first deflection level. It was found that in all tested specimens the bore cracks started appearing at 90º and –90º, relatively to the vertical charging plane, in the outside layer and at 0º and 180º in the inside layer.

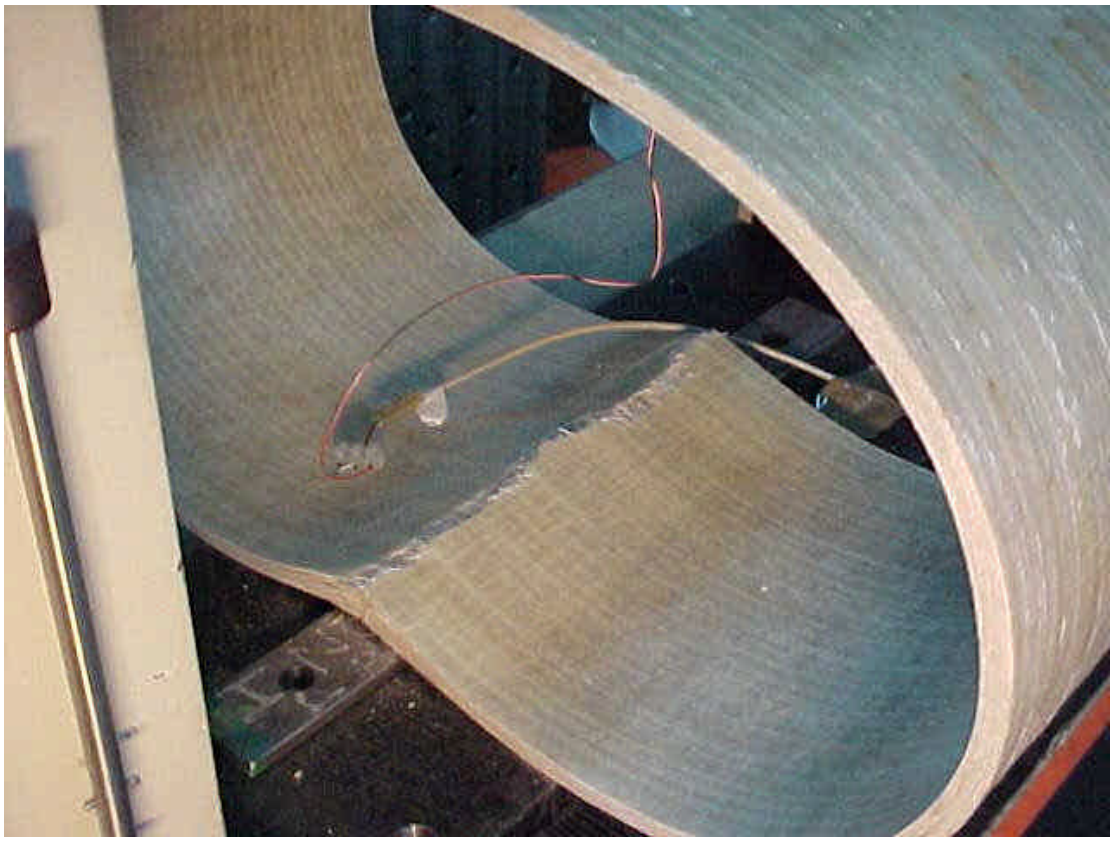

Fig. 26 – After structural failure

Fig. 27 – Detail of the failure zone (transverse cracking and delaminating)

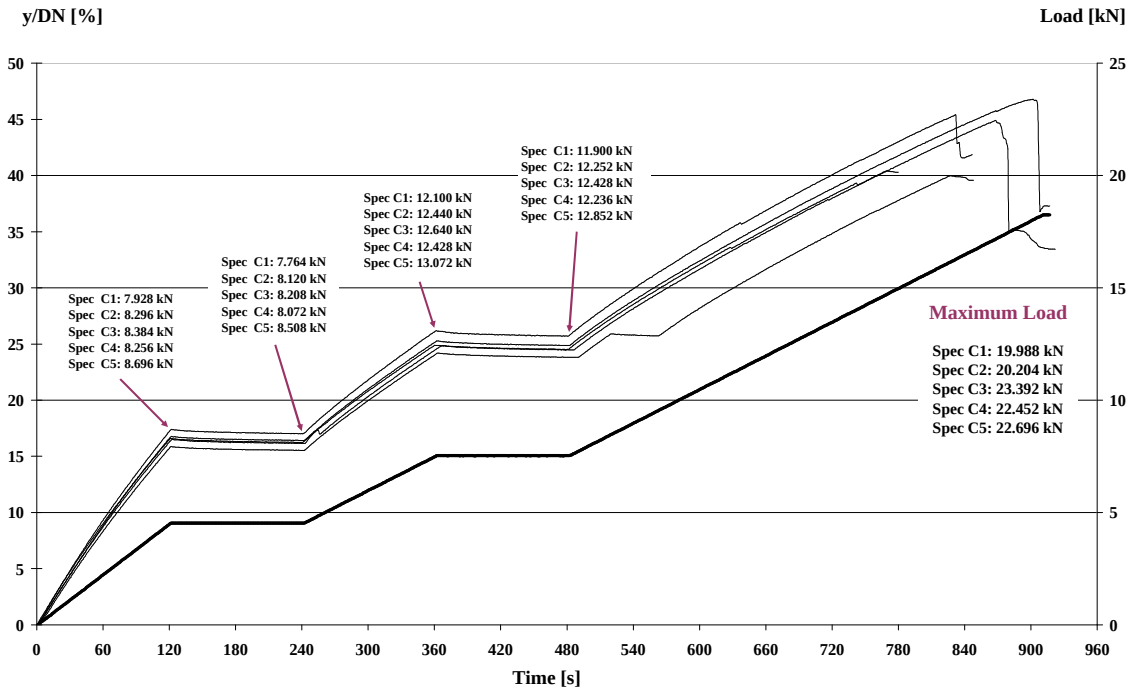

Fig. 28 – Reaction ring force *versus* Time

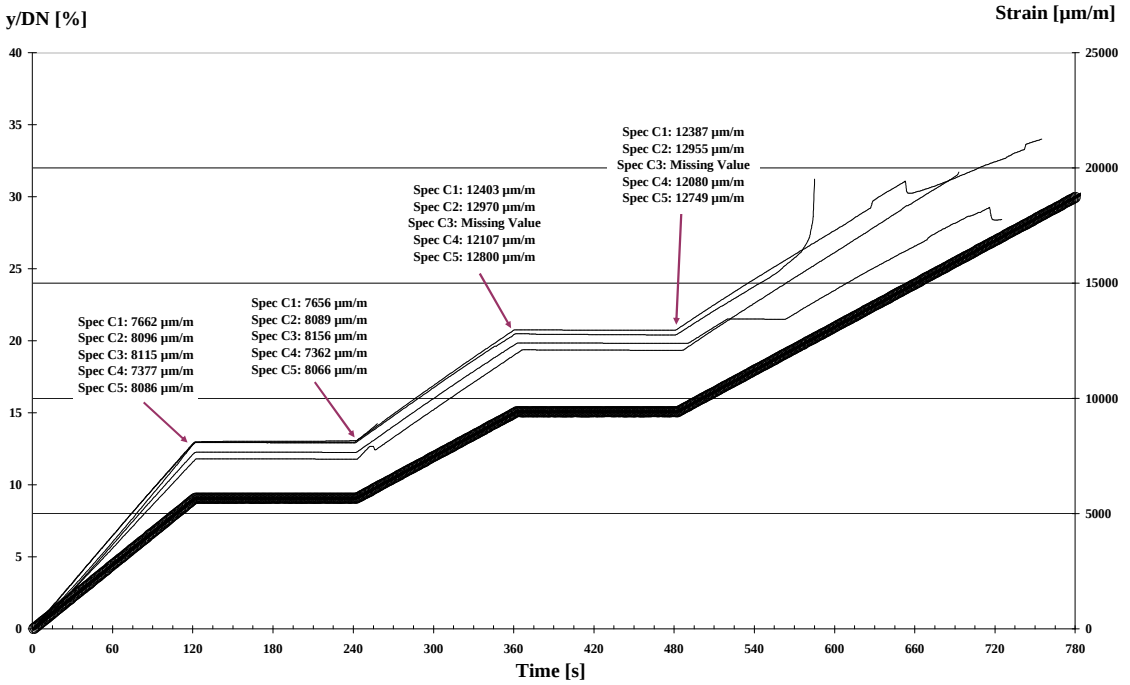

Fig. 29– Strain *versus* Time

The formation of bore cracks is due to high levels of tensile stress. Figure 31 shows outside surface with and without bore cracks (superficial fissures at the inner and/or outer liners).

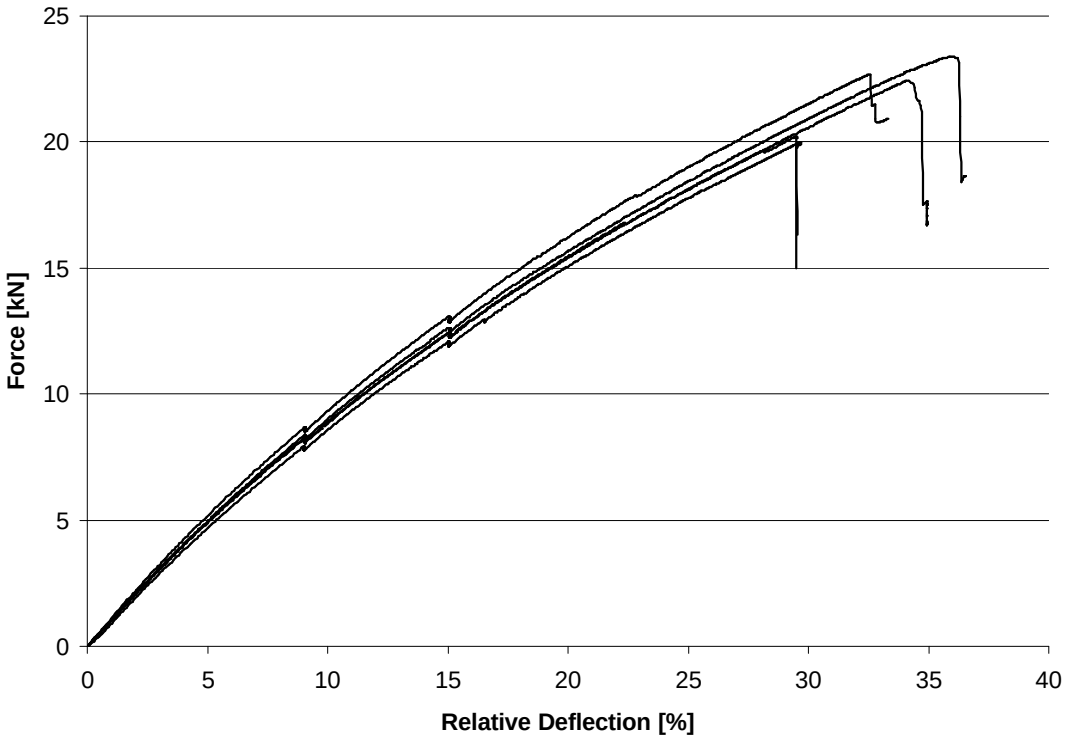

Fig. 30 – Reaction ring force *versus* relative ring deflection (man. C specimens DN500 SN10000)

Fig. 31 – Outside layer with (left) and without (right) bore cracks

Structural failure presents different mechanisms. The formation of buckling, due to high levels of compression stress, is the one verified in test specimens 2 and 5. On test pieces 3 and 4 there was interlaminar separation (delamination) around the charging plane. Figures 32-35 confirm these considerations.

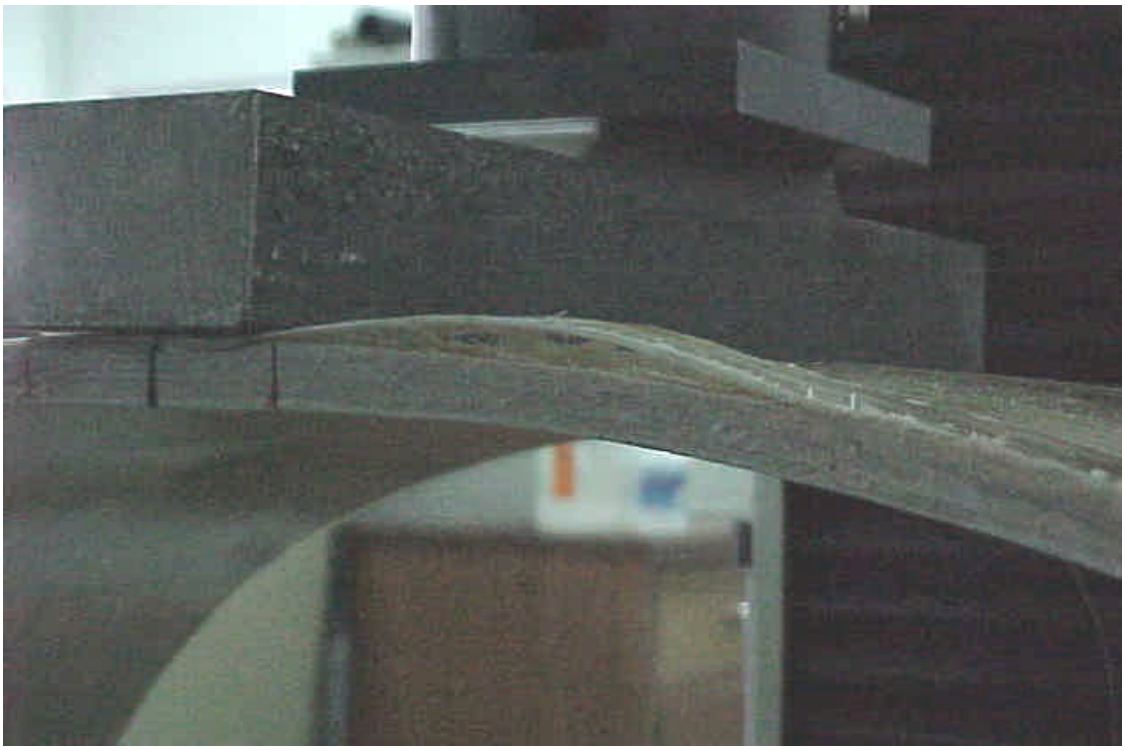

Fig. 32 – Test piece 2. Buckling of pipe wall around upper bar

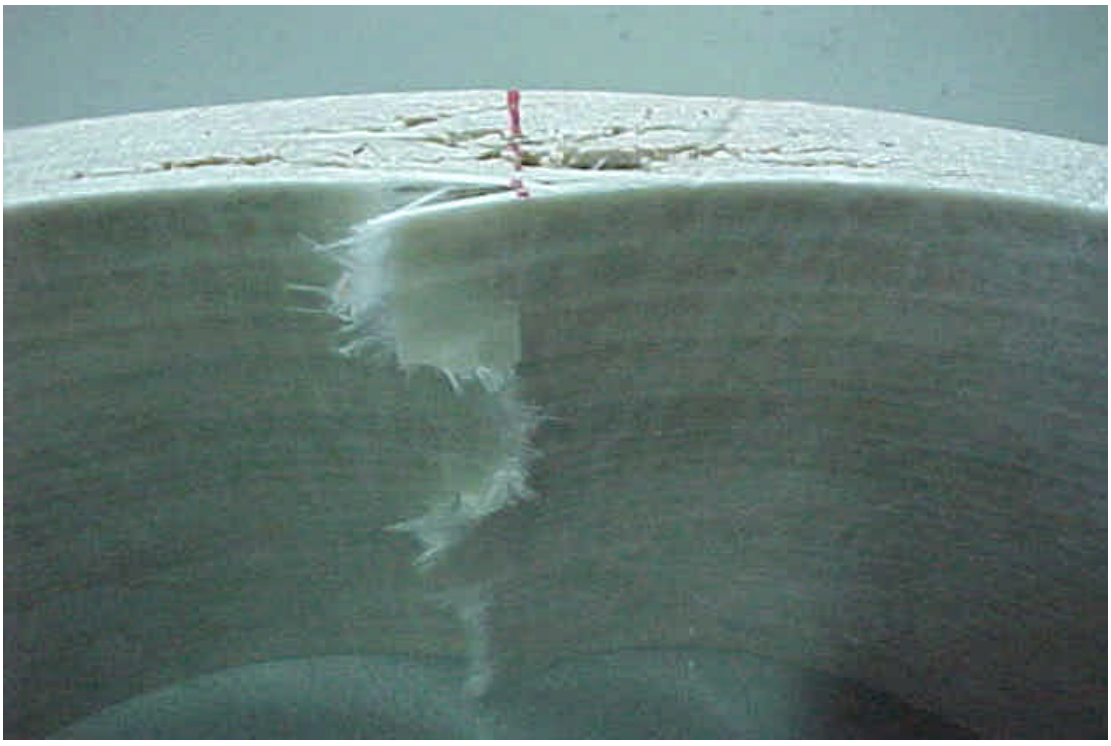

Fig. 33 – Test piece 3. Fibre rupture and delaminating from inner surface

The amount of the drop of reaction ring force during the second deflection stage was determined in absolute (F_3-F_4) and percentage terms [100×(F_3-F_4)/F_3]. It was found that in all five specimens the amount of the drop at the second level was less

than 10%. The increase of load by twice the amount of drop [F_3+2×(F_3-F_4)] was achieved in all five specimens.

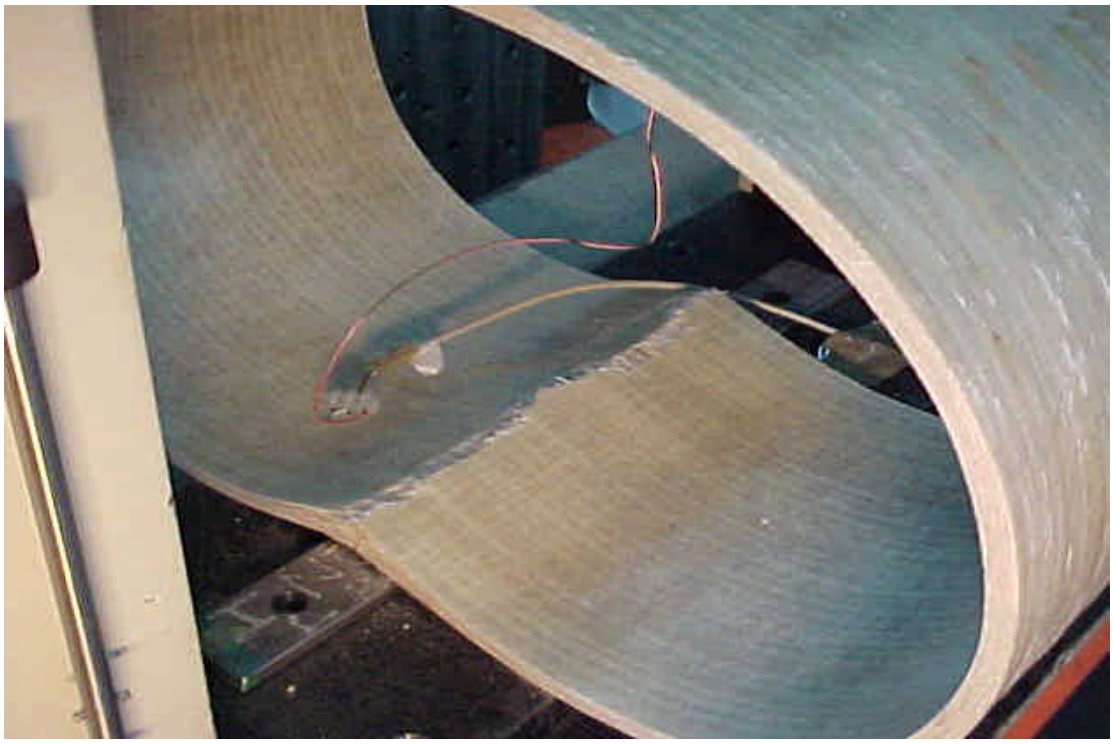

Fig. 34 – Test piece 4. Delamination and fibre rupture along transverse direction of the pipe

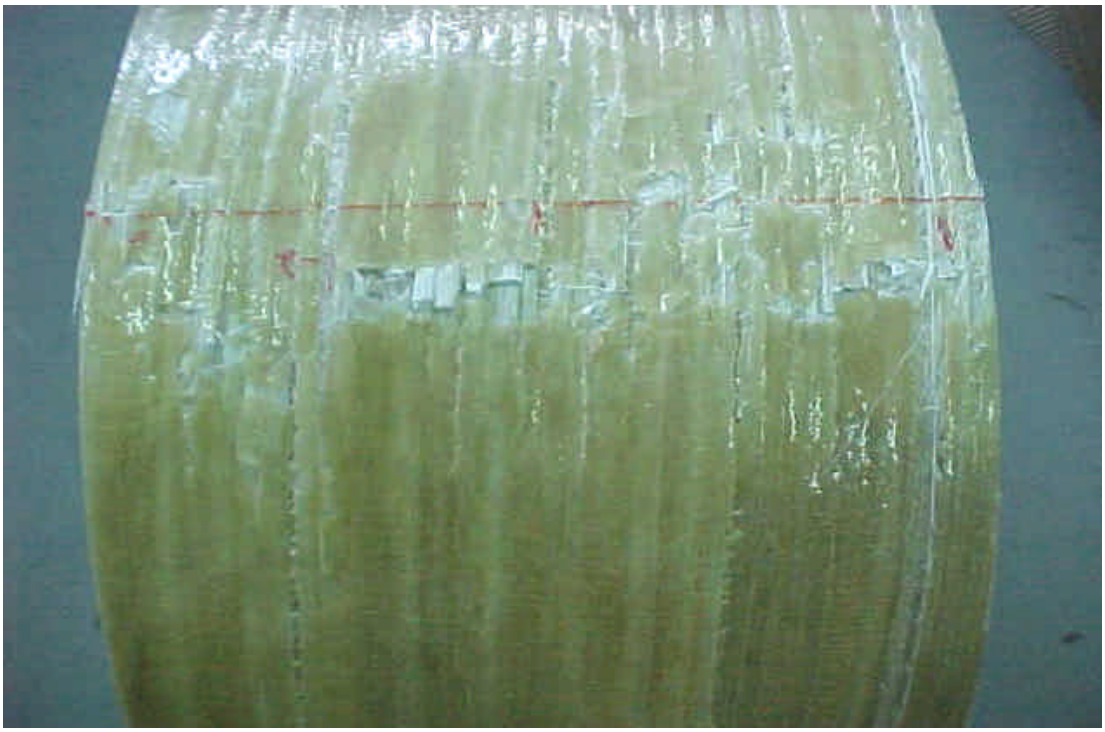

Fig. 35 – Test piece 5. Buckling of pipe wall around upper bar

From the observations one can say that the main damage mechanisms leading to structural failure of GRP pipes[10] under static ring deflection are delamination between plies and rupture of fibres. It seems properly to assume that bore cracks verified at surface have no structural origin and influence, as they appear at inner and outer surfaces where liners with no structural relevance are applied.

The softening process that is presented by all tested specimens (see figure 30) makes one think of the combination of damage phenomena together with the geometric non-linearity that characterize these structures.

Creeping In Wet Conditions

Each test piece was a complete ring cut from a pipe type DN500 SN10000 supplied by manufacturer C and made by filament winding and short fibres deposition, a hybrid process, with 300 mm long (specs 36 to 60).

The evolution of the relative ring deflection during each individual test is represented in the following figure. These curves refer to the 23 valid tests conducted within this campaign and are drawn in a log-log scale.

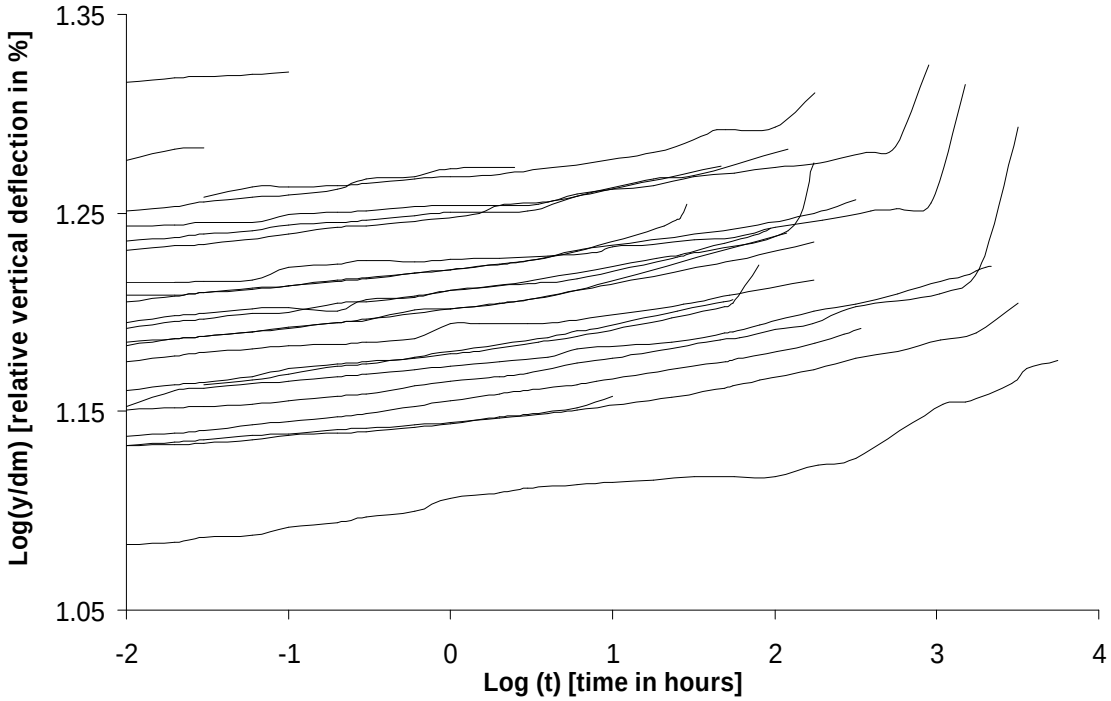

Fig. 36 - Relative ring deflections (specimens DN500 SN10000 from manufacturer C)

[10] the five specimens tested were made by filament winding and short fibre deposition. One may not assume that all types of GRP pipes behave in the same way.

One should notice that, by being in a tenth based logarithm ($\log_{10}t$), failure times within the third positive decade ($3<\log_{10}t<4$) are relatively near[11] of the equivalent time representation for 50 years ($\log_{10}438300$˜ 5.642). This is still the main reason for requiring long-term tests of 10000h long by existing standard.

Limitations of the test arrangement, namely the impossibility of registering online the increasing deflection (measurements were made only at intervals of time), explains the lack of data at the end stages of many of the individual curves presented.

Every specimens tested presented wall rupture before 10000h test duration ($\log_{10}10000=4$) and the longest assay lasted 5623h. So, there is no necessity of applying complementary equations, defined in EN1227:1997 [21] for the case of a not ruptured test piece.

Table 5 summarize the relevant parameters, measured and output during tests developed. Coefficients *a*, *b*, *c*, *d* and *e* relate to the fourth order polynomial curve that fits each experimental curve (see equation 10), according to EN 1227:1997 [21].

Table 5 - Data output (relevant parameters) for Man. C specimens DN500 SN10000

Man	DN	SN	F [kN]	y_0/dm	y_u/dm	t_u [h]	a	b	c	d	e
C	500	10000	8.842*	0.121	0.150	5623	1.1040	0.0105	-0.0019	-0.0001	0.0004
C	500	10000	10.129*	0.136	0.144	10	1.1438	0.0078	0.0028	0.0023	0.0007
C	500	10000	10.381	0.142	0.167	2163	1.1728	0.0069	0.0008	0.0008	-0.0001
C	500	10000	10.431	0.136	0.160	3162	1.1450	0.0071	0.0010	0.0003	0.0001
C	500	10000	10.644	0.142	0.197	3162	1.1681	0.0146	-0.0041	-0.0018	0.0012
C	500	10000	11.140	0.137	0.156	341	1.1552	0.0109	0.0000	-0.0001	0.0002
C	500	10000	11.411	0.145	0.167	80.5	1.1800	0.0064	-0.0020	0.0023	0.0013
C	500	10000	11.831	0.147	0.162	174	1.1838	0.0082	0.0004	0.0003	0.0001
C	500	10000	12.087	0.150	0.169	174	1.1950	0.0104	0.0013	0.0004	-0.0000
C	500	10000	12.196	0.160	0.181	314	1.2219	0.0087	0.0008	0.0004	0.0000
C	500	10000	12.401	0.146	0.161	55	1.1801	0.0122	0.0012	0.0003	0.0000
C	500	10000	12.401	0.155	0.175	94	1.2106	0.0101	0.0011	0.0006	0.0001
C	500	10000	12.532*	0.164	0.206	1512	1.2299	0.0077	-0.0056	-0.0008	0.0012
C	500	10000	12.693	0.154	0.186	173	1.2038	0.0065	-0.0016	0.0017	0.0012
C	500	10000	12.720	0.172	0.192	120	1.2496	0.0080	0.0028	0.0008	0.0002
C	500	10000	12.831	0.168	0.185	47	1.2420	0.0106	0.0012	0.0005	0.0002
C	500	10000	13.088	0.162	0.180	28.9	1.2214	0.0081	0.0016	0.0028	0.0012
C	500	10000	13.476*	0.175	0.211	892.5	1.2557	0.0073	-0.0031	-0.0003	0.0009
C	500	10000	13.638	0.178	0.187	2.5	1.2720	0.0085	-0.0115	-0.0102	-0.0025
C	500	10000	13.970	0.204	0.206	0.1	1.3987	0.2187	0.2067	0.0852	0.0127
C	500	10000	13.988	0.153	0.174	119.5	1.2016	0.0098	0.0008	0.0008	0.0004
C	500	10000	13.990*	0.181	0.204	178	1.2682	0.0056	0.0017	0.0015	0.0001
C	500	10000	14.420	0.186	0.189	0.03	1.1869	-0.1132	-0.0359	0.0000	0.0000

[11] in the logarithmic scale

* values that could not be totally confirmed

The typical structural damages that can be observed after failure are those documented by the following figures relating to the specimen no. C50.

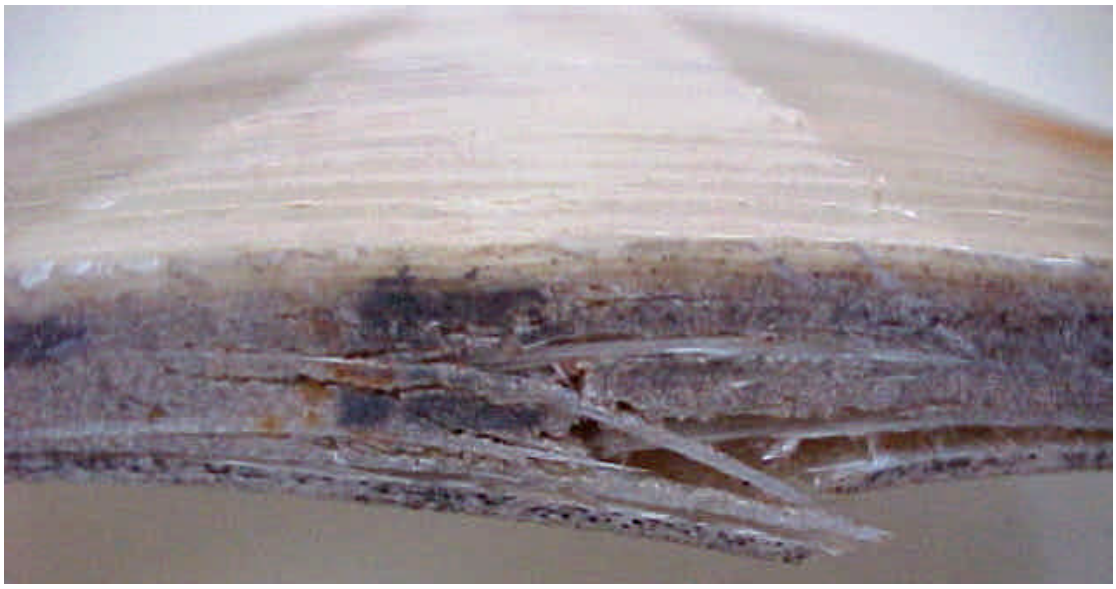

Fig. 37 – Spec. no. C50, delamination at charging zone

Fig. 38 – Spec. no. C50, plies failure from the inside wall

Once these tests were conducted according to EN 1227:1997 [21], data may be compared with other test campaigns led and published by manufacturers, final users

or even research laboratories. Output data obtained by two manufacturers that conducted tests on specimens of manufacturers A and D is then considered.

Next figures show four interesting relationships to analyse after data treatment:

- y_0/dm *vs* F, initial relative ring deflection *versus* ring force
- y_0/dm *vs* t_u, initial relative ring deflection *versus* failure time
- y_u/dm *vs* F, relative ring deflection at failure *versus* ring force
- log(y_u/dm) *vs* log(t_u), relative ring deflection at failure *versus* failure time

All available data, achieved in this work and published by two manufacturers, is integrated so that it may be analyzed in the global perspective of different types of GRP pipes selected for this study.

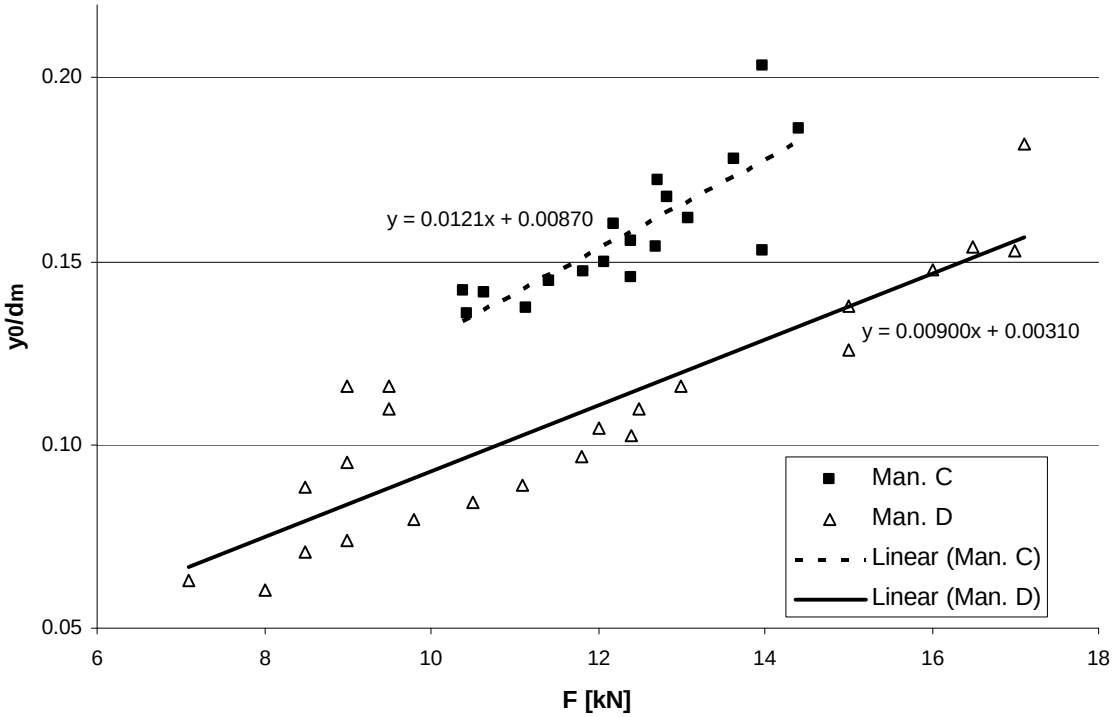

Fig. 39 – Initial relative ring deflection *vs* ring force (man. C and D)

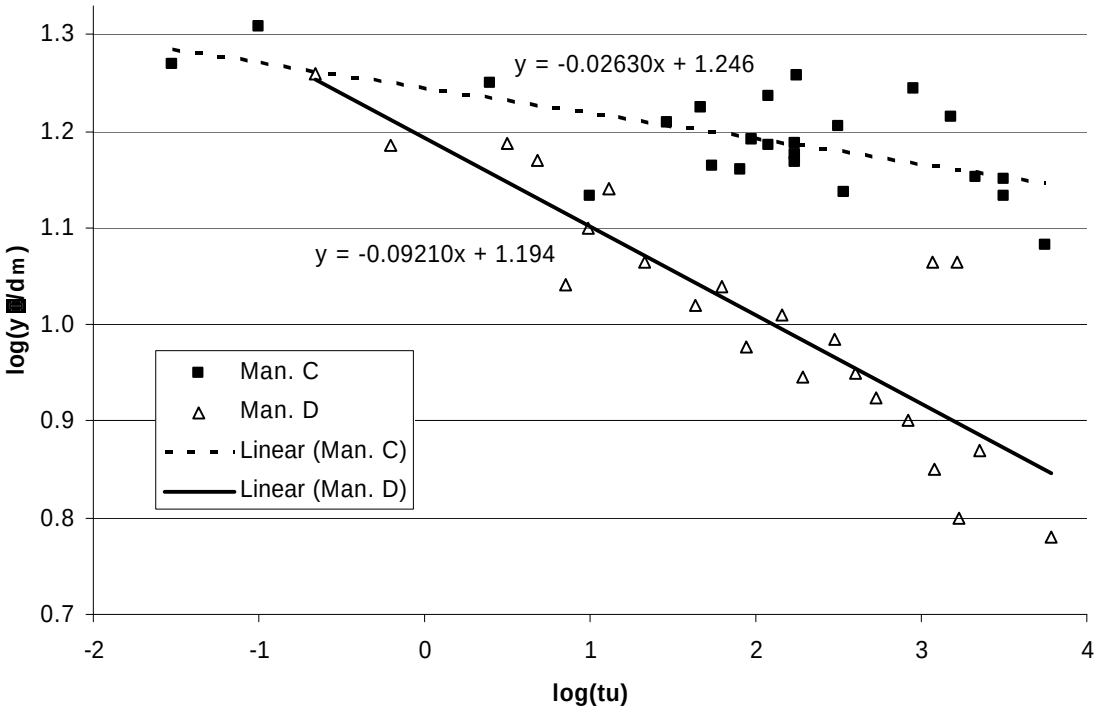

Fig. 40 – Initial relative ring deflection *vs* failure time (log-log) (man. C and D)

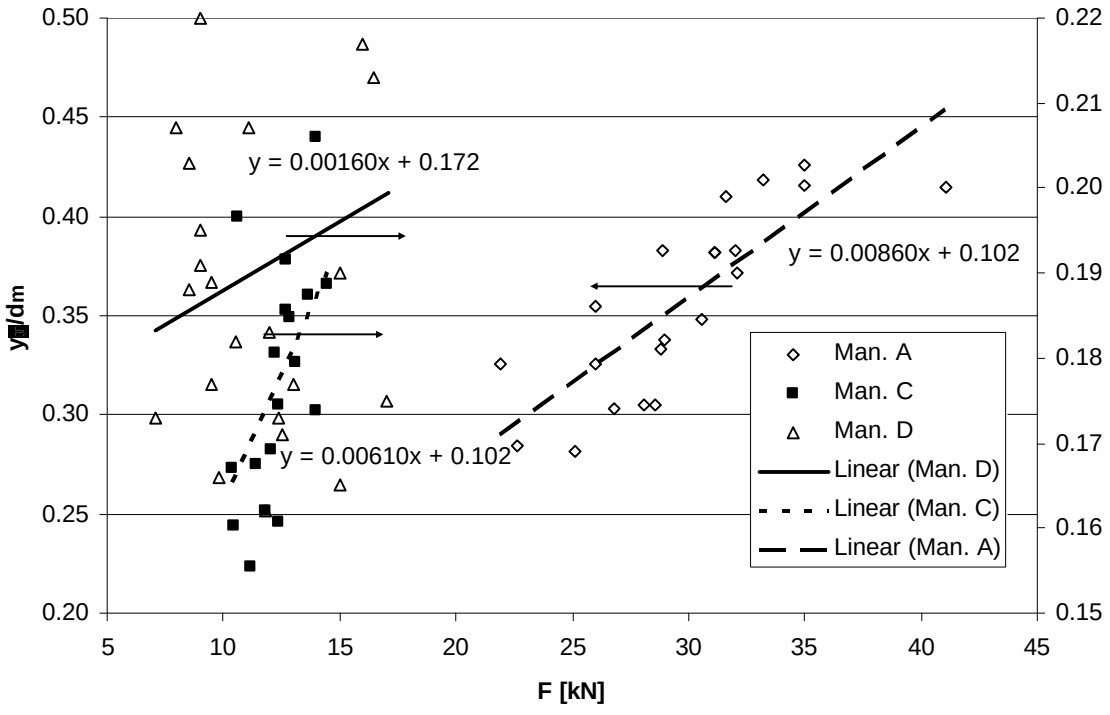

Fig. 41 – Ultimate relative ring deflection (at failure) *vs* ring force (man. A, C and D)

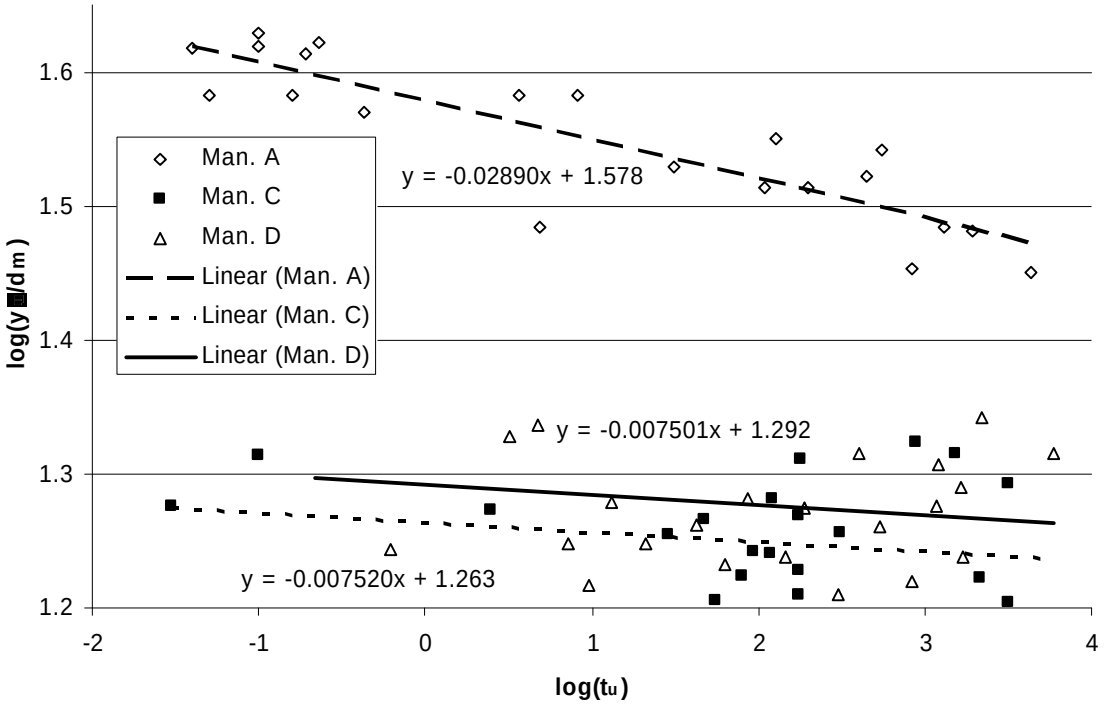

Fig. 42 – Ultimate relative ring deflection *vs* failure time (log-log) (man. A, C and D)

The extrapolated ultimate relative ring deflection for failure in 2 minutes, 6 years and 50 years are:

- specimens of manufacturer A

$$\begin{aligned}
&\log\left(y_{u,wet,2\min}/d_m\right) = +0.0289\times 1.477121 + 1.578 \approx 1.6207 &&\Leftrightarrow y_{u,wet,2\min}/d_m \approx 0.418\\
&\log\left(y_{u,wet,6}/d_m\right) = -0.0289\times 4.721 + 1.578 \approx 1.4416 &&\Leftrightarrow y_{u,wet,6}/d_m \approx 0.276\\
&\log\left(y_{u,wet,50}/d_m\right) = -0.0289\times 5.6415 + 1.578 \approx 1.4150 &&\Leftrightarrow y_{u,wet,50}/d_m \approx 0.260
\end{aligned} \quad (45)$$

- specimens of manufacturer C

$$\begin{aligned}
&\log\left(y_{u,wet,2\min}/d_m\right) = +0.007\times 1.477121 + 1.2634 \approx 1.27374 &&\Leftrightarrow y_{u,wet,2\min}/d_m \approx 0.188\\
&\log\left(y_{u,wet,6}/d_m\right) = -0.007\times 4.721 + 1.2634 \approx 1.230353 &&\Leftrightarrow y_{u,wet,6}/d_m \approx 0.170\\
&\log\left(y_{u,wet,50}/d_m\right) = -0.007\times 5.6415 + 1.2634 \approx 1.22391 &&\Leftrightarrow y_{u,wet,50}/d_m \approx 0.168
\end{aligned} \quad (46)$$

- specimens of manufacturer D

$$\begin{aligned}
&\log\left(y_{u,wet,2\min}/d_m\right) = +0.0075\times 1.477121 + 1.2919 \approx 1.30298 &&\Leftrightarrow y_{u,wet,2\min}/d_m \approx 0.201\\
&\log\left(y_{u,wet,6}/d_m\right) = -0.0075\times 4.721 + 1.2919 \approx 1.2565 &&\Leftrightarrow y_{u,wet,6}/d_m \approx 0.181\\
&\log\left(y_{u,wet,50}/d_m\right) = -0.0075\times 5.6415 + 1.2919 \approx 1.2496 &&\Leftrightarrow y_{u,wet,50}/d_m \approx 0.178
\end{aligned} \quad (47)$$

And so, the respective regression ratios, according to the standards EN1227 [21] and EN705 [18], are:

- specimens of manufacturer A $$R_{R,def} = \frac{y_{u,wet,50}/d_m}{y_{u,wet,6}/d_m} = \frac{0.260}{0.276} \approx 0.941 \quad (48)$$

- specimens of manufacturer C $$R_{R,def} = \frac{y_{u,wet,50}/d_m}{y_{u,wet,6}/d_m} = \frac{0.168}{0.170} \approx 0.985 \quad (49)$$

- specimens of manufacturer D $$R_{R,def} = \frac{y_{u,def,50}/d_m}{y_{u,def,6}/d_m} = \frac{0.178}{0.181} \approx 0.984 \quad (50)$$

These regression ratios, representing the deflection tendency by creeping effects as time under solicitation increases from short to long-term, show that specimens from manufacturers C and D have a similar behaviour with higher creeping tendency while those from manufacturer A reveal more stability during same periods of time.

Alternative procedures, with preconditioning under water for different times to determine the minimum soaking period to achieve saturation of each specimen, are now being studied in different research projects. In those tests, after a treatment of data similar to the one made in this standard procedure presented above, the influence of accelerated ageing as well as of water absorption by the pipe wall will certainly be assessed for each type of GRP pipe.

Stress Relaxation

The four types of pipes tested in this campaign (man. A, B, C and D) showed different behaviour in terms of stress relaxation when subjected to a fixed ring deflection condition. Even in those pipes having the same nominal specification for stiffness, SN 5000, and that have been subjected to similar preconditioning and charging procedures, one can observe primarily that the initial reaction ring force, i.e. the stiffness developed is different for pipes of different manufacturers.

Figure 43 shows how the three machines were disposed allowing the conduction of three tests simultaneously.

None of the tested tubes suffered structural failure neither visible damages. With acoustic emission monitoring[12] it is, however, evident the occurrence of matrix

[12] one singular test with acoustic emission monitoring was conducted in a man. B specimen

cracking during the long-term essay. Permanent emission of acoustic signals denotes the possibility of structural failure in an advanced stage of degradation of the pipe.

Fig. 43 – Arrangement developed for alternative relaxation tests

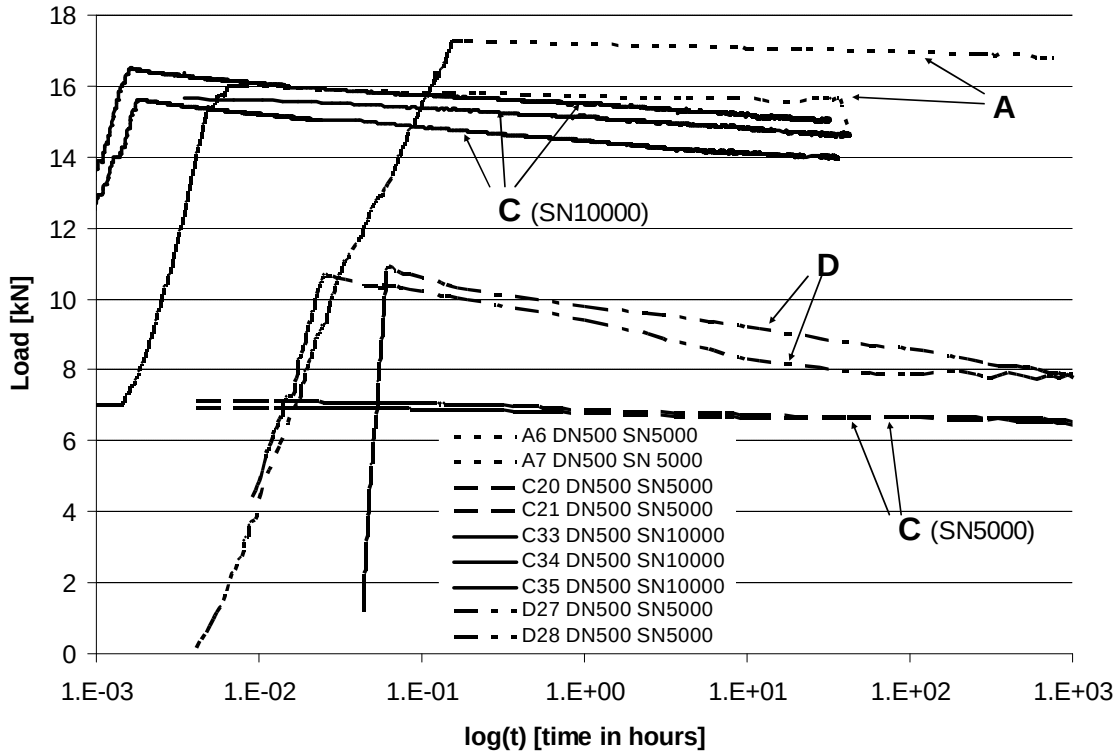

Fig. 44 – Evolution of reaction ring force in specimens subjected to 11.5% of relative ring deflection after preconditioned under water at 50ºC during 1000h

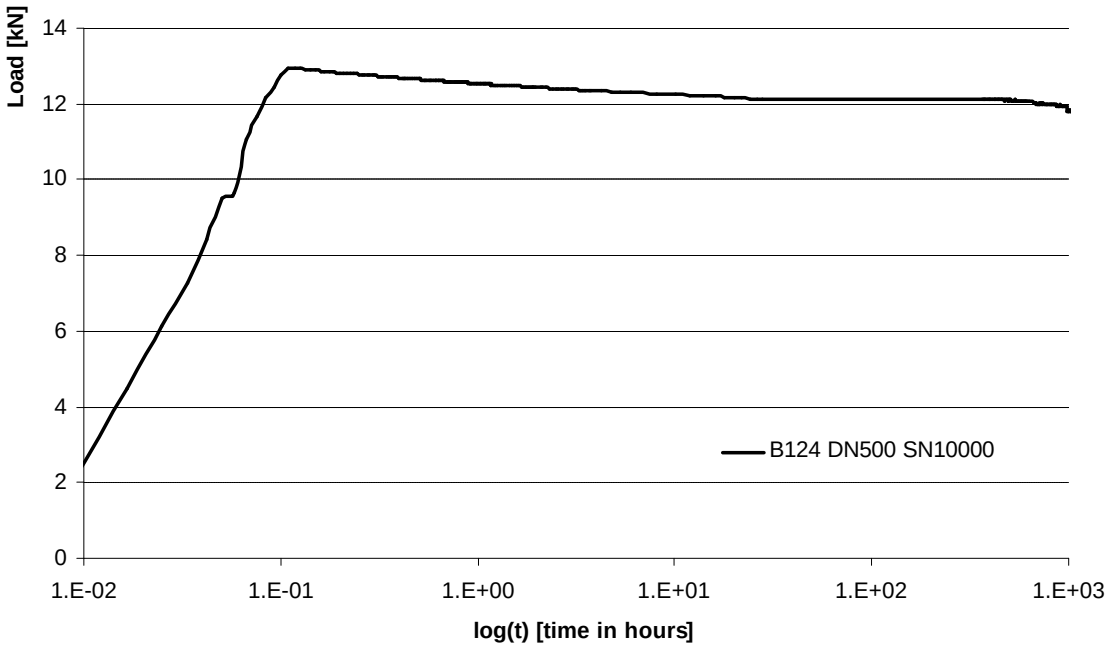

Fig. 45 – Evolution of reaction ring force in a Man. B specimen (SN5000) subjected to 24% of relative ring deflection after preconditioned under water at 50ºC during 1000h

It is also verified that these composite structures do not show a clear decreasing shape in the load *vs* time curves.

Graphics 44 and 45 compile the results obtained for several test specimens that are identified in the legend. The history output of reaction ring force during each essay is presented.

Specimens from manufacturer D SN5000 and C SN10000 showed a relevant decreasing tendency of reaction ring force, mainly at beginning of tests. The other specimens did not show that tendency, having stabilized in an early stage of the test.

Burn-off tests

Measurements made on the five samples (before and after degradation of resin) are presented in tables 6 and 7.

Figure 46 shows the type of layer-up used by manufacturer C in its production of GRP pipes (DN500 SN10000). One could observe 10 structural plies composed, each one, by a sub-layer of bundles of glass-fibre with orientation angle of 90º and another of random mat.

Table 6 – weight measurements for each sample before and after burn-off tests

sample #	Weight [g]			% resin	% fibre[13]
	sample	fibre	resin		
1	4.640	2.957	1.683	36.27	63.73
2	4.650	3.019	1.631	35.03	64.92
3	5.093	3.351	1.742	34.20	65.80
4	4.957	3.232	1.725	34.80	65.20
5	4.474	2.905	1.570	35.08	64.92

Table 7 – average results for mass contents in Man. C specimens

average results	average	S.D.
Resin [%]	35.09	0.75
Fibre + Silical charges [%]	64.91	0.75
Silical charges [%] (estimation)	35	---

The presence of silical charges (inerts) embedded in the resin, mostly introduced to reduce costs of the final product, increases the difficulty of modelling the behaviour of of these GRP pipes, once either the tension or compressive capabilities are not easily known.

Fig. 46 – Sample of one single layer free of resin and silical charges (after burning-off)

[13] this value represents, in fact, the percentage of fibre + charges (sand).

5. Numerical Models

In structural design stresses (s), displacements (d) and strains (e) that occur in each component while in service may be calculated, with more or less accuracy, recurring to analytical methods and models. However, in many practical cases that approach turns unusable due to the necessity of satisfying boundary conditions, differential equations systems with high computational demands or even of impossible resolution. Additionally, many of the cases to be studied have an empirical and/or experimental basis which allows not the recurrence to theoretical models.

Alternative methods are then frequently used for calculus, consisting typically in algebraic formulations of the problem approximating the relevant physical processes involved. One of the most used methods is finite elements method (FEM).

Simultaneously to the experimental program, numerical models were developed, in order to simulate the mechanical behaviour of a GRP pipe in a ring deflected condition. And that was, actually, its main objective: to evaluate the reproducibility of the damage mechanisms and global mechanics of these structures with numerical tools, such as finite elements method.

The reference tests were those of initial failure strain, led on specimens from manufacturer C. Although interesting is, certainly, to investigate numerical capabilities for modeling the long-term behaviour, namely recurring to viscoelastic properties, the main concern was to globally reproduce the experimental observations made in the present test campaign.

For that purpose, a 2D model was created, based in the geometry and dimensions of C specimens (table 4) with 10 plies of 1.2mm thickness each, separated by interface cohesive elements [3-5] allowing simulation of delamination and rupture of fibres, either in mode I and/or mode II.

According to the specifications of the manufacturer, a 90º winding orientation angle was assumed and so the 2D model seemed to fit all the requirements for this study, once the main properties governing the mechanical behaviour act in each cross section plane. However, to verify those assumptions, simplified 3D models were firstly developed and influence of winding angle was analyzed.

Next section presents the modeling methodologies implemented as it describes the objectives, assumptions and parametric studies. Results achieved are then presented.

Modelling Approaches

3D models

The objective of developing simplified 3D models was to evaluate either the influence of the fibres winding orientation angle on the pipe behaviour and, moreover, the reasonability of studying the specimens of manufacturer C only with 2D numerical models, once it was known that the fibres winding orientation angles of those pipes was 90º.

Within the scope established for these 3D models, for the parameterization of the results to be focused in the fibres winding orientation angle, the only difference between the several examples is the orientation of the local coordinate system, in which principal directions are defined.

The 3D models, due to its simplicity, were totally generated in CAD/CAM environment supported by ABAQUS/CAE^{TM}. Accounting the main dimensions of the specimens, a 3D shell cylinder surface was created as reported in figure 47.

It was considered a symmetric layering up of two plies with winding angles of +a and –a, respectively. Defining those angles by projecting each of the reference directions from the axis to the surface, rectangular shell elements S8R were used to mesh the geometry. The mesh configuration and refinement is shown in figure 48.

By analyzing a complete ring, making not use of the particular geometric symmetry, the boundary conditions imposed were the restraint of tangential movement of the two sections to be charged.

Elastic properties used in all 3D models were:

- E_1= 100 GPa
- E_2= 9 GPa
- $?_{12}$= 0.3
- G_{12}= 3.2 GPa
- G_{13}= 3.2 GPa
- G_{23}= 4 GPa

where E_1 is the elastic modulus in direction of fibres.

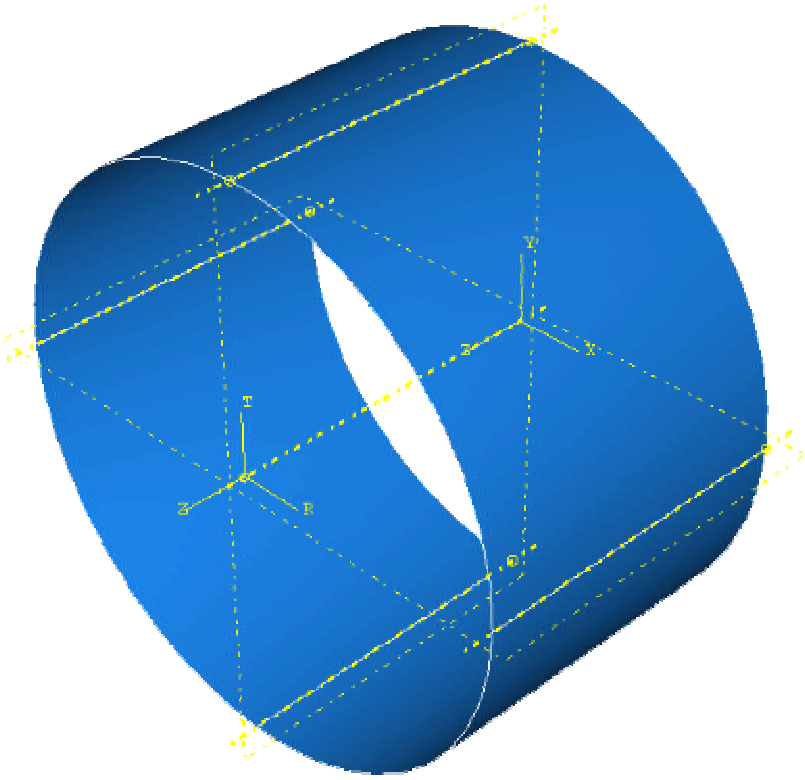

Fig. 47 – Reference shell geometry generated

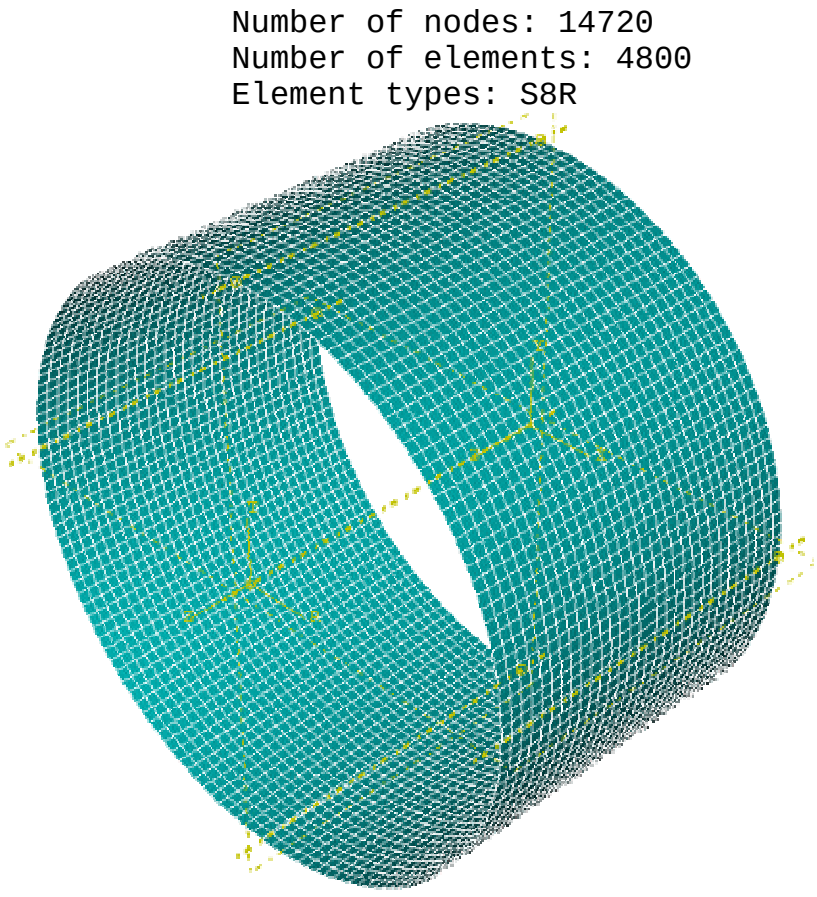

Fig. 48 – Mesh generated on the reference surface

May one notice that, by being looking for the influence of one parameter, the values attributed to the others is not quite relevant as long as they are equally defined for every examples evaluated.

The nine models run had the properties summarized in table 8.

Table 8 – Summary of the definitions of examples run

parameter	model ref.								
	1	2	3	4	5	6	7	8	9
no. plies	2	2	2	2	2	2	2	2	2
a_1 [º]	30	45	50	52.5	55	57.5	60	80	90
a_2 [º]	-30	-45	-50	-52.5	-55	-57.5	-60	-80	90
t_1 [mm]	2	2	2	2	2	2	2	2	2
t_2 [mm]	2	2	2	2	2	2	2	2	2

2D models

Due to the availability of manufacturing specifications of specimens from manufacturer C, which were chosen for initial failure strain tests, 2D numerical models were developed based on them.

The ring deflection was imposed by increasing successively the displacement of the charging section from initial undeflected condition to the final value specified. To reduce the computational weight of each model, half of the cross section was considered. Figures 49 and 50 represent schematically the load case and the equivalent configuration accounted for 2D modelling (half section) with the corresponding boundary conditions imposed.

As described before, specimens from manufacturer C are produced by a hybrid process of filament winding and short-fibre deposition. That means that between each winded ply one find complete layers of short-fibres randomly orientated impregnated with resin. Additionally, the epoxy resin used in the manufacturing process contains high levels (estimated in burn-off tests) of granulated inerts that considerably decrease the structural ability of the pipe as they allow slippering of plies, propitiating delaminations at lower stress levels.

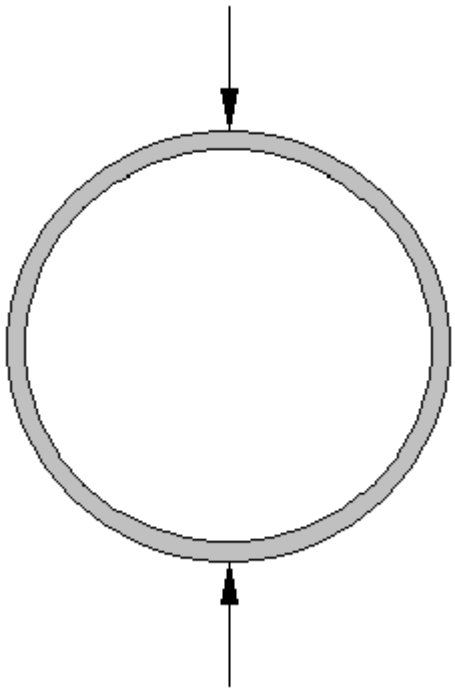

Fig. 49 – Load case of ring deflection

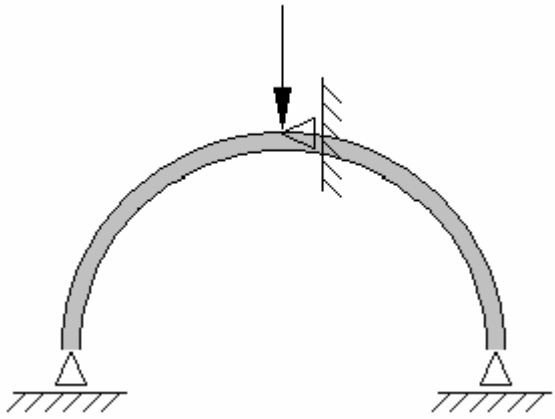

Fig. 50 – Model configuration

The stacking sequence of $[90,90,90,90,90]_s$ would make one think of no reason to assist to delamination between plies as experimental tests show. The existence of those plies formed by fibres deposition and great quantities of silical charges seems to be the reason for that phenomenon documented before.

Fracture mechanics says that cracks can propagate in three different modes, which can interact each (mixed-mode loading). Delamination is assumed to be held in the same way. Figures 51-53 show the mechanical principle of each one.

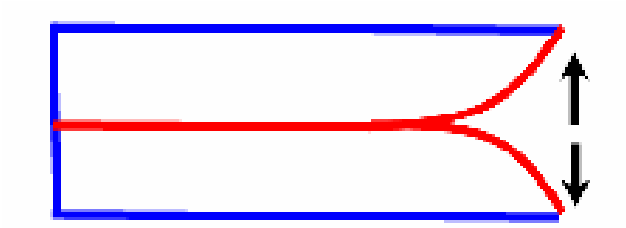

Fig. 51 – Fracture in mode I

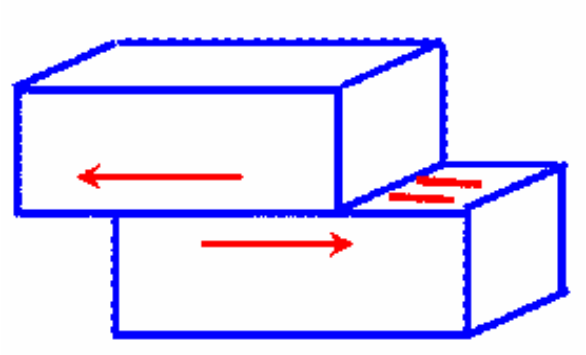

Fig. 52 – Fracture in mode II

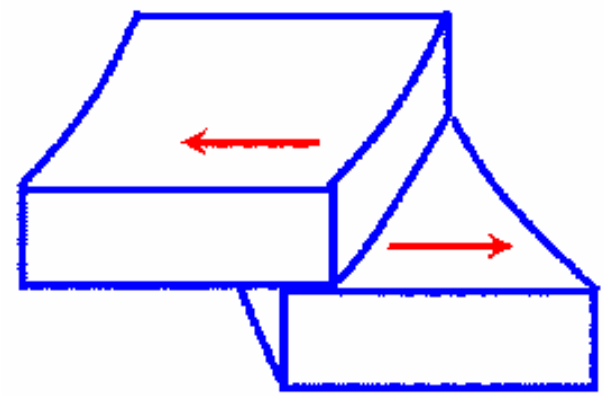

Fig. 53 – Fracture in mode III

In the present case, experimental observations showed that delamination is dominated by mode I and/or mode II, while rupture of fibres occurs in mode I.

As the strain energy release rates values are not quite easy to achieve experimentally, mainly when one look for a coherent group of values for E_1, G_{12}, G_{Id}, G_{IId}, G_{If}, it was decided to parameterize the numerical study to these variables.

Using a typical value of 0.3 kJ/m^2 for strain energy release rate in mode I delamination [23], G_{Id}, models were parameterized in the G_{If}/G_{Id} ratio, made either 10, 100, 500 and 1000.

Numerical simulation of damage propagation demand specific modelling techniques as the stress transfer from a point reaching the limit to the surrounding zone is to be gradual. Typical formulation of cohesive elements account for a softening law between interface stresses and relative displacements at homologous points of the interface elements after the stress limit is reached. This avoids mesh dependency and simultaneously accounts for the Fracture Process Zone (FPZ) which represents the region ahead of the crack tip undergoing inelastic processes, e.g., micro-cracking, voids nucleation and fibre bridging.

A two-dimensional finite element model including interface elements was used. The model considers 8-node plane strain elements of the ABAQUS^{TM} library and compatible 6-node interface finite elements specially developed (fig.54) [24].

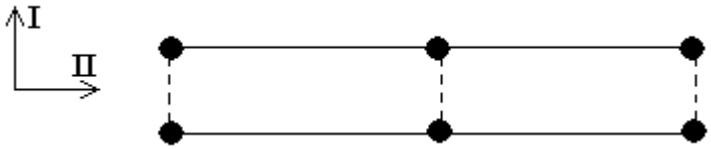

Fig. 54 –Scheme of the interface element used

Before damage starts to grow the stresses are calculated from the relative displacements doing

$$\mathbf{s} = \mathbf{D}\,\mathbf{d} \tag{51}$$

where

D is a diagonal matrix including the initial interface stiffness

At the softening region (between $d_{o,i}$ and $d_{max,i}$ as shown in figure 55) it can be written as follows

$$\mathbf{s} = (\mathbf{I} - \mathbf{E})\,\mathbf{D}\,\mathbf{d} \tag{52}$$

where

I is the identity matrix

E is a diagonal matrix containing damage parameters, e_i

These damage parameters, e_i, representing the damage accumulated at the interface, are calculated from the equation of the line representing the softening region (fig.55).

$$e_i = \frac{d_{u,i}\left(d_i - d_{o,i}\right)}{d_i\left(d_{u,i} - d_{o,i}\right)} \tag{53}$$

The maximum relative displacement, $d_{u,i}$, for which complete failure occurs is obtained by equating the area under the softening curve to the respective critical fracture energy

$$G_{ic} = \frac{1}{2} s_{u,i} d_{u,i} \tag{54}$$

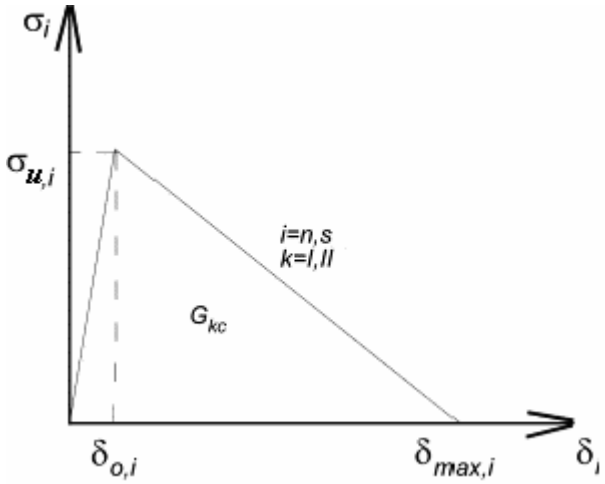

Fig. 55 – Softening stresses/relative displacements relationship for pure mode model [24]

The mixed-mode damage model used is, in this case, an extension of the pure mode model described above. Damage initiation is predicted by using a quadratic stress criterion as follows

$$\begin{aligned} &\left(\frac{s_I}{s_{u,I}}\right)^2 + \left(\frac{s_{II}}{s_{u,II}}\right)^2 = 1 \qquad if \qquad s_I \geq 0 \\ &s_{II} = s_{u,II} \qquad\qquad\qquad\qquad if \qquad s_I \leq 0 \end{aligned} \tag{55}$$

assuming that normal compressive stresses do not promote damage [24].

Simulation of damage propagation is based on the linear energetic criterion where it is assumed that complete failure occurs when

$$\frac{G_I}{G_{Ic}} + \frac{G_{II}}{G_{IIc}} = 1 \tag{56}$$

Considering this approach the failure is smooth and gradual as the energy is being released at the FPZ by several different ways (see for example fig.56).

Figure 56 represents schematically the bridging transportation principle that can be adapted for other modelling approaches, such as the one developed by F. Greco, P. Lonetti and R. Zinno [25].

As experimental results denote the damage phenomena to initiate and develop from the inside wall of the pipe around the charged section, the 2D models were designed placing cohesive elements in the inner interfaces as well as in central section of the corresponding inner plies.

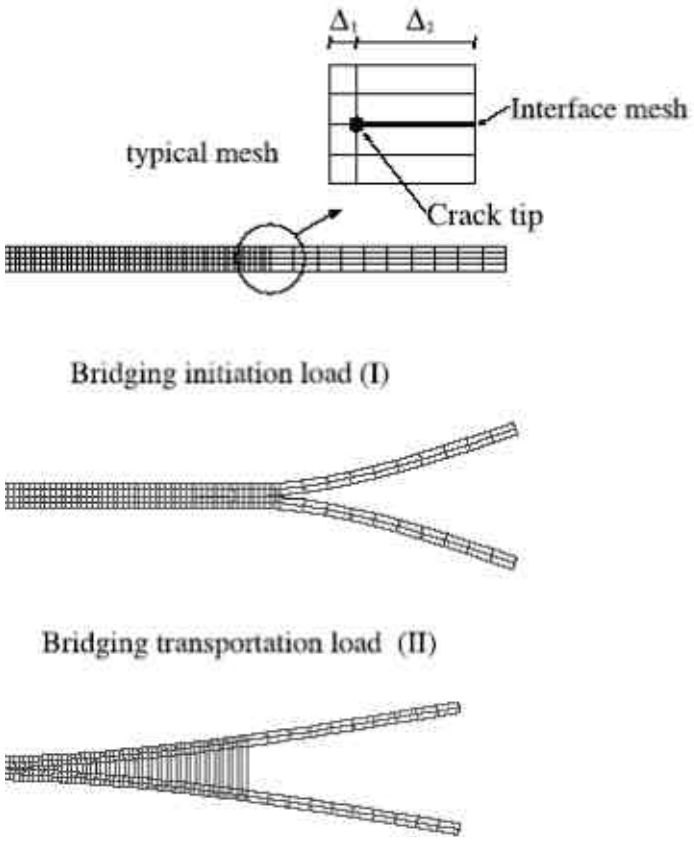

Fig. 56 – Typical undeformed mesh and deformed mesh at the initiation of the bridging creation (I), at the beginning of the bridging transportation phase (II) [25]

Three different architectures for 2D modelling were defined.

Firstly, a model with cohesive elements at the central zone of the two inner interfaces (200 elements) and another two at the charging section (202 cohesive elements total) allowing simulation of fibres rupture in the transverse direction of the cross section. CPE8R elements from processor's library were used to generate the mesh reported in figure 57. Greater refinement of mesh was promoted in the central zone, around the charging section.

The refined central zone of the mesh corresponds to the arc of 20º around the charging section (at the vertical symmetry plane) counting with 100 elements by ply.

A second approach consisted in applying the same refined level to all model and cohesive elements to the third inner interface, too. 2700 elements for delamination and the corresponding 3 central elements for ply failure (2703 cohesive elements total) were placed in this second architecture. Figure 58 shows the resulting mesh.

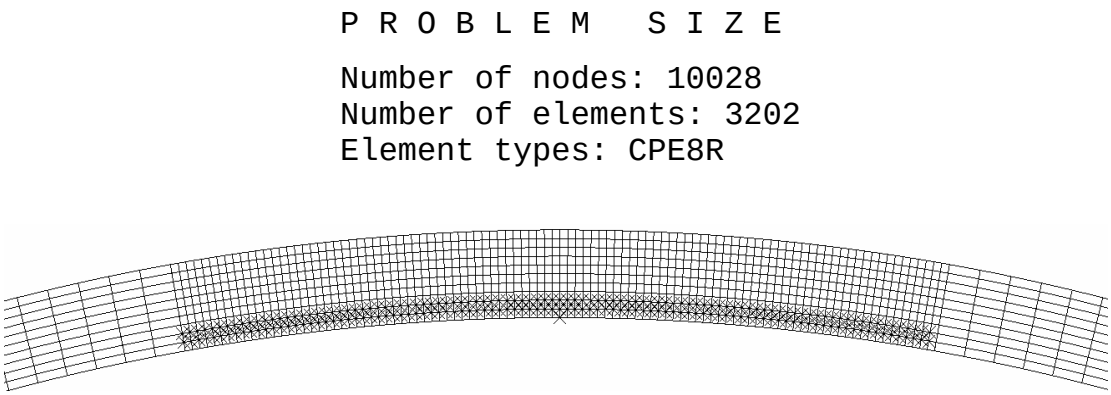

Fig. 57 – Detail of the refined zone of the mesh with cohesive elements (represented by crosses) in the two inner interfaces

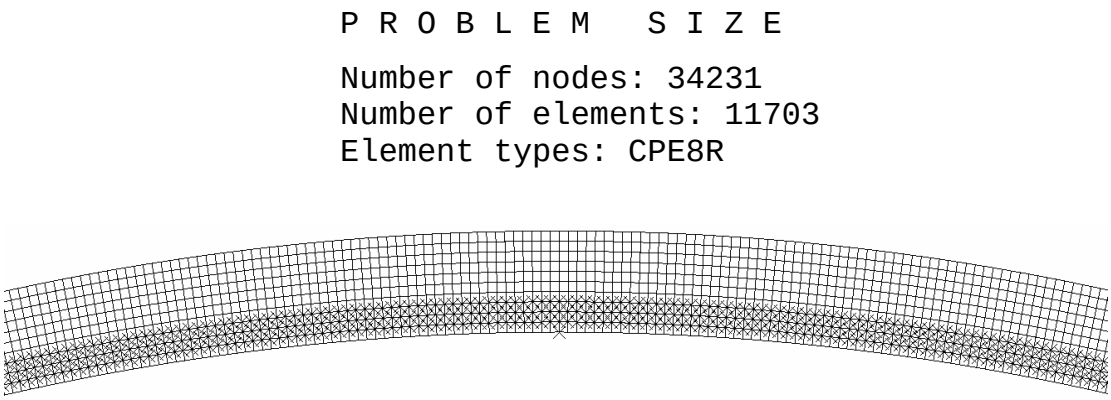

Fig. 58 – Detail of the mesh with cohesive elements (represented by crosses) in the three inner interfaces

Finally, a third configuration was designed allowing delamination in all interfaces as well as the corresponding failure of each ply at the charging section. 8100 elements for delamination and the corresponding 10 central elements for ply failure (8110 cohesive elements total) were introduced in this last mesh architecture. Figure 59 shows the respective mesh.

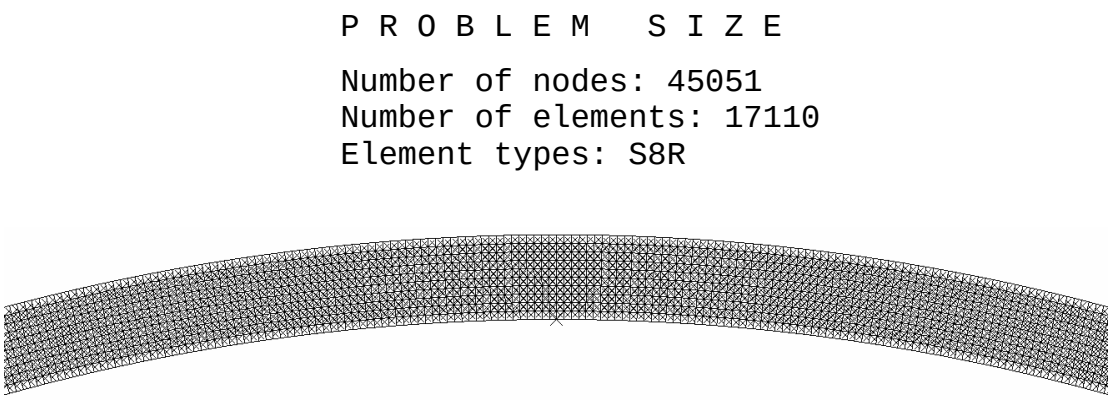

Fig. 59 – Detail of the mesh with cohesive elements (represented by crosses) in all interfaces

Several models, with distinct combinations of main parameters were run. Tables 9, 10 and 11 summarize those different combinations used to evaluate modelling applicability in simulating GRP pipes mechanics under ring deflection.

* models which correspondent input algorithm files are transcript in annex

Table 9 – List of examples run with cohesive elements in two inner interfaces

Ref.	$s_{rup\ fibres}$ [MPa]	E_1 [GPa]	no. plies	wall thickness [mm]	G_{Id} [kJ/m^2]	G_{IId} [kJ/m^2]	G_{If}/G_{Id}
1_2	300	100	10	10	0.3	0.6	10
2_2*	300	100	10	10	0.3	0.6	100
3_2	300	100	10	10	0.3	0.6	500
4_2	300	100	10	10	0.3	0.6	1000
5_2	300	60	10	10	0.3	0.6	10
6_2	300	60	10	10	0.3	0.6	100
7_2	300	60	10	10	0.3	0.6	500
8_2	300	60	10	10	0.3	0.6	1000
9_2	400	100	10	10	0.3	0.6	10
10_2	400	100	10	10	0.3	0.6	100
11_2	400	100	10	10	0.3	0.6	500
12_2	400	100	10	10	0.3	0.6	1000
13_2	400	60	10	10	0.3	0.6	10
14_2	400	60	10	10	0.3	0.6	100
15_2	400	60	10	10	0.3	0.6	500

16_2	400	60	10	10	0.3	0.6	1000
17_2	500	100	10	10	0.3	0.6	10
18_2	600	100	10	10	0.3	0.6	100
19_2	600	100	10	10	0.3	0.6	10
20_2	600	100	10	10	0.3	0.6	100

Table 10 – List of examples run with cohesive elements in three inner interfaces

Ref.	$s_{rup\ fibres}$ [MPa]	E_1 [GPa]	no. plies	wall thickness [mm]	G_{Id} [kJ/m^2]	G_{IId} [kJ/m^2]	G_{If}/G_{Id}
1_3	300	100	10	10	0.3	0.6	10
2_3*	300	100	10	10	0.3	0.6	100
3_3	300	100	10	10	0.3	0.6	500
4_3	300	100	10	10	0.3	0.6	1000
5_3	300	60	10	10	0.3	0.6	10
6_3	300	60	10	10	0.3	0.6	100
7_3	300	60	10	10	0.3	0.6	500
8_3	300	60	10	10	0.3	0.6	1000
9_3	400	100	10	10	0.3	0.6	10
10_3	400	100	10	10	0.3	0.6	100
11_3	400	100	10	10	0.3	0.6	500
12_3	400	100	10	10	0.3	0.6	1000
13_3	400	60	10	10	0.3	0.6	10
14_3	400	60	10	10	0.3	0.6	100
15_3	400	60	10	10	0.3	0.6	500
16_3	400	60	10	10	0.3	0.6	1000
17_3	500	100	10	10	0.3	0.6	10
18_3	600	100	10	10	0.3	0.6	100
19_3	600	100	10	10	0.3	0.6	10
20_3	600	100	10	10	0.3	0.6	100

Table 11 – List of examples run with cohesive elements in all interfaces

Ref.	$s_{rup\ fibres}$ [MPa]	E_1 [GPa]	no. plies	wall thickness [mm]	G_{Id} [kJ/m^2]	G_{IId} [kJ/m^2]	G_{If}/G_{Id}
1_all	100	10.5	10	12	0.3	0.6	10
2_all	100	10.5	10	12	0.3	0.6	100
3_all	100	10.5	10	12	0.3	0.6	500
4_all	100	10.5	10	12	0.3	0.6	1000
5_all	100	10.5	10	12	0.3	0.6	5000
6_all	200	10.5	10	12	0.3	0.6	10
7_all	200	10.5	10	12	0.3	0.6	100
8_all	200	10.5	10	12	0.3	0.6	500
9_all*	200	10.5	10	12	0.3	0.6	700
10_all	200	10.5	10	12	0.3	0.6	1000
11_all	200	100	10	10	0.3	0.6	1000
12_all*	300	10.5	10	12	0.3	0.6	10
13_all	300	10.5	10	12	0.3	0.6	100

14_all	300	10.5	10	12	0.3	0.6	500
15_all	300	10.5	10	12	0.3	0.6	1000
16_all	300	100	10	10	0.3	0.6	10
17_all	300	100	10	10	0.3	0.6	100
18_all	300	100	10	10	0.3	0.6	500
19_all	300	100	10	10	0.3	0.6	1000
20_all	300	10.5	10	10	0.3	0.6	1000
21_all*	300	10.5	12	12	0.3	0.6	500
22_all	300	10.5	12	12	0.3	0.6	1000
23_all	400	10.5	10	12	0.3	0.6	2
24_all	400	10.5	10	12	0.3	0.6	10
25_all	400	10.5	10	12	0.3	0.6	100
26_all	400	10.5	10	12	0.3	0.6	500
27_all	400	10.5	10	12	0.3	0.6	1000
28_all	400	100	10	10	0.3	0.6	100
29_all	400	100	10	10	0.3	0.6	1000
30_all	500	100	10	10	0.3	0.6	10
31_all	500	100	10	10	0.3	0.6	1000
32_all	500	100	10	10	0.15	0.3	10
34_all	500	60	10	10	0.3	0.6	100
37_all	500	40	12	12	0.3	0.6	100

Results

3D models

Next figures (60-62) show the stress evolution (equivalent stress state by von Mises criterion) in function of increasing deflection level forthree cases of orientation angle, ±30º, ±52.5º and ±90º. Although it is not quite understandable in selected images[14], stress increases relevantly with deflection. The instants selected for evaluation were 0, 16, 24, 32 and 40% of relative ring deflection (y/d_m).

Observing the stress distribution for each winding angle, one can see that, as expected, for a fibre orientation angle of 90º, the stress gradients, whatever their level or circumferential position are, seems not to be affected by edge effects. This assumption would not apply in any of the other cases where some distortion of gradient shapes is verified near the end of the walls.

The main scope of this simplified numerical procedure was accomplished and one could, more reliably, assume that a 2D model would fit the objectives defined for this task.

[14] because color code is automatically updated at the end of each deflection step

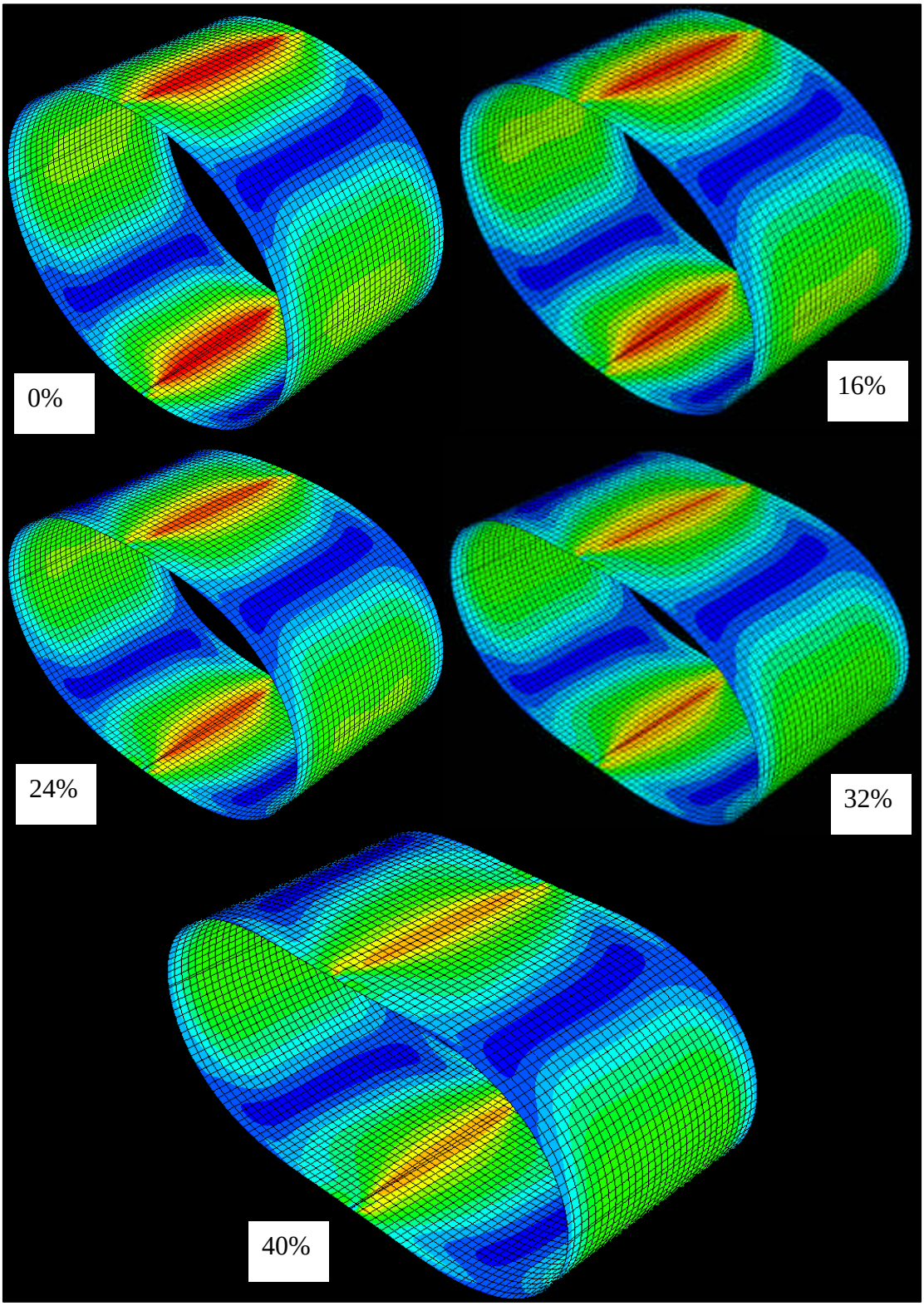

Fig. 60 – Ring deflection sequence of example ±30º

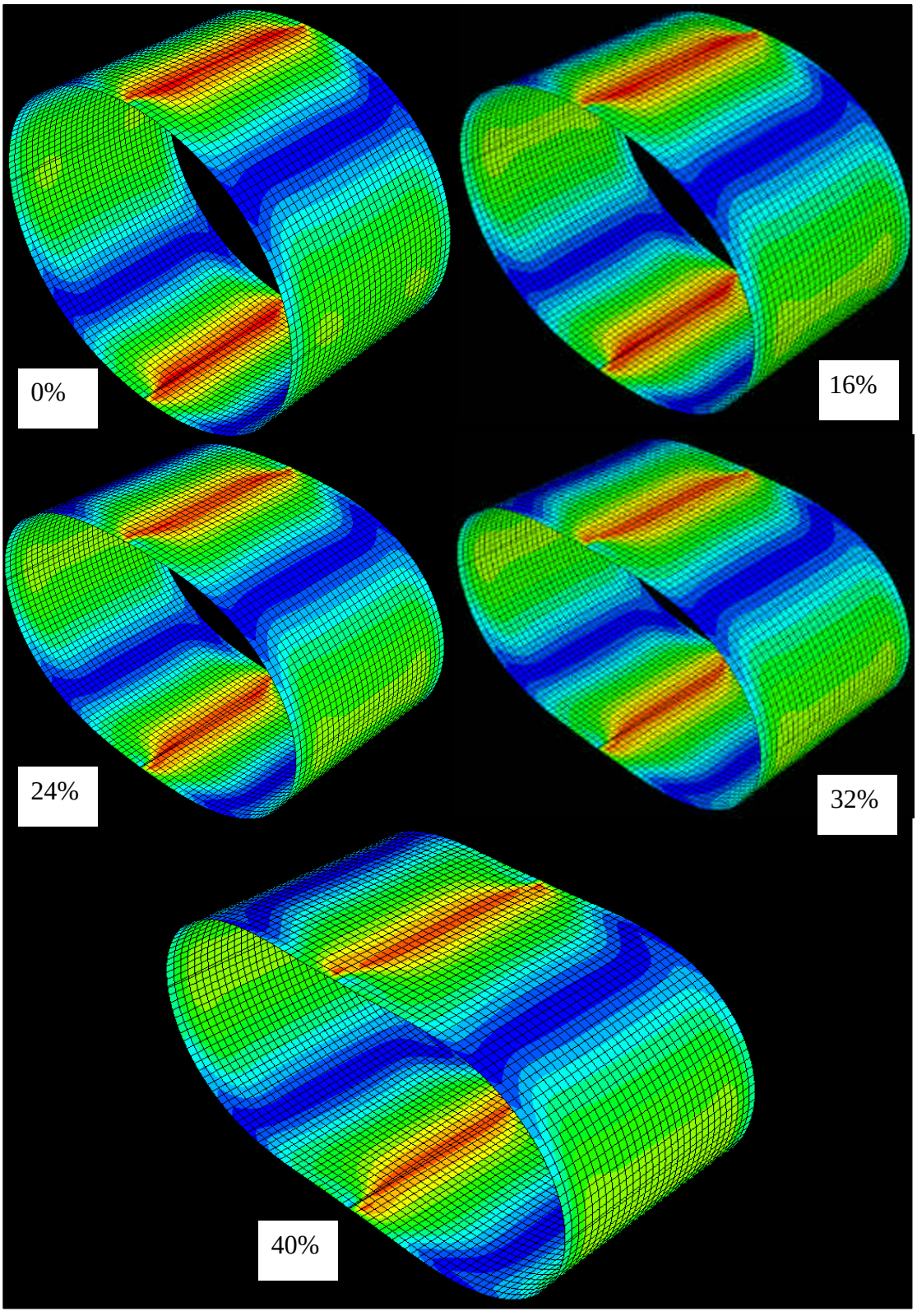

Fig. 61 – Ring deflection sequence of example ±52.5º

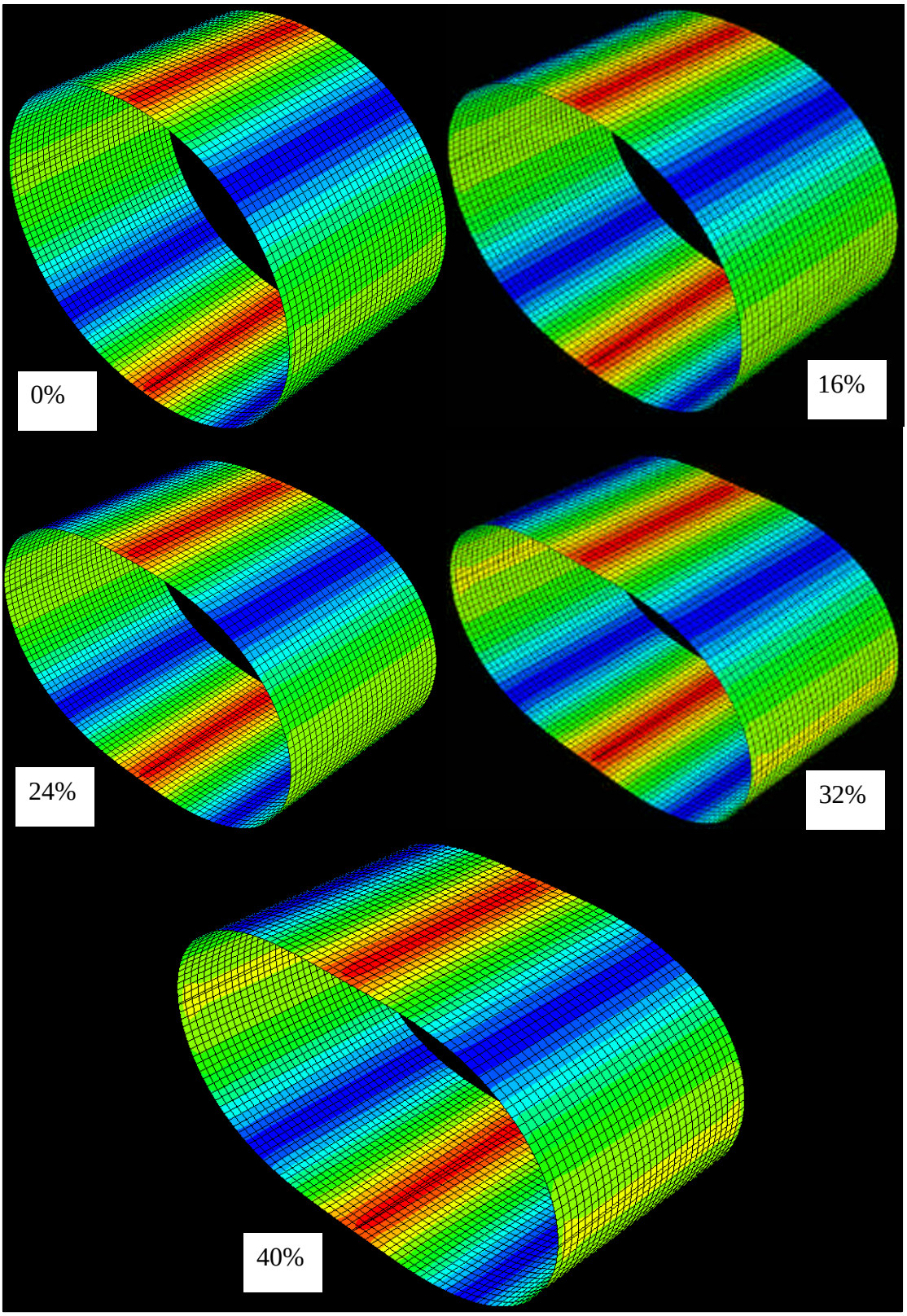

Fig. 62 – Ring deflection sequence of example 90º

Taking to advantage of having worked these models, other output data could be produced to complement the evaluation of the winding orientation angle's influence in global mechanics of GRP pipes. In that way, maximum level of strain and stress

developed in each case were registered and figures 63-66 report that data in two different ways so that conclusions can easily be taken.

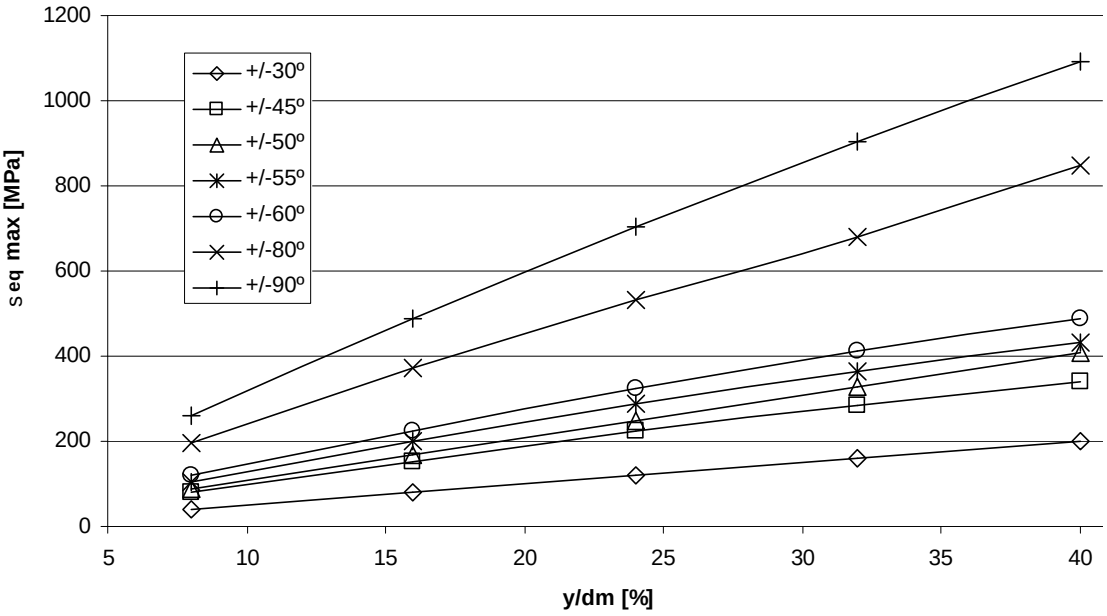

Fig. 63 – Maximum stress (von Mises equivalent) achieved in each model *versus* respective relative ring deflection

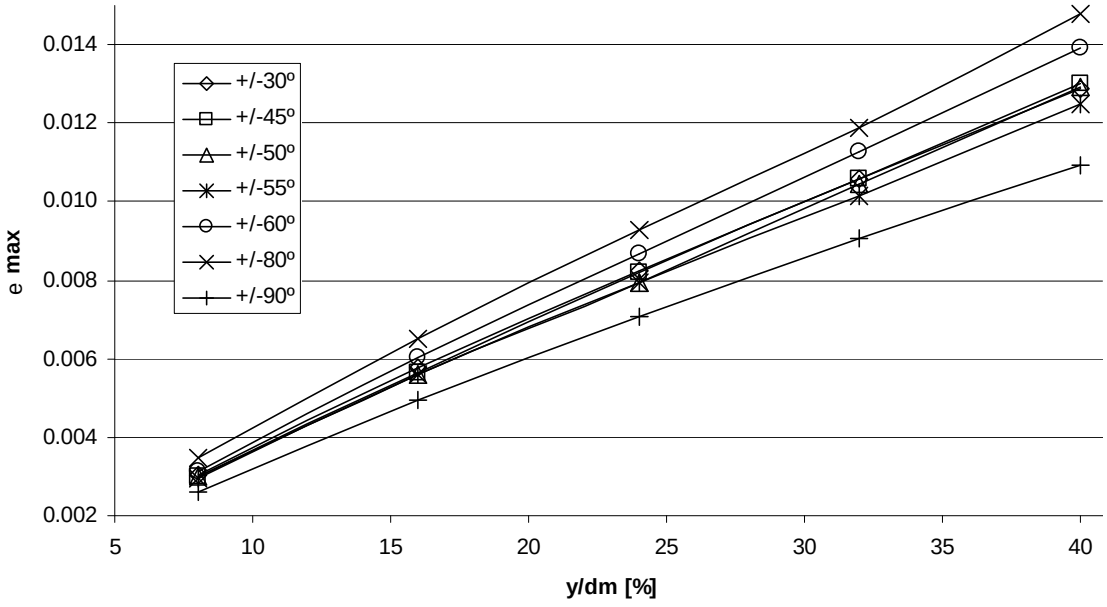

Fig. 64 – Maximum strain achieved in each model versus respective relative ring deflection

In first two graphics, figures 63 and 64, one can see curves (each one for each winding fibre orientation angle) showing the increasing tendency of stresses (von Mises equivalent) and strains (total equivalents) when increasing also the relative ring

deflection while in graphics 65 and 66 the same information is displayed using one curve for each relative ring deflection level.

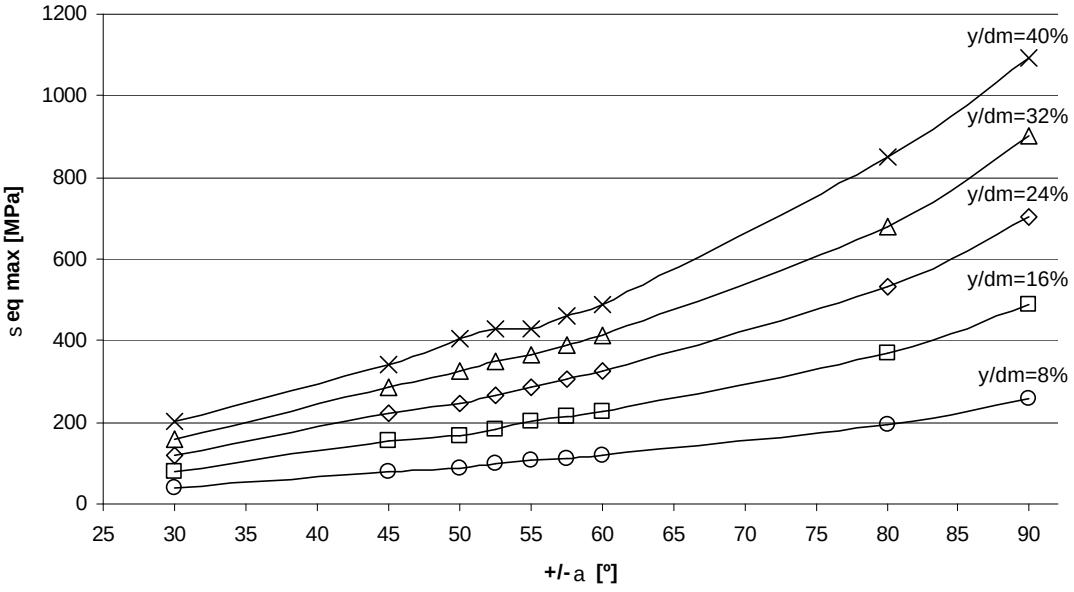

Fig. 65 – Maximum stress (von Mises equivalent) achieved at each deflection level *versus* respective winding angle

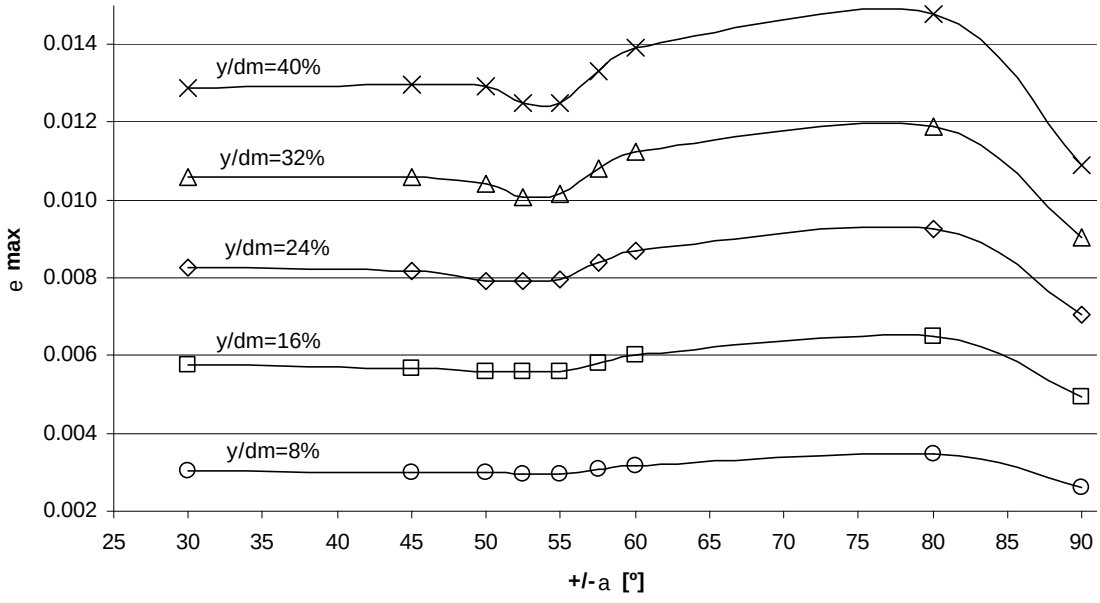

Fig. 66 – Maximum strain achieved at each deflection level *versus* respective winding angle

Higher levels of deflection lead to bigger strain reduction around 53º of winding orientation angle. For low values of ring deflection, that tendency is almost negligible.

Concerning to the maximum stress (von Mises equivalent stress), it does not seems to exist any relevant event around that winding angle value.

On the other hand, these strain numerical results were expected as winding orientation angles of 52-55º have been widely used in GRP piping manufacture in last decade, namely by two of the four manufacturers selected for test campaigns.

For a winding orientation angle of 90º it is observed a significant reduction of the maximum value of strain achieved, as well as relevant increasing of corresponding stresses. Numerically, the points where these values were obtained were in the charged section of each model.

May one note again that the absolute values, either in strain or stress, are not relevant once it is pursued only their relativity to the winding orientation angles. Additionally, in this first approach a coherent group of values was used for all relevant elastic parameters, but not necessarily suitable for modelling the experimental observations of test campaigns led in these particular GRP pipes.

2D models

Reproducibility of damage mechanisms observed in experimental tests, as well as evolution of reaction ring force during the charging procedure, imposing ring deflection, were the main outputs to analyze. However, other parameterized outputs were produced and are here presented.

Firstly, one may observe the tendency of reaction ring force *versus* displacement curves for different values of the Young modulus in circumferential direction, E_1. In the graphic of figure 67 it can be seen that as the circumferential elastic modulus is increased so the reaction ring force for the same value of deflection increases, too.

Stiffness of the pipe can be also modified by changing the geometric ratios, such as the thickness of the structural wall. That influence is drawn and may be evaluated in the same graphic. Thick curves show the value of E_1 that turns the numerical curve coincident with the experimental one. E_1 of 10.5 GPa is the value specified by manufacturer C for circumferential elastic modulus of the pipes supplied for mechanical tests.

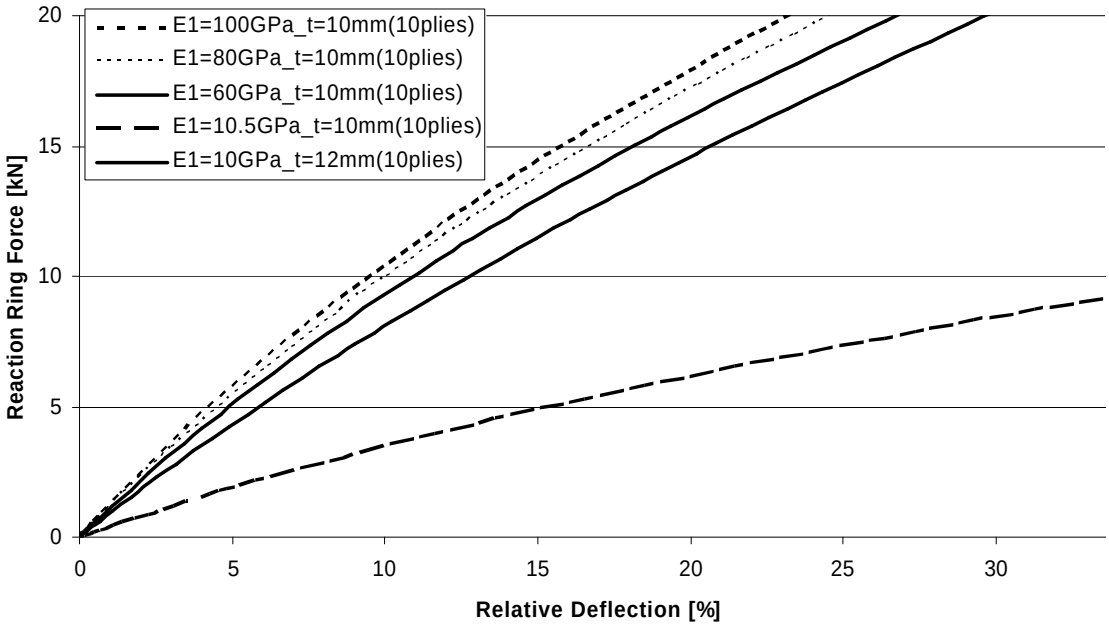

Fig. 67 – Influence of circumferential elastic modulus and wall thickness in model behaviour

As no influence of E_2 and E_3, elastic modulus in radial and axial directions, respectively, was encountered, no parameterized output was produced in those variables.

In the first two approaches, considering cohesive elements only at inner interfaces, interesting results were achieved in terms of the type of damage leading to structural failure. In fact, the occurrence of fibres rupture from the inside face at the charged section, with consequent delamination in the corresponding inner plies around that area, is quite observed in experimental tests.

Figures 68-73 show two charging sequences led in two models differing only in their mesh architecture, having the same properties (table 12). In graphic of figure 74 one can see the evolution of reaction ring force with deflection and it is observable that the damage promoted in these models was not leading to total collapse as the outer plies that suffered no delamination or fibre rupture still remain resisting. One can also observe that both *P-d* curves are similar and almost superpose each other.

Table 12 – Values of different parameters in models 2_2 and 2_3

Ref.	$s_{rup\ fibres}$ [MPa]	E_1 [GPa]	no. plies	wall thickness [mm]	G_{Id} [kJ/m^2]	G_{IId} [kJ/m^2]	G_{If}/G_{Id}
2_2	300	100	10	10	0.3	0.6	100
2_3	300	100	10	10	0.3	0.6	100

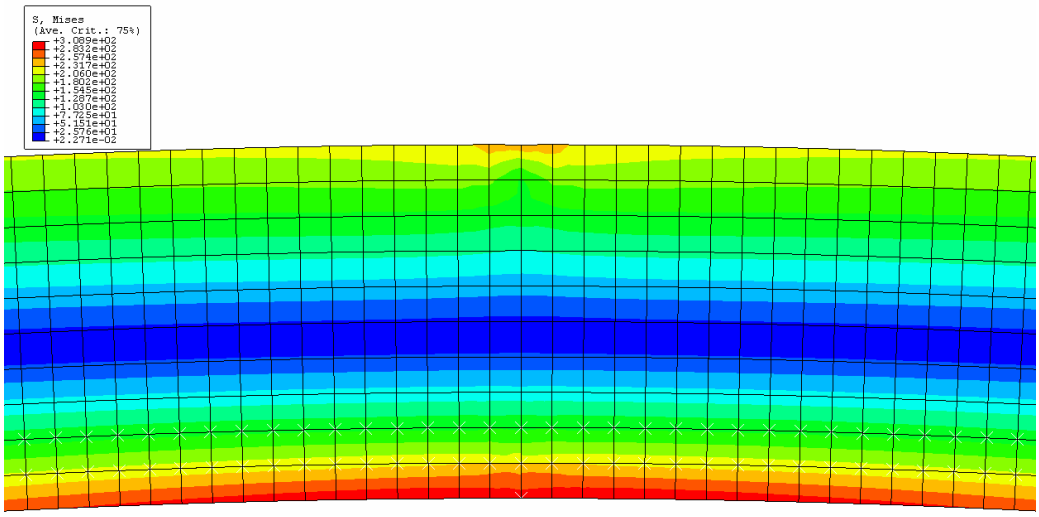

Fig. 68 – Model 2_2 at 14.31% of relative ring deflection. Instant before softening

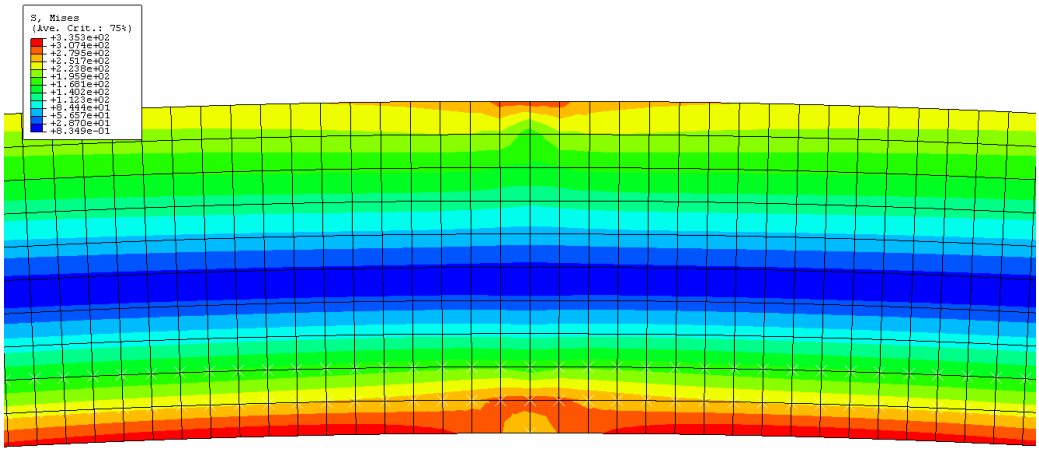

Fig. 69 – Model 2_2 at 16.94% of relative ring deflection. Damage initiation in inner ply

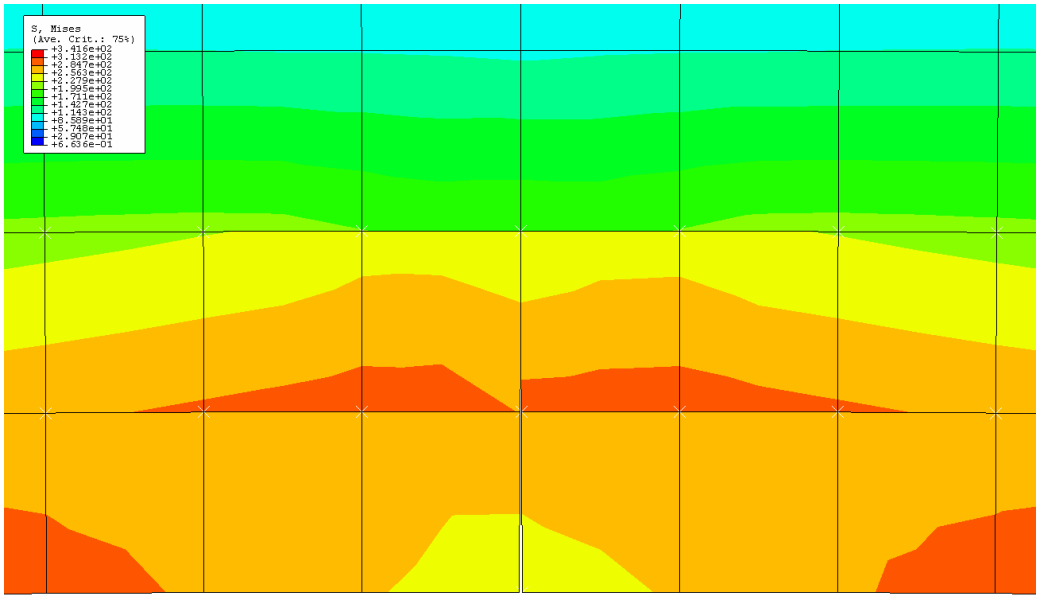

Fig. 70 – Model 2_2 at 17.81% of relative ring deflection. Fibre rupture in two inner plies and delamination of first interface due to shear stress

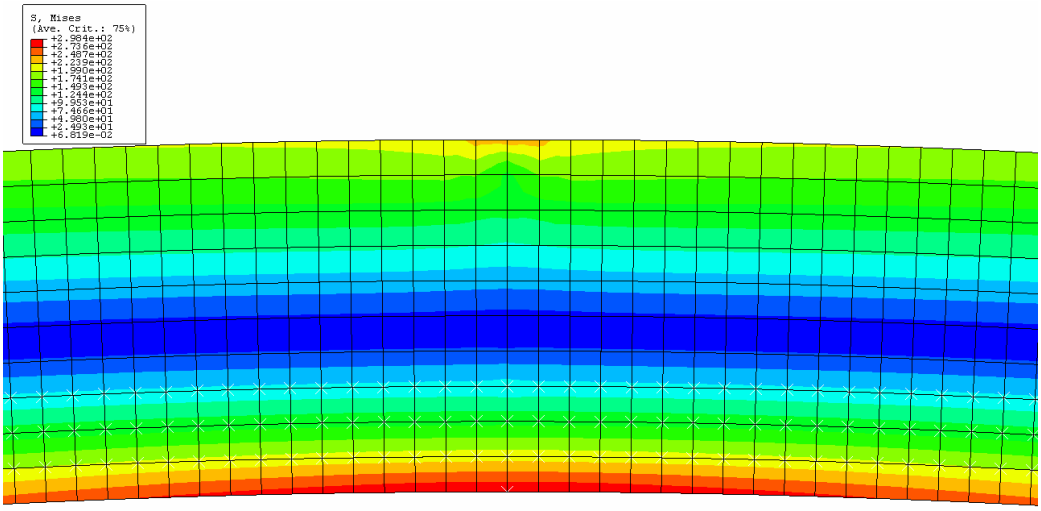

Fig. 71 – Model 2_3 at 14.42% of relative ring deflection. Instant before softening

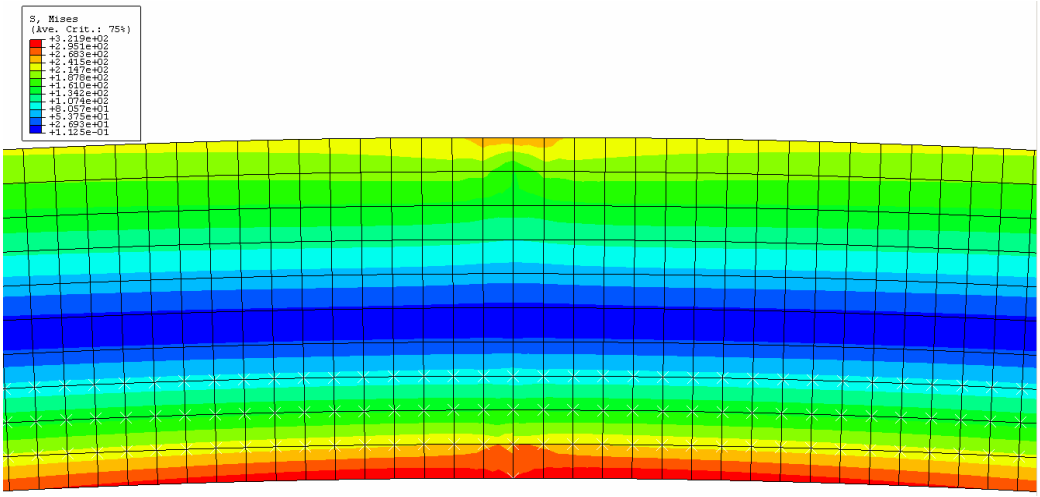

Fig. 72 – Model 2_3 at 16.63% of relative ring deflection. Softening in inner ply

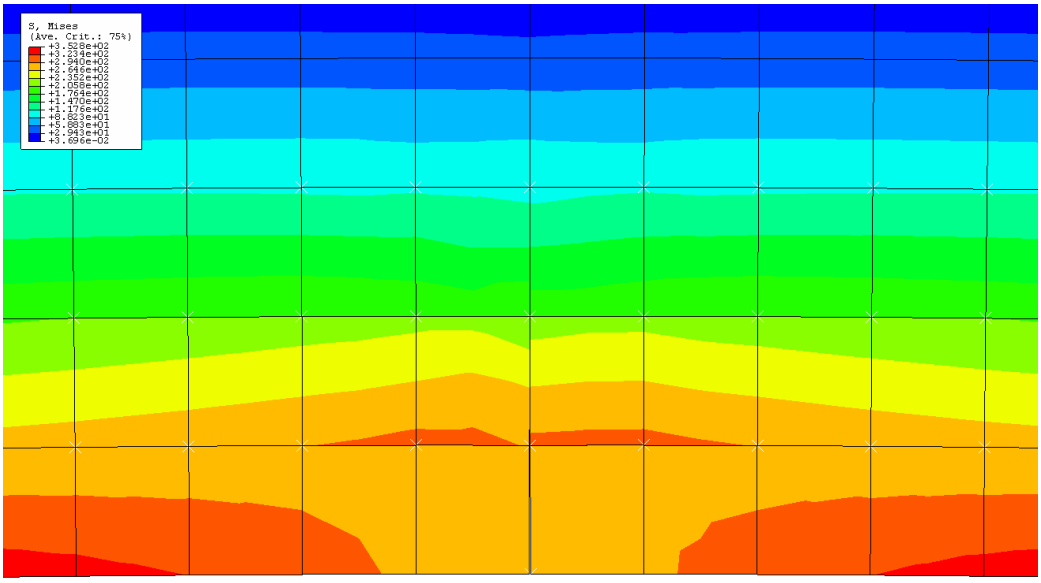

Fig. 73 – Model 2_3 at 18.51% of relative ring deflection. Fibre rupture in two inner plies and delamination of first interface due to shear stress

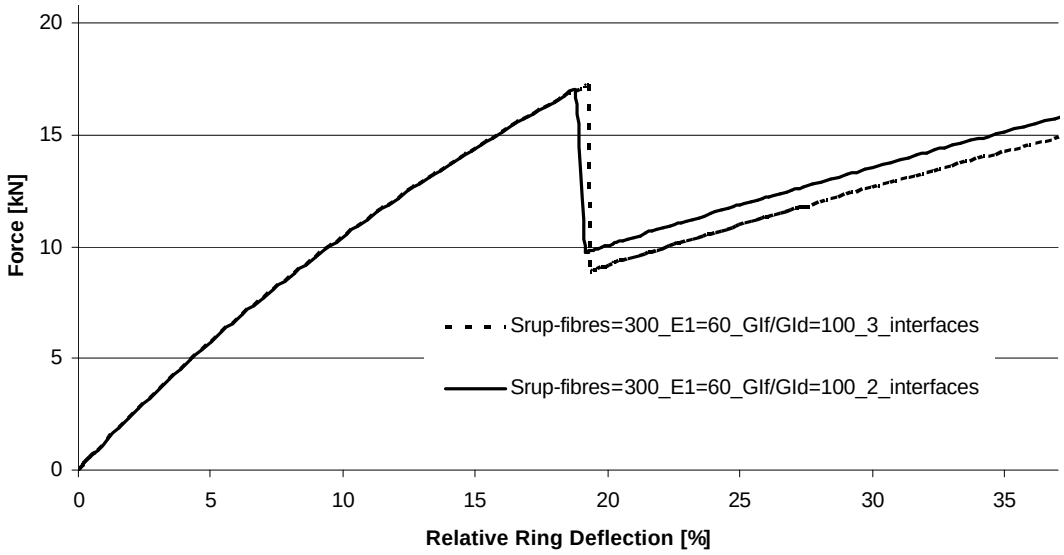

Fig. 74 – Reaction ring force *versus* relative deflection curves for models 2_2 and 2_3

With the last configuration, allowing delamination in all interfaces at all perimeter of the pipe and rupture of fibres at charging section, several outputs were produced.

Figures 75-81 show the relevant phenomena occurring at different stages of deflection in two different models, leading to degradation of the structural ability of the specimen. They are shown several moments of the two models chosen to represent the main damage occurrences detected in all models. The combinations of parameters of those two models are reported in table 11.

These two models, with 10 plies and 12mm of thickness, were chosen because, despite they both fit the experimental *P-d* curve, they present different damage phenomena and progression. And that certainly is one important factor to chose which one is better simulating the experimental tests.

So, the buckling that one can see in the model 9_all after collapse (remembering figure 32) as well as its capability to delaminate before loosing the structural ability leads to the conclusion that the real values of parameters such as $s_{rup\ fibres}$ and G_{If}/G_{Id} ratio are those applied in that successful model.

Table 13 – Values of different parameters in models reported in next figures

Ref.	$s_{rup\ fibres}$ [MPa]	E_1 [GPa]	no. plies	wall thickness [mm]	G_{Id} [kJ/m^2]	G_{IId} [kJ/m^2]	G_{If}/G_{Id}
9_all	200	10.5	10	12	0.3	0.6	700
12_all	300	10.5	10	12	0.3	0.6	10

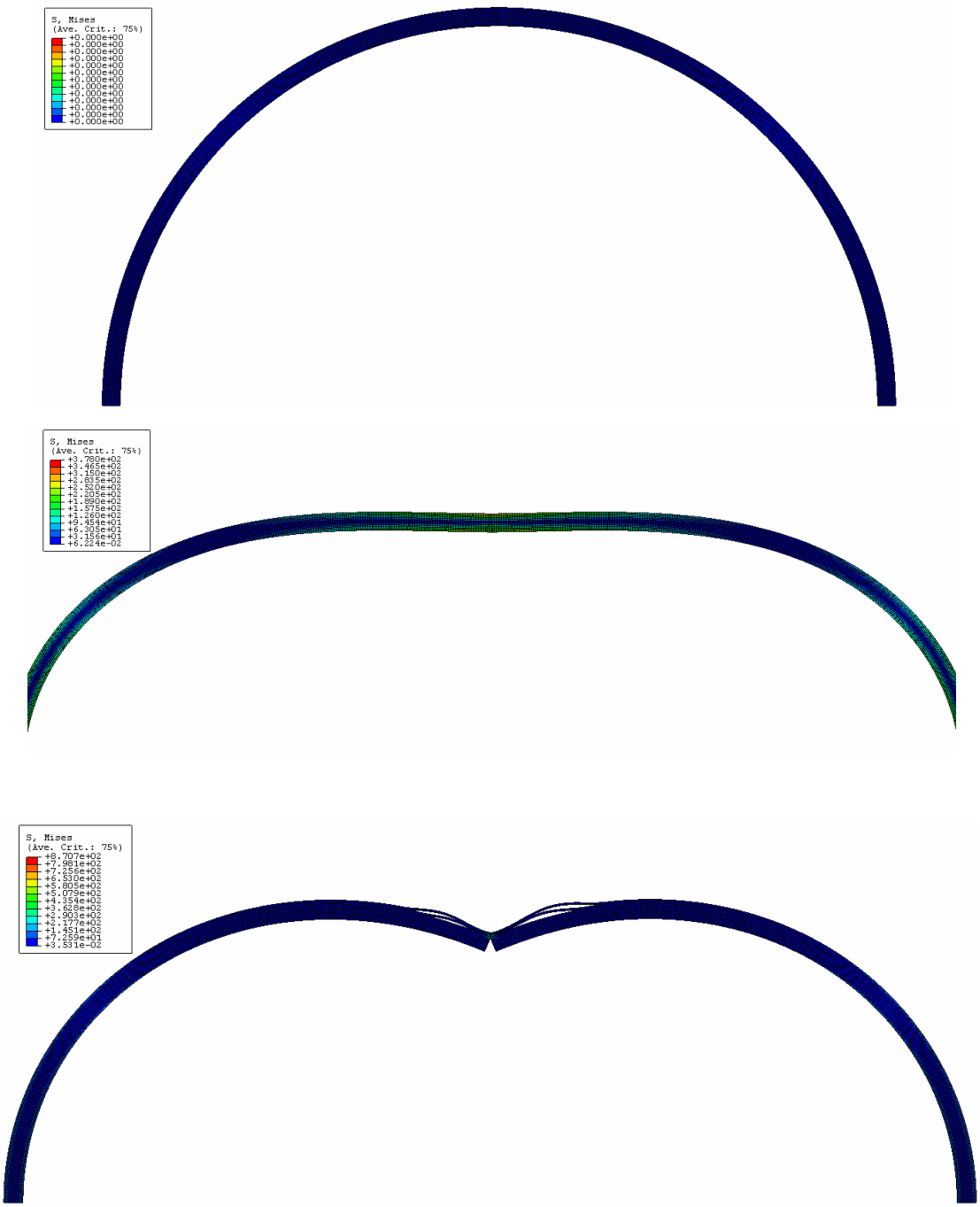

Fig. 75 – Entire view of model 9_all at initial stage, at instant before structural collapse and immediately after structural collapse

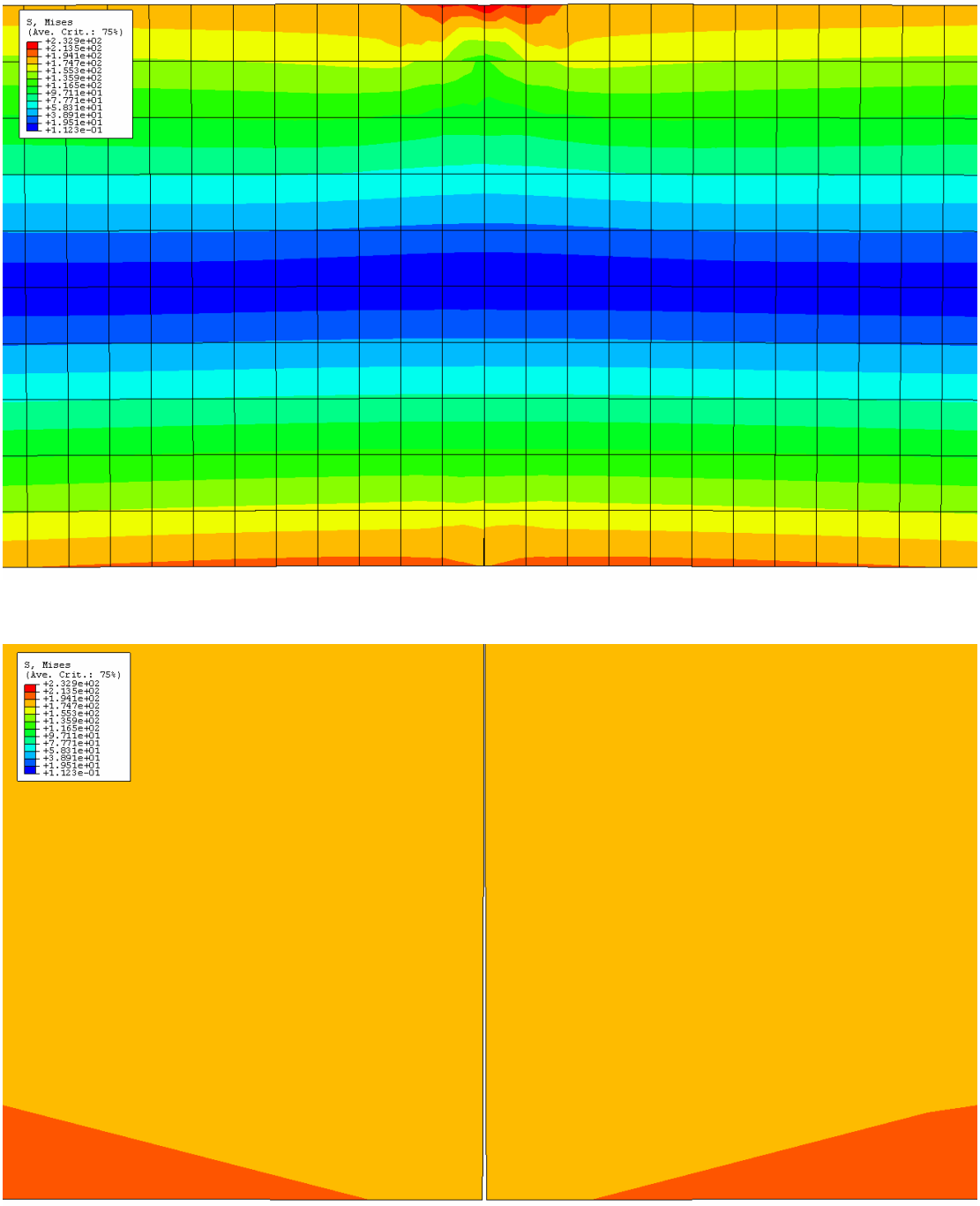

Fig. 76 - Model 9_all at 23.06% of relative ring deflection. Initiation of softening in inner ply. Normal and detailed views.

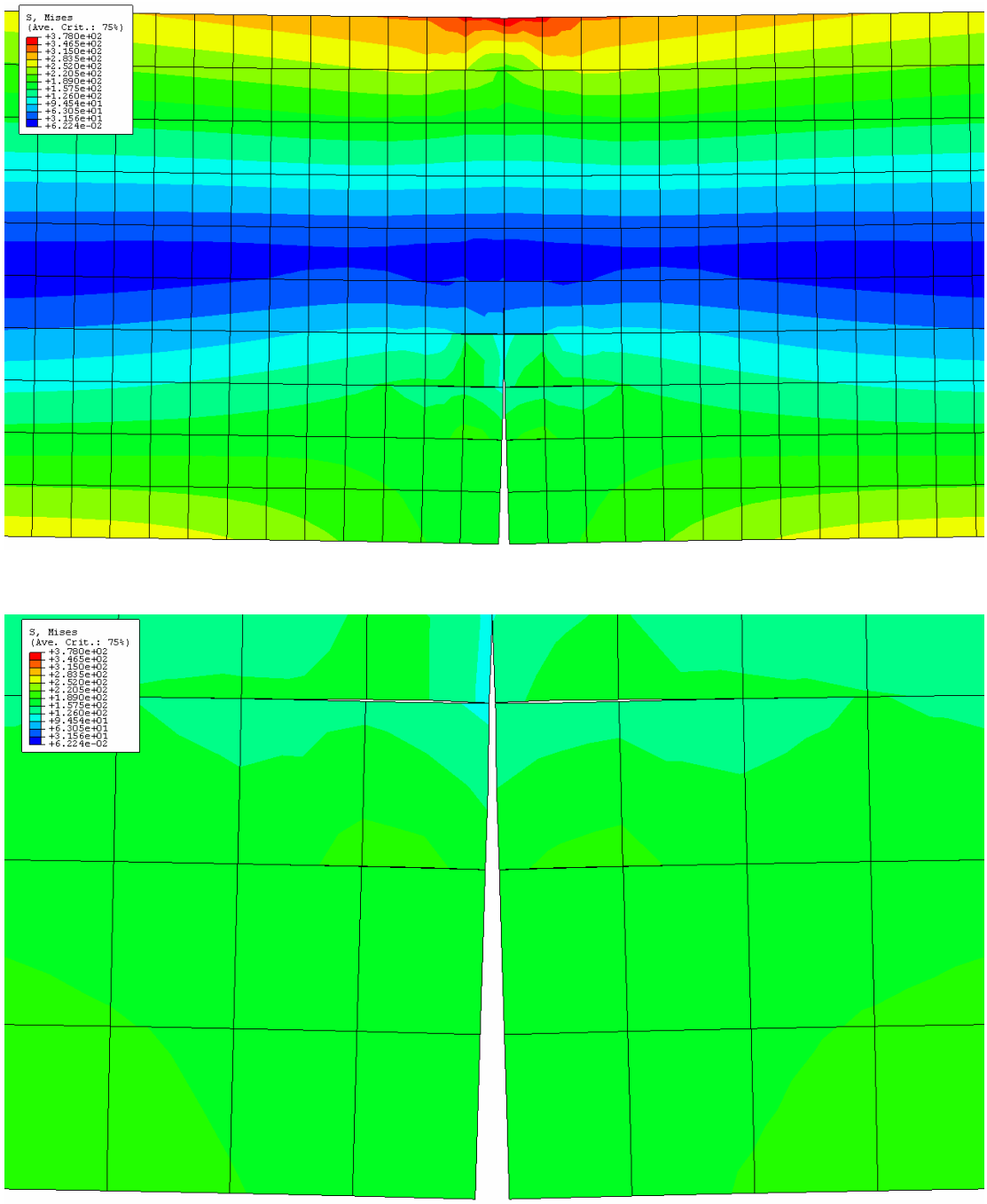

Fig. 77 - Model 9_all at 35.95% of relative ring deflection. Rupture of fibres in the five inner plies and delamination by shear stress until the 4th inner interface. Normal and detailed views.

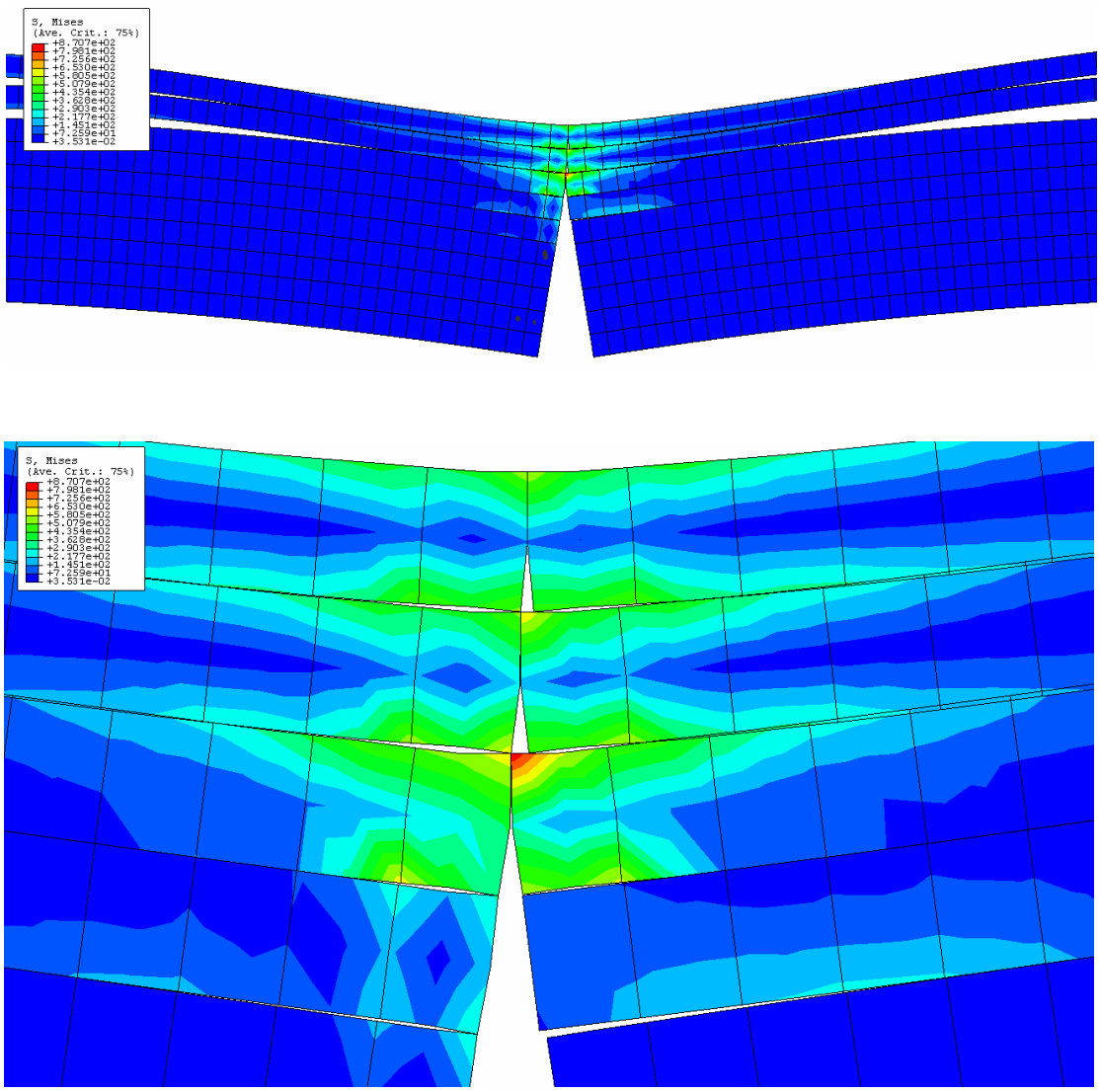

Fig. 78 - Model 9_all at 36.51% of relative ring deflection. Fibres rupture in all plies, structural collapse. Normal and detailed views.

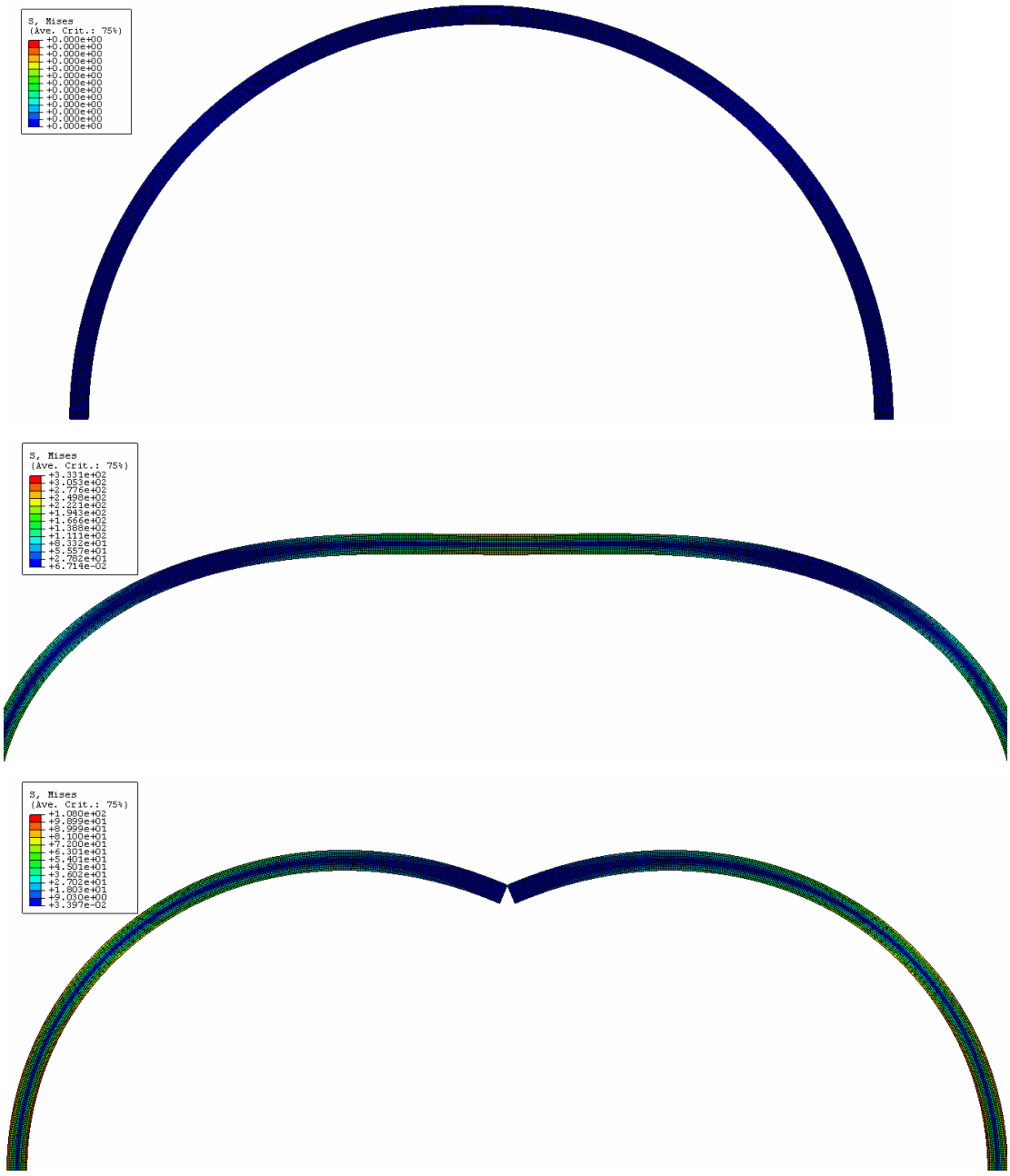

Fig. 79 – Entire view of model 12_all at initial stage, at instant before structural collapse and immediately after structural collapse

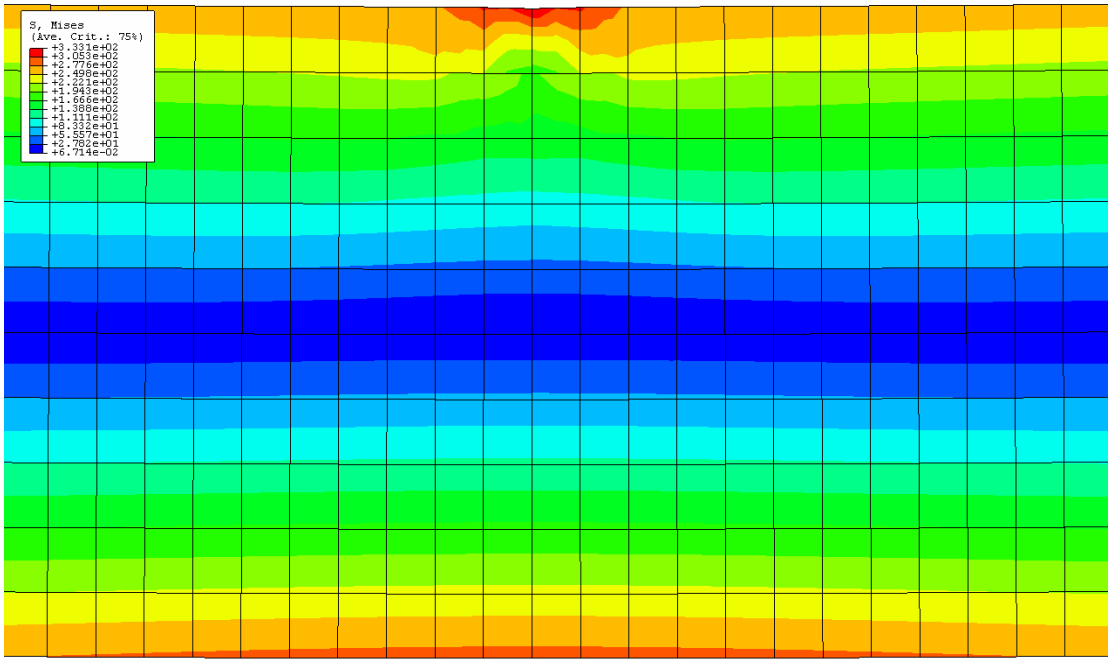

Fig. 80 - Model 12_all at 34.78% of relative ring deflection immediately before structural collapse, apparently with no relevant damage.

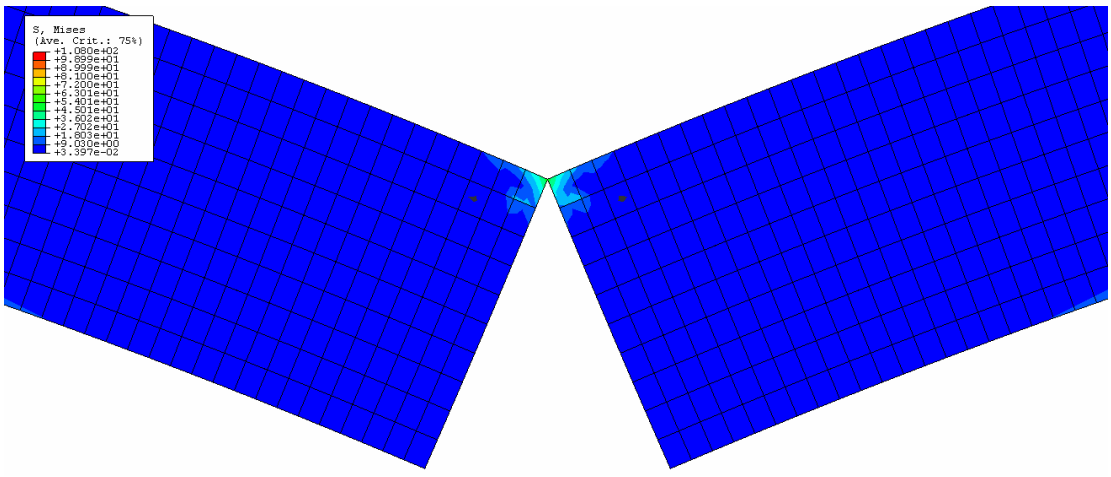

Fig. 81 - Model 34_all at 35.36% of relative ring deflection. Fibres rupture in all plies, structural collapse.

Figures 82-85 show the different curves for reaction ring force *versus* relative ring deflection achieved with different combinations of the parameters. The parameterization is made on $s_{rup\ fibres}$ (fig.82), G_{If}/G_{Id} (fig.83), G_{Id} and G_{IId} (fig.84). In figure 85 one can see that similar results can be achieved with different combinations of parameters.

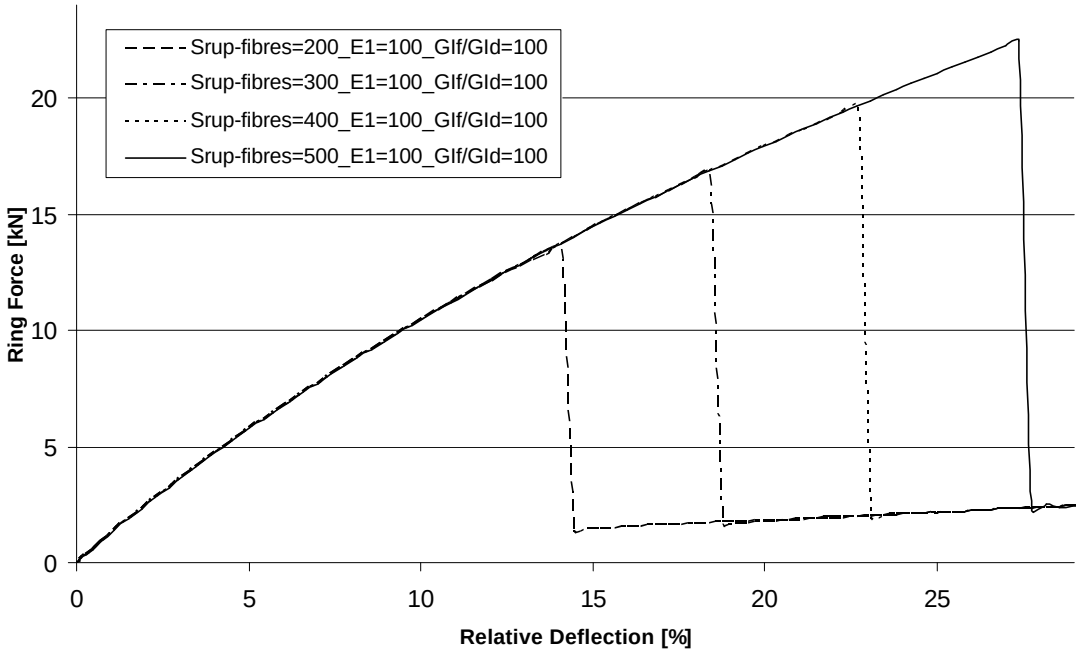

Fig. 82 – Dependence of the models on the parameter $s_{rup\ fibres}$

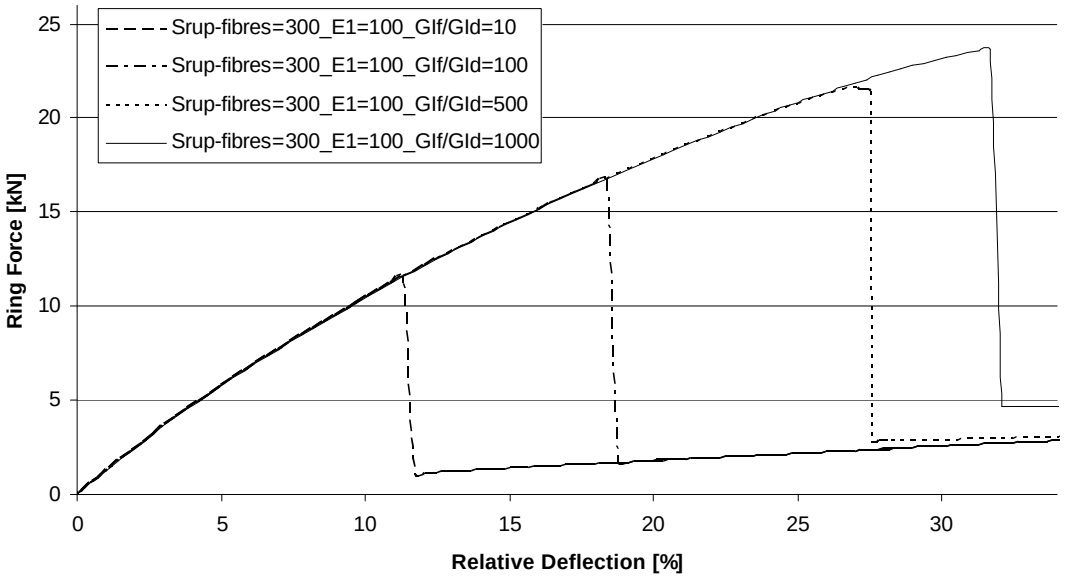

Fig. 83 – Dependence of the models on the parameter G_{If}/G_{Id}

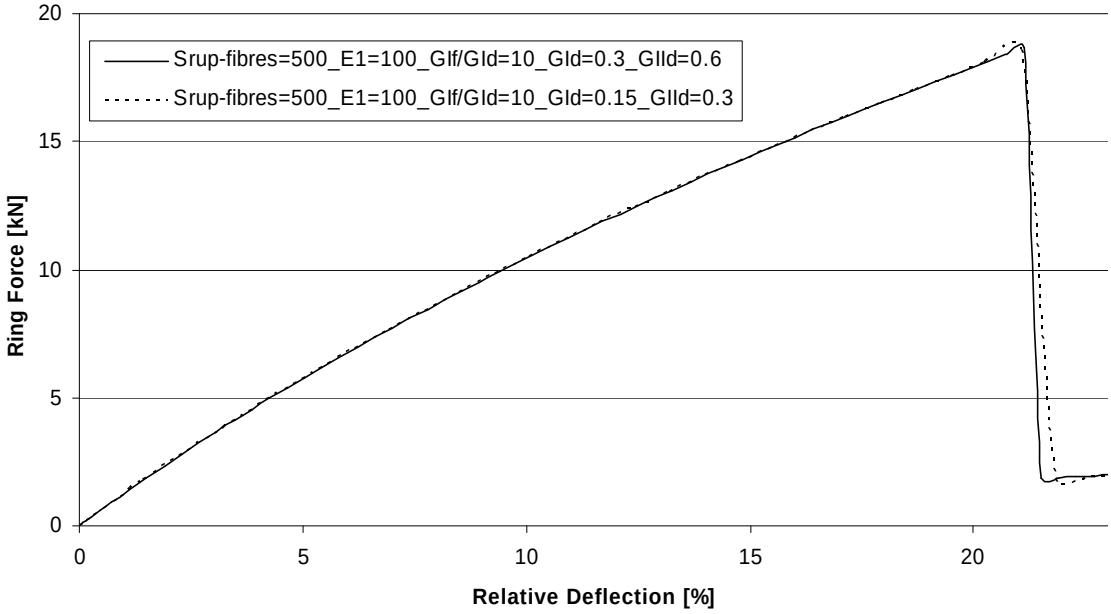

Fig. 84 – Dependence of the models on the parameters G_{Id} and G_{IId}

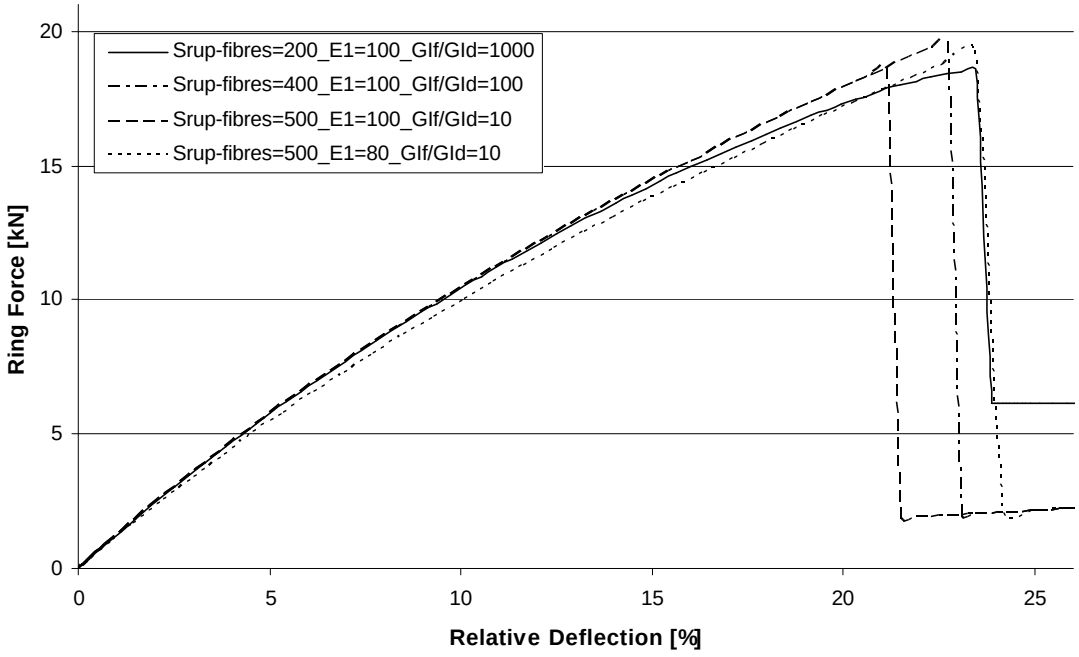

Fig. 85 – Different combinations of parameters leading to similar results

One can see superposition of curves until failure of models that differ only either in G_{If}/G_{Id} ratio, $s_{rup\ fibres}$ or G_{Id}. The only parameters that seems to affect global curves inclination are E_1 (fig.67) and wall thickness t. Actually, changing parameters like G_{If}/G_{Id} ratio, $s_{rup\ fibres}$ or G_{Id} is observed to alter only the collapse point (and respective

collapse load and/or ultimate ring deflection) of that model making no difference in terms of the initial and intermediate behaviour.

Graphics of figures 86 and 87, show the influence of G_{If}/G_{Id} ratio on collapse conditions, reaction force and relative ring deflection at failure, by representing their evolution on models differing only in that parameter. Different curves correspond to different values of $s_{rup\ fibres}$.

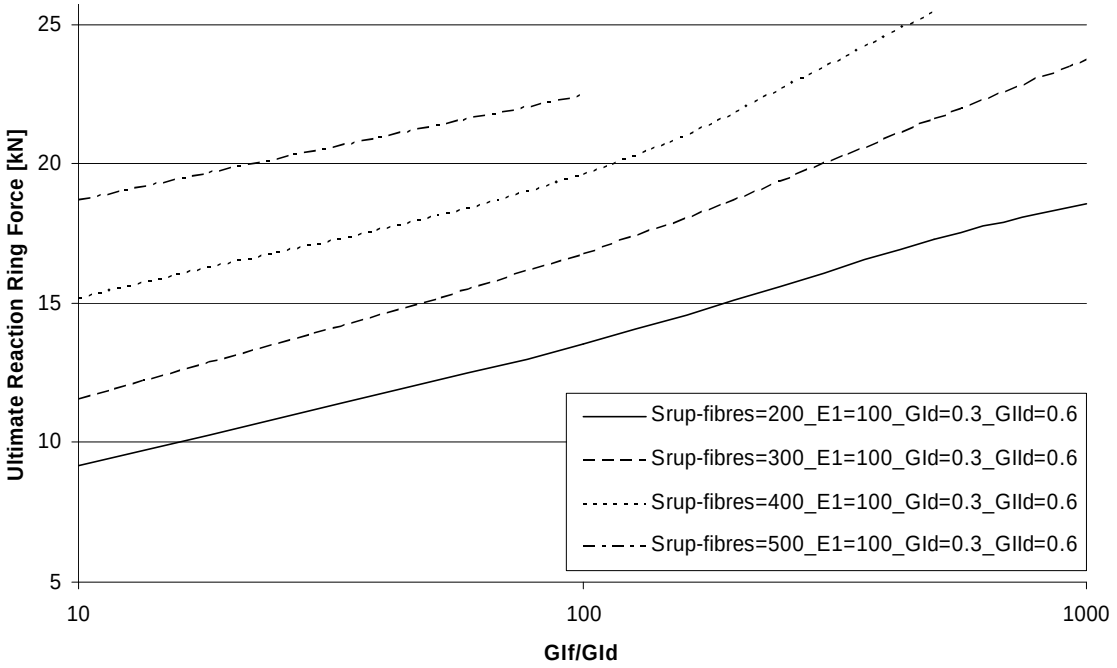

Fig. 86 – Evolution of ultimate reaction ring force with G_{If}/G_{Id} ratio

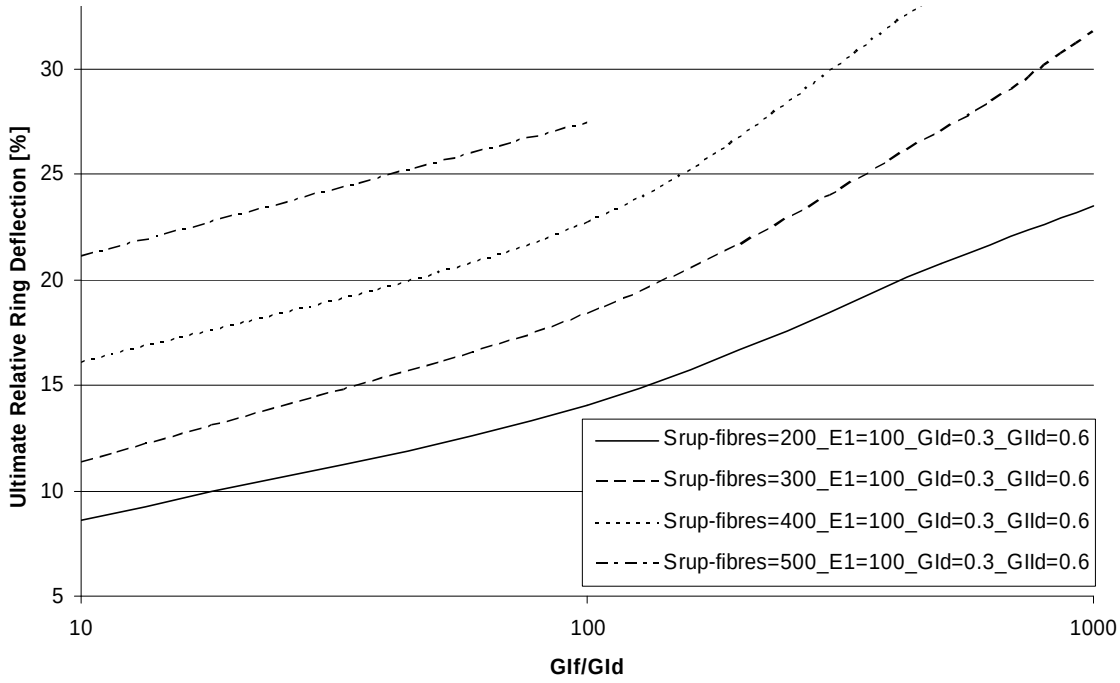

Fig. 87 – Evolution of ultimate deflection with G_{If}/G_{Id} ratio

The increasing tendency of ultimate reaction ring force and ultimate relative ring deflection with G_{If}/G_{Id} ratio that is observed fits the expectations, once it corresponds to the necessity of spending more energy to produce rupture of fibres as the value of G_{If} (strain energy release rate for rupture of fibres in mode I) increases.

Further considerations on these outputs, as well as comparison between numerical and experimental results were made and are reported in the next section.

6. Analysis of Results

In this section experimental and numerical results are analyzed in terms of the relevant conclusions they allow.

Relating to the experimental campaigns, comments shall be done on the pipe behaviour under ring load or deflection conditions, namely concerning to the influence of a wet environment and test duration. Differences in the global behaviour of GRP pipes from different manufacturers and corresponding damage mechanisms, eventually leading to structural failure, are to be analyzed.

In terms of numerical modeling, the influence of several parameters in the pipe shape and evolution of curves of ring force *versus* ring deflections are the main conclusions to be taken.

Finally, confrontation of numerical and experimental results is operated accomplishing the main objective of evaluating the reproducibility of GRP pipes mechanics under ring deflection condition. Therefore, the applicability of numerical tools, such as FEM, to simulate the ring deflection condition, the damage phenomena, by inferring coherent groups of values for relevant parameters, is analyzed.

The first idea one may confirm from the mechanical tests is the scatter in results which denotes the difficulty in establishing a reliable prediction of the long-term behaviour of GRP pipes once any data analysis is significantly affected by that scatter. Even the short-term properties, namely within the static tests, show it. This reinforces the idea of the high dependence of FRP materials properties on their manufacturing conditions.

Initial ring stiffness, creeping in wet conditions and stress relaxation tests outputted interesting data as the three procedures respect to different ring compression conditions. Having not been subjected to previous preconditioning in wet conditions (they were stored in dry air condition at room temperature) the 5 specimens from manufacturer C showed relatively coherent properties in initial ring stiffness tests. However, relevant scatter of results appeared when creeping in wet conditions tests were led on 23 specimens from the manufacturer C as well. Besides that, scatter can also be observed in data published by other two manufacturers (A and D) concerning

similar testing campaigns on pipes with the same nominal specifications. Different regression ratios were calculated for each one of these three types of GRP pipes. As referred above, these different values denote different abilities to sustain creeping effects as time increases during tests. Particularly, specimens from manufacturer A SN10000 showed to be more stable during the time period from 6 minutes to 50 years of in-service application. However, they showed higher levels of ultimate ring deflection either for short as for long-term predictions when compared with specimens SN10000 from manufacturers C and D.

In stress relaxation alternative procedures, specimens from the four selected manufacturers, preconditioned under water at 50ºC for 1000h, revealed no relevant relaxation of stress after the initial phase of few hours. However, test pieces from manufacturer D showed greater relaxation tendency than the others specimens.

Confronting experimental creeping scattered results with the apparent proximity of the resulting curves achieved in stress relaxation tests for specimens from the same manufacturer (either A, B, C or D) and nominal specifications makes one conclude that:

- as preconditioning under water at high temperature tends to accelerate degradation of GRP materials, it seems to stabilize the pipes behaviour, potentially reducing the scatter of results; preconditioning conditions may be adapted to creeping tests;
- mechanical tests imposing a ring compressive condition with constant load (instead of constant deflection) fit better the objective of simulating sub-soil service installation of pipes;
- regression lines obtained after treating the creeping data of up to 10000 hours tests could be equivalently assessed regarding only data from tests during between 0 and 1000 hours. This certainly is a relevant point for discussion within the normalization work groups;
- different types of GRP pipes, manufactured in different ways, have different behaviours under similar testing conditions, meaning that standard procedures shall account for that;
- the same typical damage mechanisms of rupture of fibres and delamination are observed either in short and long-term tests; these seem to be the damage phenomena leading to long-term in-service failure;

- experimental observations showed that delamination is dominated by mode I and/or mode II, while transverse rupture of plies (transversally to the direction of fibres) occur mostly in mode I.

Introducing changes in actual standards to reduce tests duration will require strong and reliable regression methods accounting the scatter in data. This turns especially important when considering the reduction of tested specimens that is another objective of piping industries.

Generally, the numerical models run, either the 3D or the 2D approaches, outputted their tendencies and dependencies on several variables on which results were parameterized.

The 3D models showed that winding angles of around 53º and 90º minimize the value of maximum strain achieved at the charging section. It was seen that for this loading configuration of diametrically opposed charged sections a winding orientation angle of 90º is the best possibility, as far as no relevant solicitation occur in the longitudinal direction of the pipe. Actually, the use of winding orientation angles of 90º is being an increasing tendency in GRP piping manufacture.

Within the reverse engineering process of sharpening parameters value to obtain numerical results fitting reasonably the experimental curves one could assess the main tendencies depending on those parameters:

- the inclination of the reaction ring force *versus* relative ring deflection curves is controlled either by E_1 (circumferential elastic modulus) and/or wall thickness;
- the failure point of each model moves forward on that tendency curve when either G_{If}/G_{Id} ratio and/or $s_{rup\ fibres}$;
- values of G_{Id} and/or G_{IId} have no visible effect.

One may observe, additionally, that the different behaviour of models having cohesive elements in the two inner interfaces only at a limited zone around charged section or in three inner interfaces in all perimeter denote the existence of relevant softening phenomena in sided regions of the pipe wall.

Numerical modelling of GRP pipes subjected to a ring deflection condition using FEM tools showed to be an interesting way of simulating these structures. Additionally, the simplicity of the mesh design makes this a potential method to be

included in future developments promoted by piping industries or standardization committees.

Comparison of experimental and numerical data is mainly done in two specific ways: similarity of the damage mechanisms developed in the two procedures and the proximity of values achieved for stiffness, ultimate ring deflection and ultimate ring load.

Concerning to the damage phenomena leading to structural failure, the same mechanisms are developed either in experimental tests and numerical modelling. Rupture of fibres and delamination are the relevant occurrences.

Qualitatively, the mechanics of the GRP pipe seems reproducible.

Specimens of manufacturer C were expected to have, according to the manufacturers specifications a specific ring stiffness of

$$S = \frac{E\,I}{d_m^3} = \frac{10.5E6 \times \frac{p \times \left(0.5225^4 - 0.500^4\right)}{64}}{0.51125^3} = 46410\ N/m^2 \qquad (57)$$

and, with the values used for circumferential apparent modulus (fitting the experimental curves) and the wall thickness (experimentally measured), the specific ring stiffness came

$$S = \frac{E\,I}{d_m^3} = \frac{10.5E6 \times \frac{p \times \left(0.524^4 - 0.500^4\right)}{64}}{0.512^3} = 49507\ N/m^2 . \qquad (58)$$

This very good proximity between manufacturer's information and the values achieved by integrating our own experimental measurements in the numerical models certainly is a good sign to the numerical approach and methodology worked out in this thesis programme. This good correlation makes one think that the 2D modelling methodology (mesh and geometry design) is acceptable and so it allows the study of the influence of other relevant parameters (G_{If}/G_{Id} ratio, E_2, E_3, $s_{rup\ fibres}$) as the model

seems to simulate quite well the real behaviour of these GRP pipes under ring deflection conditions.

As the models were being improved during this study, better results were achieved, until the moment when, using the same properties for wall thickness, *t*, and apparent circumferential elastic modulus, E_1, as those measured and/or given by manufacturer, the *P-d* curves fitted the experimental one. At that time, parameters as G_{If}/G_{Id} ratio, E_2, E_3, $s_{rup\ fibres}$ were given acceptable values and so these best numerical results totally accomplished the initial goals for this task that were the simulation of experimental evidences either qualitatively, reproducing the damage leading to structural failure, as well as in terms of the *P-d* curves.

In figure 88 three numerical outputs fitting reasonably the experimental one can be observed.

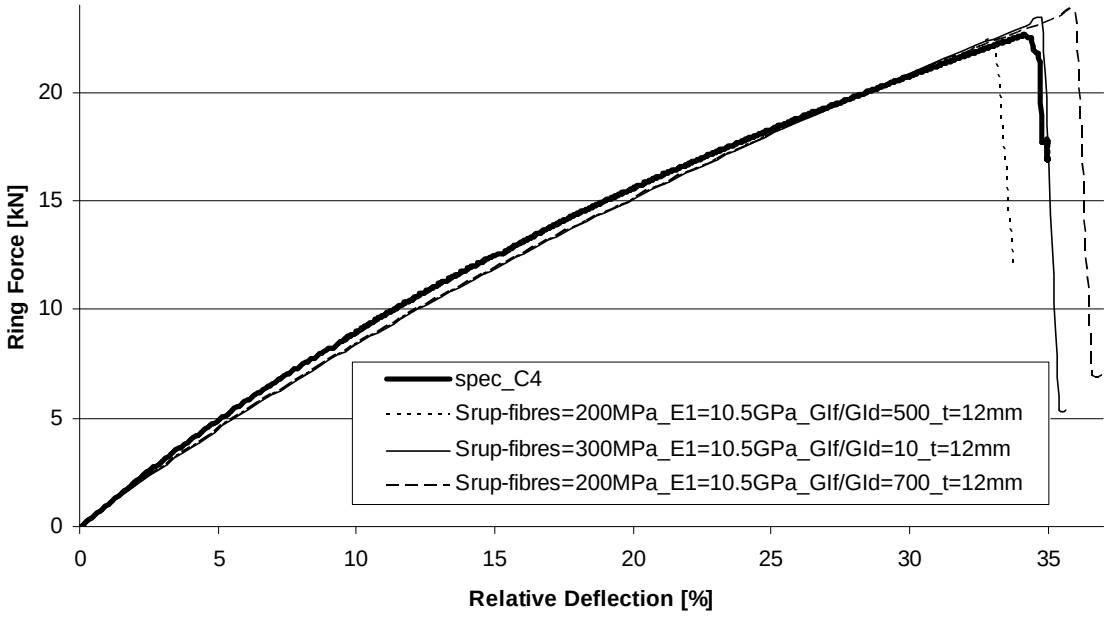

Fig. 88 – Several combinations of parameters leading to results fitting experimental data

As modelling with $s_{rup\ fibres}$=100MPa or $s_{rup\ fibres}$=400MPa would never reach those results (models 5_all and 23_all support this statement), whatever the value of G_{If}/G_{Id} was, one can say that the correct/real values are within the following ranges:

- 200 MPa < $s_{rup\ fibres}$ < 300 MPa
- 0.15 kJ/m^2 < G_{Id} < 0.3 kJ/m^2
- 10 < G_{If}/G_{Id} < 600

Ratios like G_{IId}/G_{Id}=0.5 are quite well accepted, specially when studying problems with nonlinearities [26,27].

According to some authors, and since the exact G_{Id} and G_{IId} critical values for the selected glass/epoxy system are not known, predictions shall be made using typical values of G_{Id} =0.2 kJ/m^2 and G_{IId} =1.5 kJ/m^2[23].

As no coherent groups of values of G_{Id}, G_{IId} and G_{If} for one same composite system were found, even when searching for publications on carbon fibre reinforced plastics (CFRP), one can not assure the reasonability of the values presented for G_{If}/G_{Id} ratio.

However, the values within the range of 3kJ/m^2 to 180kJ/m^2 presented for strain energy release rate in mode I for rupture of fibres, G_{If}, may be analyzed in a simple exercise as follows (let's remember the principle schematized in figure 55):

Assuming, for instance,

- $s_{rup\ fibres}$= 300 MPa,
- e=0.048 (elongation of glass fibre, type E, at total collapse) [28],
- L=0.5mm (thickness of the crack field under analysis, arbitred[15])
- $d_u = e \times L$ ˜ 2.4E-5m

the equation 56 shows how can one get an idea of the greatness of the value of G_{If}

$$G_{If} \equiv \frac{s_{rup\ fibres} \times d_u}{2} = \frac{300E6 \times 2.4E-5}{2} = 3.6\,kJ/m^2 \qquad (59)$$

and it confirms once more that, depending on the value of the strain of the fibre (and even more of the composite ply) at total collapse, the range of values presented in this work are very acceptable.

[15] this value was achieved by experimental observations of the wall section of man. C specimens

7. Conclusion

By the end of this study several conclusions could be made as experimental and numerical outputs were produced. The main objectives of testing GRP pipes under compressive ring conditions using different loading configurations, conduct standard and alternative testing procedures and evaluate the numerical reproducibility of damage phenomena and global mechanics of the pipe were accomplished.

The comparison of some of the experimental data outputted from the testing campaigns conducted here with results published by foreign manufacturers relating to similar campaigns, made the global analysis of GRP pipes behaviour more complete and profitable.

In another way, supporting numerical procedures in experimental results achieved, in a typical reverse engineering process, allowed understanding and choosing the main variables to parameterize the study on.

Globally, the study on the behaviour of GRP pipes under compressive ring loads, which is one of the most used in-service loading conditions, was led in three ways. The experimental program intended to evaluate the influence of ageing conditions by preconditioning test tubes in specific conditions and the interest of applying either loading or deflection conditions. The development of numerical models had the main scopes of reproduce damage mechanisms and main static behaviour of the selected pipes. Confrontation of numerical and experimental results was made iteratively so that numerical modeling fitted gradually the experimental observations and so it could be validated.

The relevant evidences and conclusions taken during this work are analyzed in the previous section, by criticizing the experimental and numerical results as well as by comparing them up to conclude for the global validaton of the procedures conducted.

As outputted data was analyzed, it is expectable that this study may support future investigations on this matter, mainly considering the GRP piping industries demands on lighter standard procedures for certification of products. In this particular area, work is already being done by technical committees of CEN as well as by the leading manufacturers of GRP piping systems

8. References

References

[1] – Morgan, R; Dunn, C; Edwards, C; *Gap Analysis for Durability of Fiber Reinforced Polymer Composites in Civil Infrastructure – Effects of creep and relaxation (Chap 6)*, CERF-ASCE, 2001

[2] – *Composite Engineering Materials: Guide to Composites*, SP systems, 1999

[3] – M. F. S. F. de Moura; J. P. M. Gonçalves; A. T. Marques; P. M. S. T. de Castro; *Prediction of Compressive Strength of Carbon-Epoxy Laminates Containing Delamination by Using a Mixed-Mode Damage Model*, Composite Structures, Vol. 50, Nº2, pg. 151-157, 2000

[4] – J. P. M. Gonçalves; M. F. S. F. de Moura; P. M. S. T. de Castro; A. T. Marques; *Interface Element Including Point-to-Surface Constraints for Three-Dimensional Problems With Damage Propagation*, Engineering Computations: International Journal for Computer-Aided Engineering and Software, Vol. 17, Nº1, pg. 28-47, 2000

[5] – M. F. S. F. de Moura; J. P. M. Gonçalves; A. T. Marques; P. M. S. Tavares de Castro; *Modeling Compression Failure After Low Velocity Impact on Laminated Composites Using Interface Elements*, Journal of Composite Materials, Vol. 31, Nº 15, pg. 1462-1479, 1997

[6] – Reeder, James R.; *Prediction of Long-Term Strength of Thermoplastic Composites Using Time-Temperature Superposition*, NASA-Langley Research Center, Hampton, Virginia, 2002

[7] – Camanho, P; Guedes, R M; *Notas de apoio à disciplina de materiais compósitos*, Curso de mestrado em engenharia mecânica, FEUP-DEMEGI, 2001

[8] – Bai, Jinbo; *Mechanical behavior of ±55º filament-wound glass-fibre/epoxy-resin tubes (I, II, III)*, Composites Science and Technology 57 (141-153), 1997

[9] – Richard, F; *Identification du comportement et evaluation de la fiabilité des composites stratifies*, thèse nº 769, Université de Franche-Comté, 1999

[10] – Marques, A.T.; de Brito, F.M.; *Comparison of methodologies for prediction of long-term properties of GRP pipes*, K L Reifsnider, D Dillard, A Cardon, eds., *'Progress in Durability Analysis of Composite Systems; proceedings of the 3rd int conference on the subject DURACOSYS 97'*, Blacksburg, VA, USA, 14-17 Sept 1997; A A Balkema, **1998**, pp.289-294

[11] – Chouchaoui, C S; Ochoa, O O; *Similitude study for a laminated cylindrical tube under tensile, torsion, bending, internal and external pressure.(Part I, PartII)*, Composite Structures 44 (221-229), 1999

[12] – Parnas, Levend; Katrici, Nuran; *Design of fiber-reinforced composite pressure vessels under various loading conditions*, Composite Structures, 2002

[13] – Ghorbel, J; Spiteri, P; *Durability of closed-end pressurized GRP pipes under hygrothermal conditions (Part I and Part II)*, Journal of Composite Materials, vol 30 nº14 (1562-1595), 1996

[14] – Ferry, L; Perreux, D; Varchon, D; Le Bras, L; *Tensile failure of filament wound pipes under long-term creep loading: a probabilistic analysis*, Composites Science and Technology 57 (1281-1288), 1997

[15] – Toutanji, H; Dempsey, S; *Stress modeling of pipelines strengthened with advanced composites materials*, Thin-Walled Structures 39 (153-165), 2001

[16] – Tarakçioglu, N; Akdemir, A; Avci, A; *Strength of filament wound pipes with surface crack*, Composites: Part B 32 (131-138), 2001

[17] – Marques, A. T.; Brito, F. M.; *Comparison of methodologies for prediction of long-term properties of GRP pipes*, Third International Conference on Progress in Durability Analysis of Composite Systems, 1997
[18] – EN 705, CEN, 1994
[19] – EN 1225, CEN, 1995
[20] – EN 1226, CEN, 1995
[21] – EN 1227, CEN, 1997
[22] – EN 1228, CEN, 1997
[23] – Kashtalyan, M Yu; Soutis, C; *Strain energy release rate for off-axis ply cracking in laminated composites*, International Journal of Fracture, no.112, pp L3-L8, 2001
[24] – de Moura, M.F.S.F.; Gonçalves, J.P.M.; *Modelling the interaction between matrix cracking and delamination in carbon-epoxy laminates under low velocity impact*; Composites Science and Technology 64, pp 1021-1027, 2004
[25] – Greco, F; Lonetti, P; Zinno, R; *An analytical delamination model for laminated plates including bridging effects*, International Journal of Solids and Structures 39, pp 2435-2463, 2002
[26] – Morais, A B; *Analysis of mode II interlaminar fracture of multidirectional laminates*, Composites: Part A, no.35, pp 51-57, 2004
[27] – Buchholz, F G; Rikards, R;; Wang, H; *Computational analysis of interlaminar fracture of laminated composites*, International Journal of Fracture, no.86, pp 37-57, 1997
[28] – MatWeb, Material Property Data - www.matls.com

Consulted Bibliography

[29] – Richard, F; Perreux, D; *The safety-factor calibration of laminates for long-term applications: behaviour model and reliability method*, Composites Science and Technology 61 (2087-2094), 2001
[30] – Richard, F; Perreux, D; *A reliability method for optimization of [+f ,- f] fiber reinforced composite pipes*, Reliability Engineering & System Safety 68 (53-59), 2000
[31] – Rousseau, J; Perreux, D; *The influence of winding patterns on the damage behavior of filament-wound pipes*; Composites Science and Technology 59 (1439-1449), 1999
[32] – Kaynak, C; Mat, O; *Uniaxial fatigue behavior of filament-wound glass-fiber/epoxy composite tubes*, Composites Science and Technology 61 (1833-1840), 2001
[33] – Xia, M; Takayanagi, H; *Analysis of transverse loading for laminated cylindrical pipes*, Composite Structures 53 (279-285), 2001
[34] – Perreux, D; Joseph, E; *The effect of frequency on the fatigue performance of filament-wound pipes under biaxial loading: experimental results and damage model*, Composites Science and Technology 57 (353-364), 1997

[35] – Xia, M; Takayanagi, H; *Analysis of multi-layered filament-wound composite pipes under internal pressure*, Composite Structures 53 (483-491), 2001
[36] – Jacquemin, F; Vautrin, A; *The effect of cyclic hygrothermal conditions on the stresses near the surface of a thick composite pipe*, Composites Science and Technology 62 (567-570), 2002
[37] – Nishizaki, I; Meiarashi, S; *Long-term deterioration of GFRP in water and moist environment*, Journal of Composites for Construction, February 2002
[38] – Liao, K; Tan, Y; *Influence of moisture-induced stress on in situ fiber strength degradation of unidirectional polymer composite*, Composites Part B 32 (265-370), 2001
[39] – Perreux, D; Suri, C; *A study of the coupling between the phenomena of water absorption and damage in glass/epoxy composite pipes*, Composites Science and Technology 57 (1403-1413), 1997

[40] – Perreux, D; Choqueuse, D; *Anomalies in moisture absorption of glass fibre reinforced epoxy tubes*, Composites Part A 33 (147-154), 2002
[41] – Guedes, R. M.; *Long-term behaviour predictions polymeric matrix composite materials*, Modelling of sandwich structures and adhesive bonded joints, FEUP
[42] – Young, Warren C.; *Roark's Formulas for stress and strain*, 6th edition, McGraw Hill, 1988
[43] – Janson, L.; *Plastics pipes for water supply and sewage disposal*; Borealis, 3rd ed., Stockholm, 1999
[44] – Sims, Graham; Bishop, Gordon; *UK Polymer Composites Systems – Foresight Study and Competitive Analysis*, Crown, 2001
[45] – Kim, C W; Hwang, W; Park H C; Han, K S ; *Stacking sequence optimization of laminated plates*, Composite Structures vol.39, pp 283-288, 1997
[46] – Zhang Y; Wang, S; Petersson B; *Large deflection analysis of composite laminates*, Journal of Materials Processing Technology, no.138, pp 34-40, 2003
[47] – Lee, C S; Hwang, W.; Park H.C.; Han, K.S.; *Failure of carbon/epoxy composite tubes under combined axial and torsional loading. 1. Experimental results and predicion of biaxial strength by the use of neural networks*, Composites Science and Technology, no.59, pp 1779-1788, 1999
[48] – Binienda, W K; Robinson, D N; Ruggles, M B; *Creep of polymer matrix composites. II: Monkman-Grant failure relationship for transverse isotropy*, Journal of Engineering Mechanics, vol.129, no.3, pp 310-315, 2003
[49] – Lee, C S; Hwang, W.; Park H.C.; Han, K.S.; *Failure of carbon/epoxy composite tubes under combined axial and torsional loading. 2. Morphology and failure mechanism*, Composites Science and Technology, no.59, pp 1789-1804, 1999
[50] – Kashtalyan, M Yu; Soutis, C; *Mechanisms of internal damage and their effect on the behaviour and propertie of cross-ply composite laminates*, International Applied Mechanics, vol.38, no.6, pp 641-657, 2002
[51] – Kashtalyan, M Yu; Soutis, C; *The effect of delaminations induced by transverse cracks and splits on stiffness properties of composite laminates*, Composites: Part A, no.31, pp 107-119, 2000
[52] – Carreira, R P; Caron, J F; Diaz Diaz A; *Model of multilayered materials for interface stress estimation and validation by finite element calculations*, Mechanics of Materials, no.34, pp 217-230, 2002
[53] – Li, C F; Hu, N; Yin, Y J; Sekine, H; Fukunaga, H; *Low-velocity impact-induced damage of continuous fiber-reinforced composite laminates. Part I. An FEM numerical model*, Composites: Part A, no.33, pp 1055-1062, 2002
[54] – Kashtalyan, M Yu; Soutis, C; *Stiffness degradation in cross-ply laminates damaged by transverse cracking and splitting*, Composites: Part A, no.31, pp 335-351, 2000
[55] – Demianouchko, E; Bai, J; *Stress state analyses of a ±55º filament-wound composite tube with damage effect*, Composite Structures, no.37, pp 233-239, 1997
[56] – Hwang, T; Hong, C; Kim, C; *Probabilistic deformation and strength prediction for a filament wound pressure vessel*, Composite Structures vol.39, pp 283-288, 1997
[57] – Flanagan, G; *A general sublaminate analysis method for determining strain energy release rates in composites*, Materials Science Corporation, 1998
[58] – O'Brien, T K; *PCharacterization, Analysis and prediction of delamination in composites using fracture mechanics*, NASA Oral Reference No. ICF100942OR, 2001
[59] – Hwang, T; Hong, C; Kim, C; *Probabilistic deformation and strength prediction for a filament wound pressure vessel*, Composite Structures vol.39, pp 283-288, 1997
[60] – Pereira, A B; Morais, A B; *Mode II interlaminar fracture of glass/epoxy multidirectional laminates*, Composites: Part A, no.35, pp 265-272, 2004
[61] – Korjakin, A; Rikards, R; Buchholz, F G; Wang, H; Bledzki, A K; Kessler, A; *Comparative study if interlaminar fracture toughness of GFRP with different fiber surface treatments*, Polymer Composites, vol.19, no.6, pp 793-806, 1998

[62] – Golub, V P; Kryzhanovskii, V I; *Long-term strength criteria for some polymer materials under a plane stress state*, Mechanics of Composite Materials, vol.38, no.6, pp 471-484, 2002
[63] – Mertiny, P; Ellyin, F; *LInfluence of the filament winding tension on physical and mechanical properties of reinforced composites*, Composites: Part A, no.33, pp 1615-1622, 2002
[64] – Mieras, H J M A; *Irrevesible creep of filament-wound glass-reinforced resin pipes*, Plastics & Polymers, 1973
[65] – Nishiwaki, T; Yokoyama, A; Maekawa, Z; Hamada, H; Mori, S; *A quasi-three-dimensional lateral compressive analysis method for a composite cylinder*, Composite Structures, no.32, pp 293-298, 1995
[66] – Nishiwaki, T; Yokoyama, A; Maekawa, Z; Hamada, H; *A new numerical modeling for laminated composites*, Composite Structures, no.32, pp 641-647, 1995
[67] – Diggwa, A D S; Norman, R H; *Mechanism of creep of GRP. 1. Shape of creep curves*, Rubber and Plastics Research Association of Great Britain, Research report 193, 1971
[68] – Diggwa, A D S; Norman, R H; *Mechanism of creep of GRP. 1. Microfailures*, Rubber and Plastics Research Association of Great Britain, Research report 194, 1971
[69] – Sudduth, R D; *Development of a simplified relationship between uniaxial creep, stress relaxation, and constant strain-rate results for viscoelastic polymeric materials*, Journal of Applied Polymer Science, vol.82, pp 527-540, 2001
[70] – Sudduth, R D; *Comparison of the failure conditions for creep, stress relaxation, and constant strain rate measurements to predict pipe burst for two ABS materials using the universal viscoelastic model*, Journal of Applied Polymer Science, vol.93, pp 247-260, 2004
[71] – Guedes, R M; *Mathematical analysis of energies for viscoelastic materials and energy based failure criteria for creep loading*, Mechanics of Time-Dependent Materials, no.8, pp 169-192, 2004
[72] – Robinson, D N; Binienda, W K; Ruggles, M B; *Creep of polymer matrix composites. I: Norton/Bailey creep law for transverse isotropy*, Journal of Engineering Mechanics, vol.129, no.3, pp 310-315, 2003

the author

Hugo Faria

9. Annex

input files

Ref.	$s_{rup\ fibres}$ [MPa]	E_1 [GPa]	no. plies	wall thickness [mm]	G_{Id} [kJ/m^2]	G_{IId} [kJ/m^2]	G_{If}/G_{Id}
2_2	300	100	10	10	0.3	0.6	100
2_3	300	100	10	10	0.3	0.6	100
9_all	200	10.5	10	12	0.3	0.6	700
12_all	300	10.5	10	12	0.3	0.6	10
21_all	300	10.5	12	12	0.3	0.6	500

2_2	300	100	10	10	0.3	0.6	100

```
*HEADING
Tubo de DN500 (500mm)
**
*NODE
1
10001,-250,0
11801,250,0
210001,-260,0
211801,260,0
**
**  Geração das linhas circulares interior e exterior
*NGEN,LINE=C,NSET=LINHA_A
10001,11801,1, , 0., 0., 0., 0., 0., -1
**
*NGEN,LINE=C,NSET=LINHA_B
210001,211801,1, , 0., 0., 0., 0., 0., -1
**
**  Geração de nós entre as linhas
**
*NFILL,NSET=ALL
LINHA_A,LINHA_B,20,10000
**
*NSET,NSET=ZC1,GENERATE
30800,31001,1
*NSET,NSET=ZC2,GENERATE
50800,51001,1
*NSET,NSET=VERT,GENERATE
10901,50901,10000
**
*NCOPY, CHANGE NUMBER=500000, OLDSET=ZC1, NEWSET=ZC1DUP, SHIFT
0.,0.,0.
0.,0.,0.,0.,0.,10.,0.
*NCOPY, CHANGE NUMBER=500000, OLDSET=ZC2, NEWSET=ZC2DUP, SHIFT
0.,0.,0.
0.,0.,0.,0.,0.,10.,0.
*NCOPY, CHANGE NUMBER=1000000, OLDSET=VERT, NEWSET=VERTDUP, SHIFT
0.,0.,0.
0.,0.,0.,0.,0.,10.,0.
**-----------------------------------------------------
**  Criação dos elementos laterais
**-----------------------------------------------------
*ELEMENT,TYPE=CPE8R
100000,10001,10009,30009,30001,10005,20009,30005,20001
200000,11001,11009,31009,31001,11005,21009,31005,21001
3000,50801,50803,70803,70801,50802,60803,70802,60801
1000,10801,10803,530803,530801,10802,20803,530802,20801
1050,10899,1010901,1030901,530899,10900,1020901,530900,20899
1051,10901,10903,530903,530901,10902,20903,530902,20901
*ELGEN,ELSET=ALL
100000,100,8,1,10,20000,1000,1
200000,100,8,1,10,20000,1000,1
3000,100,2,1,8,20000,1000,1
1000,49,2,1,2,20000,1000,1
1050,1,2,1,2,20000,1000,1
```

```
1051,50,2,1,2,20000,1000,1
**-----------------------------------------------------
**  Elementos de Interface
**-----------------------------------------------------
*USER ELEMENT, TYPE=U1,NODES=6,COORDINATES=2,VARIABLES=6,PROPERTIES=6
1,2
*ELEMENT, TYPE=U1
1,530801,530802,530803,30801,30802,30803
50,530899,530900,1030901,30899,30900,30901
51,530901,530902,530903,30901,30902,30903
201,10901,20901,530901,1010901,1020901,1030901
202,30901,40901,550901,1030901,1040901,1050901
*ELGEN,ELSET=INTERF1
1,49,2,1,2,20000,100
50,2,20000,100
51,50,2,1,2,20000,100
*ELSET, ELSET=INTERF2
201,202
** Interf1 - Elementos de ligaçao entre camadas
*UEL PROPERTY, ELSET=INTERF1
**GIC, GIIC, S11, T13, PEN, WIDTH
.3,.6,20,20,1E6,300.0
** interf2 - Elementos de rotura da camada
*UEL PROPERTY, ELSET=INTERF2
**GIC, GIIC, S11, T13, PEN, WIDTH
30,6,300,20,1E6,300.0
**-----------------------------------------------------
**  Propriedades do tubo
**-----------------------------------------------------
*SOLID SECTION, MATERIAL=GLASS,ELSET=ALL,ORIENTATION=OR0
300.0
**
*MATERIAL,NAME=GLASS
*ELASTIC, TYPE=ENGINEERING CONSTANTS
12000,3800,3800,0.3,0.3,0.4,3200,3200,
4000
*ORIENTATION,NAME=OR0
1,0,0,0,1,0
3,0
**
*NSET, NSET=COSE1
30801
50801
31001
51001
*NSET, NSET=COSE2
530801
550801
531001
551001
*MPC
TIE,COSE1,COSE2
**
**-----------------------------------------------------
**  STEP
**-----------------------------------------------------
*RESTART,WRITE,OVERLAY
**
```

```
*STEP,NLGEOM,INC=10000,UNSYMM=YES
*STATIC
0.002,1,1E-5,1.
**----------------------------------------------------------
**  Condições de Fronteira
**----------------------------------------------------------
*NSET, NSET=BOUND1, GENERATE
10001,210001,10000
11801,211801,10000
*NSET, NSET=BOUND2, GENERATE
210901,210901,1
*BOUNDARY
BOUND1,2,2
BOUND2,1,1
*BOUNDARY
BOUND2,2,2,-200
*OUTPUT,HISTORY,FREQ=1
*NODE OUTPUT,NSET=BOUND1
RF1,RF2,U1,
*NODE OUTPUT,NSET=BOUND2
RF2,U2,
*OUTPUT,FIELD,FREQ=1
*NODE OUTPUT
U,
*ELEMENT OUTPUT
S,
*EL PRINT, FREQ=1
S,
*NODE PRINT, TOTALS=YES,NSET=BOUND1
RF,
*CONTROLS,PARAMETERS=FIELD,FIELD=DISPLACEMENT
.1,1.0
*CONTROLS,PARAMETERS=TIME INCREMENTATION
1500,1500,,1500,1500
*NODE FILE,NSET=BOUND1
RF,U,
*NODE FILE,NSET=BOUND2
RF,U,
*NODE PRINT,TOTALS=YES,NSET=BOUND1
RF,U,
*NODE PRINT,TOTALS=YES,NSET=BOUND2
RF,U,
*END STEP
```

2_3	300	100	10	10	0.3	0.6	100

```
*HEADING
Tubo de DN500 (500mm)
**
*NODE
1
10001,-250,0
11801,250,0
210001,-260,0
211801,260,0
**
**  Geração das linhas circulares interior e exterior
*NGEN,LINE=C,NSET=LINHA_A
10001,11801,1, , 0., 0., 0., 0., 0., -1
**
*NGEN,LINE=C,NSET=LINHA_B
210001,211801,1, , 0., 0., 0., 0., 0., -1
**
**  Geração de nós entre as linhas
**
*NFILL,NSET=ALL
LINHA_A,LINHA_B,20,10000
**
*NSET,NSET=INTERCAM1,GENERATE
30001,31801,1
*NSET,NSET=INTERCAM2,GENERATE
50001,51801,1
*NSET,NSET=INTERCAM3,GENERATE
70001,71801,1
*NSET,NSET=VERT,GENERATE
10901,70901,10000
**
*NCOPY, CHANGE NUMBER=500000, OLDSET=INTERCAM1, NEWSET=INTERCAM1DUP,
SHIFT
0.,0.,0.
0.,0.,0.,0.,0.,10.,0.
*NCOPY, CHANGE NUMBER=500000, OLDSET=INTERCAM2, NEWSET=INTERCAM2DUP,
SHIFT
0.,0.,0.
0.,0.,0.,0.,0.,10.,0.
*NCOPY, CHANGE NUMBER=500000, OLDSET=INTERCAM3, NEWSET=INTERCAM3DUP,
SHIFT
0.,0.,0.
0.,0.,0.,0.,0.,10.,0.
*NCOPY, CHANGE NUMBER=1000000, OLDSET=VERT, NEWSET=VERTDUP, SHIFT
0.,0.,0.
0.,0.,0.,0.,0.,10.,0.
**-----------------------------------------------------------
**  Criação dos elementos laterais
**-----------------------------------------------------------
*ELEMENT,TYPE=CPE8R
40000,70001,70003,90003,90001,70002,80003,90002,80001
10000,10001,10003,530003,530001,10002,20003,530002,20001
10449,10899,1010901,1030901,530899,10900,1020901,530900,20899
10450,10901,10903,530903,530901,10902,20903,530902,20901
```

```
*ELGEN,ELSET=ALL
40000,900,2,1,7,20000,10000,1
10000,449,2,1,3,20000,10000,1
10449,1,2,1,3,20000,10000,1
10450,450,2,1,3,20000,10000,1
**-----------------------------------------------------
**  Elementos de Interface
**-----------------------------------------------------
*USER ELEMENT, TYPE=U1,NODES=6,COORDINATES=2,VARIABLES=6,PROPERTIES=6
1,2
*ELEMENT, TYPE=U1
1,530001,530002,530003,30001,30002,30003
450,530899,530900,1030901,30899,30900,30901
451,530901,530902,530903,30901,30902,30903
2701,10901,20901,530901,1010901,1020901,1030901
2702,30901,40901,550901,1030901,1040901,1050901
2703,50901,60901,570901,1050901,1060901,1070901
*ELGEN,ELSET=INTERF1
1,449,2,1,3,20000,900
450,3,20000,900
451,450,2,1,3,20000,900
*ELSET, ELSET=INTERF2
2701,2702,2703
** Interf1 - Elementos de ligaçao entre camadas
*UEL PROPERTY, ELSET=INTERF1
**GIC, GIIC, S11, T13, PEN, WIDTH
.3,.6,20,20,1E6,300.0
** interf2 - Elementos de rotura da camada
*UEL PROPERTY, ELSET=INTERF2
**GIC, GIIC, S11, T13, PEN, WIDTH
30,6,300,20,1E6,300.0
**-----------------------------------------------------
**  Propriedades do tubo
**-----------------------------------------------------
*SOLID SECTION, MATERIAL=GLASS,ELSET=ALL,ORIENTATION=OR0
300.0
**
*MATERIAL,NAME=GLASS
*ELASTIC, TYPE=ENGINEERING CONSTANTS
100000,9000,9000,0.3,0.3,0.4,3200,3200,
4000
*ORIENTATION,NAME=OR0
1,0,0,0,1,0
3,0
**
*NSET, NSET=COSE1
30001
50001
70001
31801
51801
71801
*NSET, NSET=COSE2
530001
550001
570001
531801
551801
```

```
571801
*MPC
TIE,COSE1,COSE2
**
**------------------------------------------------------
**  STEP
**------------------------------------------------------
*RESTART,WRITE,OVERLAY
**
*STEP,NLGEOM,INC=10000,UNSYMM=YES
*STATIC
0.002,1,1E-5,1.
**------------------------------------------------------
**  Condições de Fronteira
**------------------------------------------------------
*NSET, NSET=BOUND1, GENERATE
10001,210001,10000
11801,211801,10000
*NSET, NSET=BOUND2, GENERATE
210901,210901,1
*BOUNDARY
BOUND1,2,2
BOUND2,1,1
*BOUNDARY
BOUND2,2,2,-100
*OUTPUT,HISTORY,FREQ=1
*NODE OUTPUT,NSET=BOUND1
RF1,RF2,U1,
*NODE OUTPUT,NSET=BOUND2
RF2,U2,
*OUTPUT,FIELD,FREQ=1
*NODE OUTPUT
U,
*ELEMENT OUTPUT
S,
*EL PRINT, FREQ=1
S,
*NODE PRINT, TOTALS=YES,NSET=BOUND1
RF,
*CONTROLS,PARAMETERS=FIELD,FIELD=DISPLACEMENT
.1,1.0
*CONTROLS,PARAMETERS=TIME INCREMENTATION
1500,1500,,1500,1500
*NODE FILE,NSET=BOUND1
RF,U,
*NODE FILE,NSET=BOUND2
RF,U,
*NODE PRINT,TOTALS=YES,NSET=BOUND1
RF,U,
*NODE PRINT,TOTALS=YES,NSET=BOUND2
RF,U,
*END STEP
```

9_all	200	10.5	10	12	0.3	0.6	700

```
*HEADING
Tubo de DN500 (500mm)
**
*NODE
1
10001,-250,0
11801,250,0
210001,-262,0
211801,262,0
**
**  Geração das linhas circulares interior e exterior
*NGEN,LINE=C,NSET=LINHA_A
10001,11801,1, , 0., 0., 0., 0., 0., -1
**
*NGEN,LINE=C,NSET=LINHA_B
210001,211801,1, , 0., 0., 0., 0., 0., -1
**
**  Geração de nós entre as linhas
**
*NFILL,NSET=ALL
LINHA_A,LINHA_B,20,10000
**
*NSET,NSET=INTERCAM1,GENERATE
30001,31801,1
*NSET,NSET=INTERCAM2,GENERATE
50001,51801,1
*NSET,NSET=INTERCAM3,GENERATE
70001,71801,1
*NSET,NSET=INTERCAM4,GENERATE
90001,91801,1
*NSET,NSET=INTERCAM5,GENERATE
110001,111801,1
*NSET,NSET=INTERCAM6,GENERATE
130001,131801,1
*NSET,NSET=INTERCAM7,GENERATE
150001,151801,1
*NSET,NSET=INTERCAM8,GENERATE
170001,171801,1
*NSET,NSET=INTERCAM9,GENERATE
190001,191801,1
*NSET,NSET=VERT,GENERATE
10901,210901,10000
**
*NCOPY, CHANGE NUMBER=500000, OLDSET=INTERCAM1, NEWSET=INTERCAM1DUP,
SHIFT
0.,0.,0.
0.,0.,0.,0.,0.,10.,0.
*NCOPY, CHANGE NUMBER=500000, OLDSET=INTERCAM2, NEWSET=INTERCAM2DUP,
SHIFT
0.,0.,0.
0.,0.,0.,0.,0.,10.,0.
*NCOPY, CHANGE NUMBER=500000, OLDSET=INTERCAM3, NEWSET=INTERCAM3DUP,
SHIFT
0.,0.,0.
```

```
0.,0.,0.,0.,0.,10.,0.
*NCOPY, CHANGE NUMBER=500000, OLDSET=INTERCAM4, NEWSET=INTERCAM4DUP,
SHIFT
0.,0.,0.
0.,0.,0.,0.,0.,10.,0.
*NCOPY, CHANGE NUMBER=500000, OLDSET=INTERCAM5, NEWSET=INTERCAM5DUP,
SHIFT
0.,0.,0.
0.,0.,0.,0.,0.,10.,0.
*NCOPY, CHANGE NUMBER=500000, OLDSET=INTERCAM6, NEWSET=INTERCAM6DUP,
SHIFT
0.,0.,0.
0.,0.,0.,0.,0.,10.,0.
*NCOPY, CHANGE NUMBER=500000, OLDSET=INTERCAM7, NEWSET=INTERCAM7DUP,
SHIFT
0.,0.,0.
0.,0.,0.,0.,0.,10.,0.
*NCOPY, CHANGE NUMBER=500000, OLDSET=INTERCAM8, NEWSET=INTERCAM8DUP,
SHIFT
0.,0.,0.
0.,0.,0.,0.,0.,10.,0.
*NCOPY, CHANGE NUMBER=500000, OLDSET=INTERCAM9, NEWSET=INTERCAM9DUP,
SHIFT
0.,0.,0.
0.,0.,0.,0.,0.,10.,0.
*NCOPY, CHANGE NUMBER=1000000, OLDSET=VERT, NEWSET=VERTDUP, SHIFT
0.,0.,0.
0.,0.,0.,0.,0.,10.,0.
**------------------------------------------------------
**  Criação dos elementos laterais
**------------------------------------------------------
*ELEMENT,TYPE=CPE8R
100000,190001,190003,210003,210001,190002,200003,210002,200001
100449,190899,1190901,1210901,210899,190900,1200901,210900,200899
100450,190901,190903,210903,210901,190902,200903,210902,200901
10000,10001,10003,530003,530001,10002,20003,530002,20001
10449,10899,1010901,1030901,530899,10900,1020901,530900,20899
10450,10901,10903,530903,530901,10902,20903,530902,20901
*ELGEN,ELSET=ALL
100000,449,2,1,1,20000,10000,1
100450,450,2,1,1,20000,10000,1
10000,449,2,1,9,20000,10000,1
10449,1,2,1,9,20000,10000,1
10450,450,2,1,9,20000,10000,1
*ELSET,ELSET=ALL
100449
**------------------------------------------------------
**  Elementos de Interface
**------------------------------------------------------
*USER ELEMENT, TYPE=U1,NODES=6,COORDINATES=2,VARIABLES=6,PROPERTIES=6
1,2
*ELEMENT, TYPE=U1
1,530001,530002,530003,30001,30002,30003
450,530899,530900,1030901,30899,30900,30901
451,530901,530902,530903,30901,30902,30903
8101,10901,20901,530901,1010901,1020901,1030901
8102,30901,40901,550901,1030901,1040901,1050901
8103,50901,60901,570901,1050901,1060901,1070901
```

```
8104,70901,80901,590901,1070901,1080901,1090901
8105,90901,100901,610901,1090901,1100901,1110901
8106,110901,120901,630901,1110901,1120901,1130901
8107,130901,140901,650901,1130901,1140901,1150901
8108,150901,160901,670901,1150901,1160901,1170901
8109,170901,180901,690901,1170901,1180901,1190901
8110,190901,200901,210901,1190901,1200901,1210901
*ELGEN,ELSET=INTERF1
1,449,2,1,9,20000,900
450,9,20000,900
451,450,2,1,9,20000,900
*ELSET, ELSET=INTERF2
8101,8102,8103,8104,8105,8106,8107,8108,8109,8110
** Interf1 - Elementos de ligaçao entre camadas
*UEL PROPERTY, ELSET=INTERF1
**GIC, GIIC, S11, T13, PEN, WIDTH
.3,.6,20,20,1E6,300.0
** interf2 - Elementos de rotura da camada
*UEL PROPERTY, ELSET=INTERF2
**GIC, GIIC, S11, T13, PEN, WIDTH
210,6,200,20,1E6,300.0
**-------------------------------------------------------
**  Propriedades do tubo
**-------------------------------------------------------
*SOLID SECTION, MATERIAL=GLASS,ELSET=ALL,ORIENTATION=OR0
300.0
**
*MATERIAL,NAME=GLASS
*ELASTIC, TYPE=ENGINEERING CONSTANTS
10500,3800,3800,0.3,0.3,0.4,3200,3200,
4000
*ORIENTATION,NAME=OR0,DEFINITION=OFFSET TO NODES
2,4
3,0
**
***NSET, NSET=COSE1
**30001
**50001
**70001
**90001
**110001
**130001
**150001
**170001
**190001
**31801
**51801
**71801
**91801
**111801
**131801
**151801
**171801
**191801
***NSET, NSET=COSE2
**530001
**550001
**570001
```

```
**590001
**610001
**630001
**650001
**670001
**690001
**531801
**551801
**571801
**591801
**611801
**631801
**651801
**671801
**691801
***MPC
**TIE,COSE1,COSE2
**
**------------------------------------------------------
**  STEP
**------------------------------------------------------
*RESTART,WRITE,OVERLAY
**
*STEP,NLGEOM,INC=10000,UNSYMM=YES
*STATIC
0.002,1,1E-5,0.05
**------------------------------------------------------
**  Condições de Fronteira
**------------------------------------------------------
*NSET, NSET=BOUND1, GENERATE
10001,210001,10000
510001,710001,10000
11801,211801,10000
511801,711801,10000
*NSET, NSET=BOUND2, GENERATE
210901,210901,1
1210901,1210901,1
*BOUNDARY
BOUND1,2,2
BOUND2,1,1
*BOUNDARY
BOUND2,2,2,-150
*OUTPUT,HISTORY,FREQ=1
*NODE OUTPUT,NSET=BOUND1
RF1,RF2,U1,
*NODE OUTPUT,NSET=BOUND2
RF2,U2,
*OUTPUT,FIELD,FREQ=1
*NODE OUTPUT
U,
*ELEMENT OUTPUT
S,
*EL PRINT, FREQ=1
S,
*NODE PRINT, TOTALS=YES,NSET=BOUND1
RF,
*CONTROLS,PARAMETERS=FIELD,FIELD=DISPLACEMENT
.1,1.0
```

```
*CONTROLS,PARAMETERS=TIME INCREMENTATION
1500,1500,,1500,1500
*NODE FILE,NSET=BOUND1
RF,U,
*NODE FILE,NSET=BOUND2
RF,U,
*NODE PRINT,TOTALS=YES,NSET=BOUND1
RF,U,
*NODE PRINT,TOTALS=YES,NSET=BOUND2
RF,U,
*END STEP
```

12_all	300	10.5	10	12	0.3	0.6	10

```
*HEADING
Tubo de DN500 (500mm)
**
*NODE
1
10001,-250,0
11801,250,0
210001,-262,0
211801,262,0
**
**  Geração das linhas circulares interior e exterior
*NGEN,LINE=C,NSET=LINHA_A
10001,11801,1, , 0., 0., 0., 0., 0., -1
**
*NGEN,LINE=C,NSET=LINHA_B
210001,211801,1, , 0., 0., 0., 0., 0., -1
**
**  Geração de nós entre as linhas
**
*NFILL,NSET=ALL
LINHA_A,LINHA_B,20,10000
**
*NSET,NSET=INTERCAM1,GENERATE
30001,31801,1
*NSET,NSET=INTERCAM2,GENERATE
50001,51801,1
*NSET,NSET=INTERCAM3,GENERATE
70001,71801,1
*NSET,NSET=INTERCAM4,GENERATE
90001,91801,1
*NSET,NSET=INTERCAM5,GENERATE
110001,111801,1
*NSET,NSET=INTERCAM6,GENERATE
130001,131801,1
*NSET,NSET=INTERCAM7,GENERATE
150001,151801,1
*NSET,NSET=INTERCAM8,GENERATE
170001,171801,1
*NSET,NSET=INTERCAM9,GENERATE
190001,191801,1
*NSET,NSET=VERT,GENERATE
10901,210901,10000
**
*NCOPY, CHANGE NUMBER=500000, OLDSET=INTERCAM1, NEWSET=INTERCAM1DUP,
SHIFT
0.,0.,0.
0.,0.,0.,0.,0.,10.,0.
*NCOPY, CHANGE NUMBER=500000, OLDSET=INTERCAM2, NEWSET=INTERCAM2DUP,
SHIFT
0.,0.,0.
0.,0.,0.,0.,0.,10.,0.
*NCOPY, CHANGE NUMBER=500000, OLDSET=INTERCAM3, NEWSET=INTERCAM3DUP,
SHIFT
```

```
0.,0.,0.
0.,0.,0.,0.,0.,10.,0.
*NCOPY, CHANGE NUMBER=500000, OLDSET=INTERCAM4, NEWSET=INTERCAM4DUP,
SHIFT
0.,0.,0.
0.,0.,0.,0.,0.,10.,0.
*NCOPY, CHANGE NUMBER=500000, OLDSET=INTERCAM5, NEWSET=INTERCAM5DUP,
SHIFT
0.,0.,0.
0.,0.,0.,0.,0.,10.,0.
*NCOPY, CHANGE NUMBER=500000, OLDSET=INTERCAM6, NEWSET=INTERCAM6DUP,
SHIFT
0.,0.,0.
0.,0.,0.,0.,0.,10.,0.
*NCOPY, CHANGE NUMBER=500000, OLDSET=INTERCAM7, NEWSET=INTERCAM7DUP,
SHIFT
0.,0.,0.
0.,0.,0.,0.,0.,10.,0.
*NCOPY, CHANGE NUMBER=500000, OLDSET=INTERCAM8, NEWSET=INTERCAM8DUP,
SHIFT
0.,0.,0.
0.,0.,0.,0.,0.,10.,0.
*NCOPY, CHANGE NUMBER=500000, OLDSET=INTERCAM9, NEWSET=INTERCAM9DUP,
SHIFT
0.,0.,0.
0.,0.,0.,0.,0.,10.,0.
*NCOPY, CHANGE NUMBER=1000000, OLDSET=VERT, NEWSET=VERTDUP, SHIFT
0.,0.,0.
0.,0.,0.,0.,0.,10.,0.
**-----------------------------------------------------
**  Criação dos elementos laterais
**-----------------------------------------------------
*ELEMENT,TYPE=CPE8R
100000,190001,190003,210003,210001,190002,200003,210002,200001
100449,190899,1190901,1210901,210899,190900,1200901,210900,200899
100450,190901,190903,210903,210901,190902,200903,210902,200901
10000,10001,10003,530003,530001,10002,20003,530002,20001
10449,10899,1010901,1030901,530899,10900,1020901,530900,20899
10450,10901,10903,530903,530901,10902,20903,530902,20901
*ELGEN,ELSET=ALL
100000,449,2,1,1,20000,10000,1
100450,450,2,1,1,20000,10000,1
10000,449,2,1,9,20000,10000,1
10449,1,2,1,9,20000,10000,1
10450,450,2,1,9,20000,10000,1
*ELSET,ELSET=ALL
100449
**-----------------------------------------------------
**  Elementos de Interface
**-----------------------------------------------------
*USER ELEMENT, TYPE=U1,NODES=6,COORDINATES=2,VARIABLES=6,PROPERTIES=6
1,2
*ELEMENT, TYPE=U1
1,530001,530002,530003,30001,30002,30003
450,530899,530900,1030901,30899,30900,30901
451,530901,530902,530903,30901,30902,30903
8101,10901,20901,530901,1010901,1020901,1030901
8102,30901,40901,550901,1030901,1040901,1050901
```

```
8103,50901,60901,570901,1050901,1060901,1070901
8104,70901,80901,590901,1070901,1080901,1090901
8105,90901,100901,610901,1090901,1100901,1110901
8106,110901,120901,630901,1110901,1120901,1130901
8107,130901,140901,650901,1130901,1140901,1150901
8108,150901,160901,670901,1150901,1160901,1170901
8109,170901,180901,690901,1170901,1180901,1190901
8110,190901,200901,210901,1190901,1200901,1210901
*ELGEN,ELSET=INTERF1
1,449,2,1,9,20000,900
450,9,20000,900
451,450,2,1,9,20000,900
*ELSET, ELSET=INTERF2
8101,8102,8103,8104,8105,8106,8107,8108,8109,8110
** Interf1 - Elementos de ligaçao entre camadas
*UEL PROPERTY, ELSET=INTERF1
**GIC, GIIC, S11, T13, PEN, WIDTH
.3,.6,20,20,1E6,300.0
** interf2 - Elementos de rotura da camada
*UEL PROPERTY, ELSET=INTERF2
**GIC, GIIC, S11, T13, PEN, WIDTH
3,6,300,20,1E6,300.0
**-----------------------------------------------------
**  Propriedades do tubo
**-----------------------------------------------------
*SOLID SECTION, MATERIAL=GLASS,ELSET=ALL,ORIENTATION=OR0
300.0
**
*MATERIAL,NAME=GLASS
*ELASTIC, TYPE=ENGINEERING CONSTANTS
10500,3800,3800,0.3,0.3,0.4,3200,3200,
4000
*ORIENTATION,NAME=OR0,DEFINITION=OFFSET TO NODES
2,4
3,0
**
***NSET, NSET=COSE1
**30001
**50001
**70001
**90001
**110001
**130001
**150001
**170001
**190001
**31801
**51801
**71801
**91801
**111801
**131801
**151801
**171801
**191801
***NSET, NSET=COSE2
**530001
**550001
```

```
**570001
**590001
**610001
**630001
**650001
**670001
**690001
**531801
**551801
**571801
**591801
**611801
**631801
**651801
**671801
**691801
***MPC
**TIE,COSE1,COSE2
**
**------------------------------------------------------
**  STEP
**------------------------------------------------------
*RESTART,WRITE,OVERLAY
**
*STEP,NLGEOM,INC=10000,UNSYMM=YES
*STATIC
0.002,1,1E-5,0.05
**------------------------------------------------------
**  Condições de Fronteira
**------------------------------------------------------
*NSET, NSET=BOUND1, GENERATE
10001,210001,10000
510001,710001,10000
11801,211801,10000
511801,711801,10000
*NSET, NSET=BOUND2, GENERATE
210901,210901,1
1210901,1210901,1
*BOUNDARY
BOUND1,2,2
BOUND2,1,1
*BOUNDARY
BOUND2,2,2,-150
*OUTPUT,HISTORY,FREQ=1
*NODE OUTPUT,NSET=BOUND1
RF1,RF2,U1,
*NODE OUTPUT,NSET=BOUND2
RF2,U2,
*OUTPUT,FIELD,FREQ=1
*NODE OUTPUT
U,
*ELEMENT OUTPUT
S,
*EL PRINT, FREQ=1
S,
*NODE PRINT, TOTALS=YES,NSET=BOUND1
RF,
*CONTROLS,PARAMETERS=FIELD,FIELD=DISPLACEMENT
```

```
.1,1.0
*CONTROLS,PARAMETERS=TIME INCREMENTATION
1500,1500,,1500,1500
*NODE FILE,NSET=BOUND1
RF,U,
*NODE FILE,NSET=BOUND2
RF,U,
*NODE PRINT,TOTALS=YES,NSET=BOUND1
RF,U,
*NODE PRINT,TOTALS=YES,NSET=BOUND2
RF,U,
*END STEP
```

21_all	300	10.5	12	12	0.3	0.6	500

```
*HEADING
Tubo de DN500 (500mm)
**
*NODE
1
10001,-250,0
11801,250,0
250001,-262,0
251801,262,0
**
**  Geração das linhas circulares interior e exterior
*NGEN,LINE=C,NSET=LINHA_A
10001,11801,1, , 0., 0., 0., 0., 0., -1
**
*NGEN,LINE=C,NSET=LINHA_B
250001,251801,1, , 0., 0., 0., 0., 0., -1
**----------------------------------------------------
**  Geração de nós entre as linhas
**----------------------------------------------------
*NFILL,NSET=ALL
LINHA_A,LINHA_B,24,10000
**
*NSET,NSET=INTERCAM1,GENERATE
30001,31801,1
*NSET,NSET=INTERCAM2,GENERATE
50001,51801,1
*NSET,NSET=INTERCAM3,GENERATE
70001,71801,1
*NSET,NSET=INTERCAM4,GENERATE
90001,91801,1
*NSET,NSET=INTERCAM5,GENERATE
110001,111801,1
*NSET,NSET=INTERCAM6,GENERATE
130001,131801,1
*NSET,NSET=INTERCAM7,GENERATE
150001,151801,1
*NSET,NSET=INTERCAM8,GENERATE
170001,171801,1
*NSET,NSET=INTERCAM9,GENERATE
190001,191801,1
*NSET,NSET=INTERCAM10,GENERATE
210001,211801,1
*NSET,NSET=INTERCAM11,GENERATE
230001,231801,1
*NSET,NSET=VERT,GENERATE
10901,250901,10000
**
*NCOPY, CHANGE NUMBER=500000, OLDSET=INTERCAM1, NEWSET=INTERCAM1DUP,
SHIFT
0.,0.,0.
0.,0.,0.,0.,0.,10.,0.
*NCOPY, CHANGE NUMBER=500000, OLDSET=INTERCAM2, NEWSET=INTERCAM2DUP,
SHIFT
```

```
0.,0.,0.
0.,0.,0.,0.,0.,10.,0.
*NCOPY, CHANGE NUMBER=500000, OLDSET=INTERCAM3, NEWSET=INTERCAM3DUP,
SHIFT
0.,0.,0.
0.,0.,0.,0.,0.,10.,0.
*NCOPY, CHANGE NUMBER=500000, OLDSET=INTERCAM4, NEWSET=INTERCAM4DUP,
SHIFT
0.,0.,0.
0.,0.,0.,0.,0.,10.,0.
*NCOPY, CHANGE NUMBER=500000, OLDSET=INTERCAM5, NEWSET=INTERCAM5DUP,
SHIFT
0.,0.,0.
0.,0.,0.,0.,0.,10.,0.
*NCOPY, CHANGE NUMBER=500000, OLDSET=INTERCAM6, NEWSET=INTERCAM6DUP,
SHIFT
0.,0.,0.
0.,0.,0.,0.,0.,10.,0.
*NCOPY, CHANGE NUMBER=500000, OLDSET=INTERCAM7, NEWSET=INTERCAM7DUP,
SHIFT
0.,0.,0.
0.,0.,0.,0.,0.,10.,0.
*NCOPY, CHANGE NUMBER=500000, OLDSET=INTERCAM8, NEWSET=INTERCAM8DUP,
SHIFT
0.,0.,0.
0.,0.,0.,0.,0.,10.,0.
*NCOPY, CHANGE NUMBER=500000, OLDSET=INTERCAM9, NEWSET=INTERCAM9DUP,
SHIFT
0.,0.,0.
0.,0.,0.,0.,0.,10.,0.
*NCOPY, CHANGE NUMBER=500000, OLDSET=INTERCAM10, NEWSET=INTERCAM10DUP,
SHIFT
0.,0.,0.
0.,0.,0.,0.,0.,10.,0.
*NCOPY, CHANGE NUMBER=500000, OLDSET=INTERCAM11, NEWSET=INTERCAM11DUP,
SHIFT
0.,0.,0.
0.,0.,0.,0.,0.,10.,0.
*NCOPY, CHANGE NUMBER=1000000, OLDSET=VERT, NEWSET=VERTDUP, SHIFT
0.,0.,0.
0.,0.,0.,0.,0.,10.,0.
**----------------------------------------------------------
**  Criação dos elementos regulares
**----------------------------------------------------------
*ELEMENT,TYPE=CPE8R
120000,230001,230003,250003,250001,230002,240003,250002,240001
120449,230899,1230901,1250901,250899,230900,1240901,250900,240899
120450,230901,230903,250903,250901,230902,240903,250902,240901
****100000,190001,190003,210003,210001,190002,200003,210002,200001
****100449,190899,1190901,1210901,210899,190900,1200901,210900,200899
****100450,190901,190903,210903,210901,190902,200903,210902,200901
10000,10001,10003,530003,530001,10002,20003,530002,20001
10449,10899,1010901,1030901,530899,10900,1020901,530900,20899
10450,10901,10903,530903,530901,10902,20903,530902,20901
*ELGEN,ELSET=ALL
120000,449,2,1,1,20000,10000,1
120450,449,2,1,1,20000,10000,1
****100000,449,2,1,1,20000,10000,1
```

```
****100450,450,2,1,1,20000,10000,1
10000,449,2,1,11,20000,10000,1
10449,1,2,1,11,20000,10000,1
10450,450,2,1,11,20000,10000,1
*ELSET,ELSET=ALL
120449
****100449
**------------------------------------------------------
**  Criação dos Elementos de Interface
**------------------------------------------------------
*USER ELEMENT, TYPE=U1,NODES=6,COORDINATES=2,VARIABLES=6,PROPERTIES=6
1,2
*ELEMENT, TYPE=U1
1,530001,530002,530003,30001,30002,30003
450,530899,530900,1030901,30899,30900,30901
451,530901,530902,530903,30901,30902,30903
9901,10901,20901,530901,1010901,1020901,1030901
9902,30901,40901,550901,1030901,1040901,1050901
9903,50901,60901,570901,1050901,1060901,1070901
9904,70901,80901,590901,1070901,1080901,1090901
9905,90901,100901,610901,1090901,1100901,1110901
9906,110901,120901,630901,1110901,1120901,1130901
9907,130901,140901,650901,1130901,1140901,1150901
9908,150901,160901,670901,1150901,1160901,1170901
9909,170901,180901,690901,1170901,1180901,1190901
9910,190901,200901,710901,1190901,1200901,1210901
9911,210901,220901,730901,1210901,1220901,1230901
9912,230901,240901,750901,1230901,1240901,1250901
****8101,10901,20901,530901,1010901,1020901,1030901
****8102,30901,40901,550901,1030901,1040901,1050901
****8103,50901,60901,570901,1050901,1060901,1070901
****8104,70901,80901,590901,1070901,1080901,1090901
****8105,90901,100901,610901,1090901,1100901,1110901
****8106,110901,120901,630901,1110901,1120901,1130901
****8107,130901,140901,650901,1130901,1140901,1150901
****8108,150901,160901,670901,1150901,1160901,1170901
****8109,170901,180901,690901,1170901,1180901,1190901
****8110,190901,200901,210901,1190901,1200901,1210901
*ELGEN,ELSET=INTERF1
1,449,2,1,11,20000,900
450,11,20000,900
451,450,2,1,11,20000,900
*ELSET, ELSET=INTERF2
9901,9902,9903,9904,9905,9906,9907,9908,9909,9910,9911,9912
** Interf1 - Elementos de ligaçao entre camadas
*UEL PROPERTY, ELSET=INTERF1
**GIC, GIIC, S11, T13, PEN, WIDTH
.3,.6,20,20,1E6,300.0
** interf2 - Elementos de rotura da camada
*UEL PROPERTY, ELSET=INTERF2
**GIC, GIIC, S11, T13, PEN, WIDTH
150,6,300,20,1E6,300.0
**------------------------------------------------------
**  Propriedades do tubo
**------------------------------------------------------
*SOLID SECTION, MATERIAL=GLASS,ELSET=ALL,ORIENTATION=OR0
300.0
**
```

```
*MATERIAL,NAME=GLASS
*ELASTIC, TYPE=ENGINEERING CONSTANTS
10500,9000,9000,0.3,0.3,0.4,3200,3200,
4000
*ORIENTATION,NAME=OR0, DEFINITION=OFFSET TO NODES
2,4
3,0
**
*NSET, NSET=COSE1
30001
50001
70001
90001
110001
130001
150001
170001
190001
210001
230001
31801
51801
71801
91801
111801
131801
151801
171801
191801
211801
231801
*NSET, NSET=COSE2
530001
550001
570001
590001
610001
630001
650001
670001
690001
710001
730001
531801
551801
571801
591801
611801
631801
651801
671801
691801
711801
731801
*MPC
TIE,COSE1,COSE2
**
**----------------------------------------------------------
```

```
**  STEP
**----------------------------------------------------------
*RESTART,WRITE,OVERLAY
**
*STEP,NLGEOM,INC=10000,UNSYMM=YES
*STATIC
0.002,1,1E-5,0.05
**----------------------------------------------------------
**  Condições de Fronteira
**----------------------------------------------------------
*NSET, NSET=BOUND1, GENERATE
10001,250001,10000
11801,251801,10000
*NSET, NSET=BOUND2, GENERATE
250901,250901,1
1250901,1250901,1
*BOUNDARY
BOUND1,2,2
BOUND2,1,1
*BOUNDARY
BOUND2,2,2,-150
*OUTPUT,HISTORY,FREQ=1
*NODE OUTPUT,NSET=BOUND1
RF1,RF2,U1,
*NODE OUTPUT,NSET=BOUND2
RF2,U2,
*OUTPUT,FIELD,FREQ=1
*NODE OUTPUT
U,
*ELEMENT OUTPUT
S,
*EL PRINT, FREQ=1
S,
*NODE PRINT, TOTALS=YES,NSET=BOUND1
RF,
*CONTROLS,PARAMETERS=FIELD,FIELD=DISPLACEMENT
.1,1.0
*CONTROLS,PARAMETERS=TIME INCREMENTATION
1500,1500,,1500,1500
*NODE FILE,NSET=BOUND1
RF,U,
*NODE FILE,NSET=BOUND2
RF,U,
*NODE PRINT,TOTALS=YES,NSET=BOUND1
RF,U,
*NODE PRINT,TOTALS=YES,NSET=BOUND2
RF,U,
*END STEP
```